UNIVERSITY OF SOUTHAMPTON

Ship Science

School of Engineering Sciences

Time domain simulation of hydroelastic response of ships in large amplitude waves

by

Jae-Hong Park

Thesis for the degree of Doctor of Philosophy

December 2006

ABSTRACT

The influence of non-linearities on wave-induced motions and loads has been the focus of many investigations in the past few years and continues to be an important issue. A number of two- and three-dimensional methodologies have been developed, by and large, partly accounting for various non-linearities. Non-linear radiation, and to an extent diffraction, is the main problem and its solution via a three-dimensional method using Eulerian-Lagrangian schemes is likely to be complex and time consuming for practical applications. On the other hand two-dimensional methods, in spite of issues associated with accounting for forward speed, offer more possibilities of making practical advances in dealing with non-linearities.

A two-dimensional hydroelasticity analysis for symmetric (i.e. vertical motions, distortions and loads) dynamic behaviour in waves, including the influence of non-linearities, is presented in this thesis using two methods. In the first method the total response is decomposed into linear and non-linear parts. The linear part is evaluated using the conventional two-dimensional linear hydroelasticity analysis. The non-linear hydrodynamic forces are due to changes in added mass and damping coefficients, as well as restoring and incident wave forces, all evaluated over the instantaneous wetted surface. Non-linear forces due to slamming (bottom impact and flare) and green water (treated in a quasi-static manner) are also added. One aim of the thesis is to investigate the influence/importance of each of the non-linear hydrodynamic forces. Furthermore, the effects of assumptions made when using these hydrodynamic forces, e.g. frequency dependence of added mass, neglecting the damping coefficients in some components and evaluation of derivatives, are investigated. The solution in the time domain is obtained using direct integration and convolution integration, the latter based on the impulse response functions of the hull in its mean wetted surface. In the second method the response, including non-

linearities, is obtained from the solution of one system of equations of motion, where the added mass and damping coefficients and the restoring, incident wave and diffraction forces are evaluated at the instantaneous draft. Non-linear forces due to slamming (bottom impact and flare) and green water (treated in a quasi-static manner) are also added.

Both methods are applied to the S-175 containership, for which experimental measurements of motions and loads in large amplitude regular head waves are available. Comparisons made between predictions and measurements (heave and pitch motions, vertical acceleration and vertical bending moment) indicate good overall agreement. The comparisons also show that the influence of flare slamming is important for the range of speeds and wave amplitudes investigated.

Contents

Ⅰ. Nomenclature

a	wave amplitude
$[A]$	generalized hydrodynamic added mass matrix
$[B]$	generalized fluid damping matrix
$[C]$	generalized fluid stiffness matrix
$[a]$	generalized structural mass matrix
$[b]$	generalized structural damping matrix
$[c]$	generalized stiffness matrix
$\{F_l\}$	generalised linear wave force
$\{F_{nl}\}$	generalised nonlinear force
E	Young's modulus
G	Shear modulus
I_y	moment of inertia about horizontal axis
L	ship length
M	bending moment
V	shear force
p_r	r^{th} principal coordinate
p_l	linear principal coordinate
p_{nl}	nonlinear principal coordinate
p_{max}	maximun slamming pressure
r, s	modal index
U	ship forward speed
w	vertical displacement
w_r	modal vertical displacement
k	wave number

z_{rel}	vertical relative displacement ($z_{rel} = w - \bar{\zeta}$)
ρ	water density
g	gravity acceleration
t	time
F_1	flare slammig force
F_2	nonlinear modification due to added mass variation
F_3	nonlinear modification due to fluid damping variation
F_4	nonlinear modification to hydrostatic restoring and Froude-Krylov force
F_5	green water effects
F_6	bottom impact slamming force
H	frequency response function
h	impulse response function
m	added mass coefficient
N	fluid damping coefficient
ζ	wave elevation
κ	Smith correction factor
χ	heading angle
ω	wave frequency
ω_e	encounter wave frequency
λ	wave length
θ	bending slope
	also pitch in graphs
ϕ	velocity potential

Ⅱ. List of figures

III. List of tables

Chapter 1

Introduction

1.1 General background

The dynamic responses of a ship advancing in a seaway are examined by evaluating the interaction between the ship and the waves. Considering the interactive process between the wave and the ship as a system, the input to the system is the irregular and randomly varying sea surface and the output of the system is the ship response, such as ship motion, hull pressure distribution, bending moment, etc. St. Denis and Pierson (1953) opened a new era in the study of ship motions and wave loads by hypothesizing that irregular sea waves can be represented as a linear superposition of a large number of regular waves of varying amplitude and frequency. The validation of the application of superposition to ship motions and wave loads is generally accepted, especially for vertical motions and loads. Naval architects and researchers calculate hull responses due to some regular (harmonic) waves and combine the sequences later. In order to represent irregular and random sea waves, statistical methods are applied (Price and Bishop 1974).

In the wave-ship system, the mechanics and dynamics of fluid flow, ship motions and ship deformations can be described by equations governing the interaction between the waves and the ship. In the equations of motion for a wave-ship system, assuming that the water particles cannot penetrate the hull and there are no viscous effects (for rolling motion, viscous effects are important and empirical corrections may be introduced (Schmitke 1978)), the nonlinearities occur due to free surface conditions as well as the instantaneous position of the ship relative to the waves. No general

solutions exist and the fully three-dimensional problem in the time domain is, at present, too complex to be of practical use in concept and preliminary design stages. Thus, several partly nonlinear numerical methods are established, mainly using two-dimensional methods.

The linear theory of ship motion may sometimes be inadequate for the estimation of wave loads and ship structure design. However, the general theory regarding the response of linear systems is of great value and also has application to the vibratory response of the ship. In addition one should note that much of the terminology used in seakeeping is based on linear theory and the concept of a frequency response function or transfer function is widely used in design. In linear theory, some assumptions have to be made. By and large two different kinds of approximation have been introduced. The first assumes small waves and small motion of the ship, by which one can use a linearised free surface condition. Assuming the wave-ship system as a linear system, a three-dimensional linear problem is obtained and can be solved. However, the influence of waves generated by the ship advancing at forward speed, i.e. the steady flow case, makes the problem difficult. Another approximation is based on the assumption that the three-dimensional effects of wave loads are so small that the longitudinal components of velocity may be ignored. In this assumption, the effect of the local steady flow around the ship is neglected. Furthermore, the linear free surface condition with forward speed is simplified so that the unsteady waves generated by the body propagate in directions perpendicular to the longitudinal axis of the ship. Thus the problem is reduced to a two-dimensional one; the so called strip theory (Korvin-Kroukovsky and Jacobs 1957, Salvesen et al. 1970).

Although the strip theory has useful applications, a three-dimensional method can account for interactions between strips, and the forward speed effect in the free surface boundary condition; thus, capable of producing three-dimensional pressure information for an arbitrary-shaped body for structural analysis. Three-dimensional panel methods have been developed using Green function methods or Rankine source methods in the frequency and in the time domain. Green function methods for the seakeeping problem which satisfy the mean body boundary condition and linear free surface boundary condition in the frequency domain were implemented by Inglis and Price (1982), Ohkusu and Iwashita (1989) and Du et al. (1999). Time domain linear solutions applying the Green function method are calculated from the frequency domain (Ballard et al. 2003). The three-dimensional linear methods have been developed using time domain Green function (Lin and Yue 1990) or Rankine source (Nakos and Sclavounos 1990). Fully three-dimensional nonlinear approach in potential flow problems was solved for mathematical hull forms using the Euler-Lagrange method (Longuet-Higgins and Cokelet 1976, Beck et al. 1994). Driven by the complexity of the fully nonlinear approach, the approximate nonlinear methods were developed based on the time domain Green function method (Lin and Yue 1993) or the Rankine source method (Nakos et al. 1993).

Rigid body methods (two or three-dimensional) can provide, in addition to motions, information that can be used for estimating wave-induced loads, such as bending moments. However, they do not include the influence of the structure and structural dynamics when solving the fluid-structure interaction problem. Two-dimensional hydroelastic theory was originated by Bishop and Price (1979) using a strip-beam model. Fluid-structure interaction problems can be analyzed by defining rigid-body motions and elastic deflections of flexural bodies as motions in ‘generalized’ modes, introducing different sets of generalised modes. The generalised modes comprise the ‘dry’ modes of ship structure in vacuo and the ‘wet’ modes including the effects of

fluid action. The evaluation of bending moment, shear force, torsional moment and stresses is affected by the distortions due to excitation by waves, machinery, etc. Two-dimensional hydroelasticity theories (the strip-beam model) were successfully applied to symmetric (Bishop et al. 1977) and antisymmetric behaviour (Bishop et al. 1978a). Bishop et al. (1986) presented a general linear potential flow theory for flexible marine structures, based on the three-dimensional Green function method. This approach is unified, comprising rigid body motions and distortions, and is applicable for any type of floating structure. Two- and three-dimensional hydroelasticity theories were applied to structures such as frigates (Bishop et al. 1984), a dry dock (Lundgen et al. 1989), a fast patrol boat (Aksu et al. 1993), SWATH (Price et al. 1994), and a trimaran (Miao et al. 2003). Bishop et al. (1978b) devised a linear method to estimate slamming excitation and response.

It has been known that the sagging bending moment is considerably larger than the hogging bending moment, because of hydrodynamic differences between the entry and exit of a body through the free surface of a fluid and for non-sinusoidal waves. Ships advancing in rough seas experience nonlinear effects due to non-vertical flare and slamming loads and these nonlinear forces, associated with the continuous change of the submerged hull surface, can only be included using a time domain solution. The methods for treatment of nonlinear forces in seakeeping and wave loads were widely discussed by ISSC (1997, 2000). Several partly nonlinear computation methods, based on the strip theory, were established (Jensen and Pedersen 1979, Gu et al. 1989). The hydrostatic and Froude-Krylov forces, which are known to be the most dominant components when dealing with large motions, are calculated considering the instantaneous wetted surface, while radiation and diffraction forces are represented by frequency dependent coefficients, which are sometimes included (Domnisoru and Domnisoru 1997, Wu and Hermunstad 2002, Gu et al. 2003) or sometimes omitted (Xia and Wang 1997) in the formulation of the

equation. Bottom slamming impact loads or green water effects can also be additionally treated in a linear manner (Wang et al. 1998).

The dynamic responses of structure due to fluid impact are decomposed into two parts: local and global hull behaviour. The local structure is rigid and its natural frequency is higher than wave excitation frequencies. Therefore, the response of local structure may be focussed on impact load prediction, the fluid-structure interaction problem and the large deformation of local structure. This local behaviour is not further examined as this research will only focus on examining the global responses associated with hydroelastic behaviour of hull girder due to steady state wave loads and impact loads (i.e. bottom slamming and green water). A ship is flexible and this property has important consequences in two main cases: (1) when the hull girder is relatively flexible such that the natural frequencies of hull girder vibration fall within the excitation frequency of wave loads, referred to as a springing; (2) when the ship undergoes impact loads and its behaviour is significantly affected by impact, i.e. whipping. Springing is a continuous resonant global vibration and may be induced by the high-frequency part of the wave spectrum and a high order wave excitation (Jensen and Dogliani 1995, Vidic-Perunovic et al. 2004). The effect of springing may increase in faster, larger, lighter and wider ships, especially with low structural damping. Full-scale measurements for various types of ships indicate that springing reduces fatigue life considerably and high springing occurs even in low sea states and ballast condition (Storhaug et al. 2003, Stiansen et al. 1978). Whipping is a transient hull vibration which is induced by bottom slamming, bow flare slamming and green water loads. It increases cumulative fatigue damage to and extreme stresses on the hull. Whipping effects on the bending moment are sensitive to ship speed and wave frequency. Full-scale measurements show that the magnitude of whipping stress can be of the same order as those of steady state wave loads (Aertssen and Sluys 1972, Meek et al. 1972).

With respect to the prediction of extreme loads and fatigue assessment, both the hydroelastic effect and nonlinear effects are important in hull response to waves. A prediction method of long term extremes using nonlinear time-domain simulations and relevant statistical approaches has been presented by Baarholm and Jensen (2004), Wu and Hermundstad (2002). It was found, for an S175 container vessel, that whipping increases the long term extreme values of vertical bending moment (especially hogging) and the correlation effects between whipping and wave-induced responses are significant (Baarholm and Jensen 2004).

1.2 Objectives and scope of the work

The objectives of the present thesis are the development of reliable and practical calculation methods for predicting ship motions and loads in large amplitude waves, considering hydroelastic effects. Time domain simulation of hydroelastic response due to large amplitude motion was carried out in regular waves.

The theoretical background is presented in Chapter 2. The generalised hydroelastic equation of motion is set up for a Timoshenko beam model. The generalised hydrodynamic mass, damping and stiffness coefficients and fluid force are derived using the classical strip theory of Salvesen et al. (1970). The nonlinear effects in large amplitude waves are considered, by modifying the fluid forces according to the instantaneous draught at each time step. A hydrodynamic formula for calculating the green water load is used. Bottom slamming impact force is predicted, using an existing empirical formula. The transient loads are included in the nonlinear equation of motion.

Linear and nonlinear numerical calculations are presented in Chapters 3 and 4 for the S175 container ship, respectively. The linear solutions in Chapter 3 are carried out for both frequency and time domain in regular head waves. A sensitivity study on the influence of higher modes and structural damping on the hydroelastic effects is performed. Comparative studies of the numerical simulation methods are carried out, using the convolution integral method and the direct numerical integration method, in order to verify the time simulation scheme to be used in nonlinear analysis.

The nonlinear forces are decomposed into six components (Method 1) and the influence of each component on the response is evaluated in Chapter 4. The nonlinear modification of the Froude-Krylov force and the hydrostatic restoring force as well as the modification of the hydrodynamic force are evaluated for response in regular waves. The green water load effects are also compared. Bottom impact induced loads and whipping responses are presented. The vertical bending moment due to the impact is amplified at the wet resonance frequency of the lower mode of the hull vibration. The nonlinear solutions are compared with the experiment results for the S175 container ship given by O'Dea et al. (1992), Watanabe et al. (1989) and Chen et al. (2001). The comparisons show that the nonlinear method provides consistent simulation for rigid body motions, bow accelerations and sagging/hogging bending moments.

In Chapter 5, the alternative method (Method 2) is introduced, based on the direct numerical integral method (Newmark-beta method) to the nonlinear problem for ships in large amplitude of motions and wave loads. In this method, all hydrodynamic coefficients are varied with the instantaneous draught of hull sections. The bottom impact and green water are estimated in the same manner as in Chapter 2 and included among the total hydrodynamic forces. The calculations were performed

for the S175 container ship and the predicted results are compared with those estimated by Method 1 in Chapter 4 and experiments.

1.3 Literature review

1.3.1 The strip method, including nonlinearities

Korvin-Kroukovsky and Jacobs (1957) published very important papers on ship motion analysis, in which, based on the slender body hypothesis, the disturbance potential in the vicinity of a slender hull is assumed locally to be two-dimensional without interaction between the flow around each section along the body. Two forces, one due to the hull motion and one due to the diffraction of the incident wave, can be represented using relative motion descriptions. Gerritsma and Beukelman (1967) extended the method for series sixty vessel, by using the close-fit method in estimating two-dimensional hydrodynamic coefficients. The calculated results have a good agreement with experiments and results according to close-fit method differed slightly from those using the Lewis transformation.

More rational approaches appeared. Ogilvie and Tuck (1969) derived strip theory, also based on slender body theory. Salvesen, Tuck and Faltinsen (1970; STF) derived a strip method, starting with the exact expressions of forces and moments for an irrotational, incompressible and inviscid fluid. Subsequently, introducing assumptions, such as slender body and high frequency, the fluid forces acting on the hull can be expressed as integrals along the ship length, expressed as a function of two dimensional velocity potential. The effect of the outgoing waves has also been included in the expression of momentum, with forward speed. The strip method

gives excellent results in an engineering sense and the paper by Salvesen et al. (1970) became one of the most cited works in seakeeping. The difference between the above two methods [i.e. STF (1970) and Gerritsma and Beukelman (1967)] is mainly the influence of the damping coefficients. The STF method may be preferred from a theoretical point of view because the limitations of the method become clear in derivations of the method. Flokstra (1974) presented an example for a container ship, where the vertical bending moments calculated by the STF method are in closer agreement with the experimental data than those of Gerritsma and Beukelman (1967). The main assumptions used in the derivation of the equation motion by the STF strip method are recalled here: Firstly, the viscous effects are disregarded, so that only the potential flow damping is considered. Damping is due to the energy loss in creating free-surface waves. Secondly, in order to linearise the potential flow problem, it is assumed that the wave-resistance perturbation potential and its derivatives are small enough to be ignored, which is reasonable for slender hull forms. Finally, in order to reduce the three-dimensional problem to a summation of two-dimensional problems, the frequency is assumed to be high. However, in the case of the STF method, the hydrodynamic coefficients and the exciting force and moment were derived without use of any strip theory approximations, so that the strip theory approximations were introduced only in order to simplify the numerical computation. In the STF method, the perturbation due to steady force is ignored; instead the Doppler effects accounting for forward speed are included.

Conformal transformation and mapping techniques in calculations of added mass and fluid damping for ship sections was derived by Lewis (1929) in fluid of infinite depth. Ursell (1949) analytically introduced frequency dependent hydrodynamic coefficients accounting for the effect of the free surface by the multipole expansion technique. A full derivation and description of Ursell's expression was given by de Jong (1973). By using the multi-parameter conformal mapping technique, Ursell's

work was extended to a ship-shaped section by Tasai (1960). Bishop et al. (1978c) calculated the hydrodynamic coefficients by using the multipole expansion and conformal mapping techniques for various types of sections, and showed the method can more effectively applied to arbitrary sections than Lewis form technique or Frank's close fit method (Faltinsen 1969).

High speed strip theory was proposed by Faltinsen and Zhao (1991). The perturbation due to forward speed affects the body boundary condition and free surface boundary condition. The surface boundary condition includes high order terms which account for the forward speed effects. The method has improved results in comparison with experimental data. However, strip theory basically ignores the interaction effect between each section, so the forward speed effect can be considered better in the three-dimensional method, especially when using translating pulsating source (Inglis and Price, 1981)

Jensen and Pedersen (1979) presented the second order strip theory hydroelastic code (SOST) in the frequency domain based on a perturbation method, in which the quadratic terms due to non-linearity of the exciting waves (Stokes waves), the non-vertical sides of the ship, and the non-linear hydrodynamic forces are added to the linear strip theory coefficients. The frequency domain method is convenient in terms of computing and represents well the difference between sagging and hogging moments and probability information. The quadratic theory extends to a hydroelastic problem in order to predict springing response due to continuous excitation from waves (Jensen and Dogliani 1995). The results for the fast container vessel are that the non-linear contributions to the springing response are as important as the linear contribution. However long-term extreme peak responses of the springing vibrations become less important.

Time domain analysis has many advantages in dealing with nonlinearities in ship motions and wave loads. The fluid force can be estimated at the exact instantaneous hull surface for large amplitude motions and the transient impact loads may be obtained in the time domain. Nonlinear time domain strip methods have been developed, extending directly from frequency domain theory formulations (Guedes Soares 1989, Chui and Fujino 1991, Chan et al. 2003). Although such methods are relatively simple and have advantages in terms of computation, the hydrodynamic coefficients are simply derived for a specific frequency, so that the application of the method for irregular waves causes a problem in the choice of frequency dependent coefficients.

Domnisoru and Domnisoru (1997) presented unified linear and nonlinear analytical models for ship dynamic response analysis, including springing and whipping, and compared this result with model test data. They used the Longuet-Higgins model for the waves and hydrodynamic force was calculated using the strip theory by Gerritsma and Beukelman (1967). They divided the total response into linear and nonlinear parts, the latter including the nonlinearities from the time variation in hydrodynamic coefficients and the impact slamming force component. For the linear part, the conventional linear modal analysis was adopted and the nonlinear system of equations was solved using a numerical integration method. The hydrodynamic coefficients were calculated such that: the hydrodynamic terms for rigid modes (r = 0,1) were calculated using ship oscillation frequency for heave mode and the terms for flexural mode (r = 2,…,N) were calculated at the frequency of the first flexural mode (r = 2). The results showed high stress levels in the hull girder induced by springing and whipping phenomena.

Cummins (1962) resolved the time domain velocity potential into the instantaneous and memory parts of the impulse response function derived from the frequency dependent transfer function. Many efforts have been focussed on this partly nonlinear time domain method. Gu et al. (1989) presented a time domain formulation of hydrodynamic loading that considered the nonlinear effect of the symmetric motion of a ship as an elastic structure. The impulse response function calculation relies on the frequency domain coefficients at mean draught. The momentum slamming force, nonlinear hydrostatic force and bottom impact slamming force were included. The Hamiltonian method was applied with a predictor-corrector method to solve the equation of motion. The approach was extended to a three-dimensional time-domain free surface potential flow method, which had been simplified to the slender body theory for application to the vertical global response of ships in order to reduce computational burden (Xia and Wang 1997). The program (THEAS) includes nonlinearities of the instantaneous hydrostatic force and nonlinear hydrodynamic force according to the momentum slamming theory. A rational expression of the higher order ordinary differential equation for the hydrodynamic memory effect was presented by Xia et al (SHIPSTAR, 1998), based on Sőding's (1982) proposal. In this method the nonlinear memory effect and the momentum slamming force are included and the hydrodynamic inertial and restoring forces are estimated over the instantaneous draught. They concluded, comparing numerical results for the S175 container ship with the results by the program THEAS and experiments, that including only nonlinearities of the momentum slamming for and restoring force is not enough for accurate prediction of vertical ship motions and wave loads.

Fonseca and Guedes Soares (1998) presented a non-linear time domain strip theory code (IST) employing convolution integral formulation for radiation related actions, related to the mean wetted surface. The diffraction excitation forces are assumed to be linear at the mean draught and calculated using the STF strip theory approach.

The non-linear hydrostatic restoring force and the Froude-Krylov force are calculated over the instantaneous wetted hull surface.

Watanabe and Guedes Soares (1999) presented comparative calculations for the S175 container ship with six different simplified nonlinear codes. In general, most of the results by each code agree with each other and with linear theory within 10% for low wave heights. At large amplitude waves, however, a significant variation is observed. They specified the main features of the methods, which make it easy to compare the assumptions in various codes: (1) elastic hull, (2) nonlinear motion, (3) nonlinear hydrostatic, (4) nonlinear Froude-Krylov force, (5) nonlinear added mass and damping, (6) relative motion concept, (7) Smith correction, (8) linear and nonlinear diffraction excitation forces, (10) free surface memory effect, (11) slamming loads by bottom slamming, (12) slamming loads by momentum slamming and (13) green water load.

The work was continued by the ISSC 2000 special task committee (ISSC 2000). The conclusion of the comparative results between measured and calculated wave bending moments is that the various nonlinear strip theory formulations in general are able to predict the magnitude and trend (hogging and sagging ratios) with reasonable accuracy in the engineering sense. However, the responses for higher order harmonics have a large scatter. This is largely because of the different approximations used to treat the non-linearities. It was, therefore, suggested to estimate carefully the different hydrodynamic coefficients and integration procedure as well as to check for possible input error. Some details of the various nonlinear strip theory methods used shown in Table 1.1..

Table 1.1 Nonlinear strip methods

Method	SOST Jensen and Pedersen 1979	THEAS Xia and Wang 1997	SHIPSTAR Xia et al. 1998	IST Fonseca and Guedes Soares 1998
Nonlinear restoring force and Froude-Krylov force	Yes	Yes	Yes	Yes
Relative motion concept	Yes	Yes	Yes	No
Nonlinear hydrodynamic coefficients	Yes	No	Yes	No
Momentum slamming	Yes	Yes	Yes	No
Green water	No	No	Yes	Yes
Steady state forward speed potential	No	No	No	No
Degree of freedom	Vertical, elastic	Vertical, elastic	Vertical, elastic	Vertical, rigid

Wu and Moan (1996) presented a practical nonlinear hydroelastic time-domain simulation method, in which the total response is divided into linear and nonlinear components. The linear part is evaluated using linear potential flow theory (high speed strip theory based on Faltinsen and Zhao's (1991) study and the nonlinear part comes from the convolution of the impulse response functions of the linear ship-fluid system and the nonlinear hydrodynamic forces based on a momentum force expression (Faltinsen 1990). They divided the nonlinear force into the momentum slamming force, nonlinear modifications of added mass/damping, and the Froude-Krylov and hydrostatic restoring force related to the current draught. Bottom impact slamming was not included. They performed a parametric study for four high speed ships of different length, in irregular waves, but similar body plan with respect to the extreme values of midship bending moment. They concluded that the nonlinear influence in high speed vessels is more remarkable at large Froude numbers,

important even in moderate sea state, and that hydrodynamic damping come from forward speed plays a leading role in higher modes of hull vibration. The nonlinear time domain simulation method was applied to the S175 container ship (Wu and Hermunstad 2002). The parametric study of the nonlinear force terms showed that the modification to the added mass/damping terms gave worse results for motions but better results for sagging/hogging bending moments in comparison with experiments. A time history depicted that a slamming impact produces a large sagging peak and high frequency whipping responses. They also calculated long-term vertical sagging moments and hogging moments amidships in a 20-hour time-domain simulation, and the results were comparable to those obtained from Classification Society rules.

1.3.2 Three-dimensional method

Though the strip theory has so far been successful in predicting wave-induced motions and loads for conventional ships, it has its limitations. In order to overcome the shortcoming of the strip theory, three-dimensional methods have been developed. The three-dimensional solution is mainly based on the boundary integral equation method and the velocity potentials (or source strengths) can be solved either in the frequency domain or the time domain. Generally there are two ways to solve the three-dimensional potential flow problem: the Green function method and the Rankine source method.

In the Green function method, the singularities are located on the discretized wetted hull surface, which satisfies the mean free surface condition, the Laplace equation and the radiation condition. Various methods for determining a velocity potential are developed in order to improve accuracy and increase computational power. Inglis

and Price (1980, 1981) used the Green function for the pulsating and translating-pulsating source to predict rigid body motion at forward speed in regular waves. They presented comparisons with experiments and strip theory for a Series 60 model (Inglis and Price 1982). The pulsating source distribution method gives mixed improvement over strip theory predictions. The translating-pulsating source distribution method gives improved result; however it causes computational complexity and large computing time which require efficient numerical scheme. In this respect, one of the best numerical schemes is the proposal by Du et al. (1999).

In order to examine the fluid-structure interaction behaviour of non-beam like floating bodies, Bishop et al. (1986) present a linear three-dimensional hydroelastic theory using the three-dimensional Green function and a finite element approach. Hirdaris et al. (2003) applied the two- and three-dimensional hydroelasticity theories (finite element idealisations combined potential flow analysis based on pulsating source distribution over the mean wetted surface) to a bulk carrier. They showed that the predicted symmetric dynamic responses obtained from two- and three-dimensional modes were in good agreement, however, differences were observed for anit-symmetric dynamic characteristics.

The time domain Green function is solved at each time step using convolution of the solution for the previous time. The LAMP software (Lin et al. 1993) is an example of this method. LAMP-4 is a nonlinear three-dimensional time domain method accounting for the exact wetted surface of the hull body when calculating hydrodynamic data at each time step. The nonlinear hydrostatic restoring and Froude-Krylov wave forces are calculated. LAMP-2 is a partly nonlinear three dimensional time domain method satisfying the free surface boundary condition on the mean wave surface. LAMP-2 is the same as LAMP-1, except that it calculates the

linear hydrostatic restoring and Froude-Krylov wave force. Actually, the LAMP software implements a hybrid numerical approach, which is a combination of the transient Green function in the outer domain and the Rankine source in the inner domain (Weems et al. 1998). Application results using the LAMP system for the S175 container ship are presented by Shin et al (1997). As the results, LAMP-2 predicted larger heave responses than the LAMP-4 results, while for the pitch responses there is good agreement between LAMP-2 and LAMP-4. The nonlinear effect of amidships bending moment (hogging/sagging) predicted by LAMP-2 is smaller than those by LAMP-4 and the trend was very much same.

The alternative method is the Rankine source method. The Rankine source method, in theory, is applicable whether linear or nonlinear free-surface boundary conditions are applied, and uses a simple Green function. As the Rankine source method does not satisfy the radiation condition, stability in both space and time may cause a problem. The SWAN system is an example of the application of the method (Sclavounos et al. 1997). SWAN-1 (Nakos and Sclavounos, 1990) is a frequency domain formulation, while SWAN-2 (Nakos et al. 1993, Huang and Sclavounos 1998) is solved in the time domain. Huang and Sclavounos (1998) developed nonlinear method based on the Weak-scatter hypothesis, which systematically accounted for hydrostatic and hydrodynamic nonlinearities. Comparing the calculation results by quasi-nonlinear method (Nakos et al. 1993) for a Series 60 hull and a S175 hull, they concluded that the hydrodynamic nonlinearities were to be as important as, if not more than, the hydrostatic and Froude-Krylov nonlinearities.

1.3.3 Transient loads

Transient response analysis concerning the bottom slamming and green water effect has to be calculated in the time domain. In the linear system, the calculation result in the frequency domain can easily be transferred to time sequences using a relevant method, such as Fourier transform. Determination of the transient response required suitable models for excitation due to slamming and green water. Bottom impact slamming is a three-dimensional phenomenon and occurs over a very short time. When a body enters the water, there is an air-gap between the body and water surface, which reduces the slamming impact force. It is well known that the slamming force is proportional to velocity squared and a function of body geometry. The distribution of slamming force in space and time is complicated to evaluate, which makes the problem difficult. Therefore, some empirical formulae for the slamming were suggested and applied.

Ochi and Motter (1971) suggested the empirical non-dimensional slamming pressure factor for Wagner's (1932) model depending on the section shape, using a seakeeping test and a drop test. The sectional coefficients are determined using the conformal mapping technique and the sectional distribution of the local pressure is assumed to be linear from maximum value at bottom to zero at the effective area level (i.e. one tenth of draught). Stavovy and Chuang (1976) suggested an empirical slamming pressure by regression analysis of measured data from drop tests as a function of deadrise angle. They also assumed the local pressure distribution as linear.

A time domain mathematical model with convolution integral formulation can consider fluid memory effects on ship response to arbitrary excitation such as transient slamming. Bishop et al. (1978b) devised a linear method to estimate

slamming responses. The slamming responses for sinusoidal waves were obtained by superimposing on the steady-state responses induced by the waves in the manner discussed by Bishop et al. (1978b). They identified two distinct ways of slamming. The first method, so-called 'impact slamming' (Ochi and Motter, 1971, Stavovy and Chuang, 1976), evaluates the forces at the instant when the hull strikes the free surface of the waves. The second method, so-called 'momentum slamming' (Leibowitz 1963), describes the effect of pressure variations around the hull surface as it penetrates the moving fluid after the initial entry. They discussed two distinct issues: One is that the hull vibrates due to slamming while the bow is deeply immersed or emerged above the mean water line; another is that the constants of hydrodynamic coefficients for added mass and damping (**A**, **B)** are, in general, frequency dependent, but treated as constant. Belik et al. (1987) considered the rate of change of fluid momentum (Leibowitz 1963) and additional flare buoyancy when bow sections plunge into/re-emerge from the water before the sea surface reaches the still water draught (flare slamming). The total transient excitation consists of impact (Ochi and Motter, 1971, Stavovy and Chuang, 1976) and momentum slamming. The results show that the flare slamming effect is important for large flared ships. Aksu et al. (1995) carried out probability analysis using time simulation results. Both hydroelasticity investigations are based on linear strip method, representation of irregular waves by a combination of a large number of regular waves.

Kaplan (1987) presented the analytical/computational determination of the slamming forces arising from flat bottom impacts on the water surface of ships advancing in waves. In this work, the concepts of fluid momentum theory, with a three-dimensional model rather than the conventional two-dimensional strip theory methods, are applied to the impact problems of a flat surface.

Zhao and Faltinsen (1993) presented a numerical method for studying water entry of a two-dimensional body of arbitrary cross-section using a nonlinear boundary element method with a jet flow approximation. This method was verified by comparison with similarity theoretical solution of water entry wedges derived by Dobrovol'skaya (1969) and Wagner's (1932) model for small dead rise angle.

Kvålsvold and Faltinsen (1995) presented a theoretical and numerical slamming model for the wet deck of a multi-hulled vessel. The disturbance of the wetted surface as well as the local hydroelastic effects in the slamming area were accounted for. The elastic deflections of the wet deck, modelled as a beam, are expressed in terms of 'dry' normal modes. The structural deformation of beam model accounts for the shear deformations and the rotary inertia effects. The results indicated that an important effect arises from the body boundary condition as an angle of attack effect. The maximum bending moment stress was proportional to curvature of the wave crest in the impact region. Both theory and drop test results did not predict the maximum pressure deterministically; however, the bending stresses and deflections agree with each other.

Ramos et al. (2000) compared the empirical formulae for the slamming forces described above and proposed a simple formula for sectional distributions of the slam force. The study showed that Ochi and Motter's (1971) formula gave a slightly smaller slamming force, whilst other empirical formulae showed good agreement.

Storhaug et al. (2003) measured global vibrations in terms of whipping and springing of a large ocean-going ship, using the DNV structural monitoring system. From the measurements it became apparent that a possible cause of vibration may be stern slamming (bottom slams are rare); hence, small impacts and low damping may cause

the springing. The predicted wave frequency results are in fairly good agreement with measurement, while, for high frequency, the results do not capture the measured trend.

Buchner (1995) presented the green water phenomena based on model tests with a frigate. He indicated that the rate of change of water height on the deck has an important effect on the maximum deck pressure as well as static load and an inertia load for vertical acceleration. The calculations showed good agreement with the measurements. Buchner's approach is widely accepted for modelling the effects of green water on the global wave-induced vertical bending moment, as shown by Wang et al. (1998) and Jensen and Mansour (2003).

Chapter 2

Theoretical Background

2.1 Equations of motion

The equilibrium coordinate system for a ship advancing at constant mean forward speed U is defined such that the origin is at the stern in the x-direction (positive to bow). The z-axis is upward positive and y is positive to port. The x-z plane coincides with the central plane of the ship and x-y plane is at the mean waterline.

The beam model for the global vibration of the ship hull gives good accuracy for mono-hulled vessels. The hull is assumed to behave as a Timoshenko beam with the assumption that the angle between the neutral axis and the normal of the cross section is proportional to the shear force. It includes the effects of shear deflection and rotational inertia as can be seen in Equations 2.1 to 2.3.

The equations of symmetric flexural motion of the Timoshenko beam are as follows (Bishop and Price 1979) :

$$\mu(x)\ddot{w}(x,t) - [kAG(x)\{\gamma(x,t) + \alpha(x)\dot{\gamma}(x,t)\}]' = F(x,t) \tag{2.1}$$

$$\begin{aligned} I_y(x)\ddot{\theta}(x,t) - [EI(x)\{\theta'(x,t) + \beta(x)\dot{\theta}'(x,t)\}]' \\ - kAG(x)[\gamma(x,t) + \alpha(x)\dot{\gamma}(x,t)] = 0 \end{aligned} \tag{2.2}$$

$$w'(x,t) = \theta(x,t) + \gamma(x,t) \tag{2.3}$$

where, $F(x,t)$ is the vertical force due to hull weight and fluid action

$\mu(x)$ is the mass per unit length

$\alpha(x)$ and $\beta(x)$ are the distributed shear and bending damping respectively

$\theta(x,t)$ is the angle due to bending

$\gamma(x,t)$ is the shear strain

$w(x,t)$ is the vertical displacement

$I_y(x)$ is the rotary inertia

$EI(x)$ is the flexural rigidity

$kAG(x)$ is the shear rigidity.

The normal-coordinate transformation, which serves to change the set of N coupled equations of motion of the N-DOF (Degrees Of Freedom) system into a set of *N* uncoupled equations, is the basis of the mode-superposition method of dynamic analysis. This method can be used to evaluate the dynamic response of any linear structure for which the displacement has been expressed in terms of a set of N principal coordinates and where the structural damping can be expressed by modal damping ratios (see Equation 2.9)

The modal superposition of the vertical displacement with respect to the r^{th} principal coordinate $p_r(t)$ is written in the form

$$w(x,t) = \sum_{r=0}^{N} w_r(x)\, p_r(t) \qquad (2.4)$$

where, w_r is the modal shape function comprising rigid (r = 0,1) and flexible (r = 2, … , N) mode shapes. The natural frequencies ω_r and corresponding principal mode shapes are obtained from "dry" or in vacuo analysis carried out in the absence of structure damping and external force (see Section 3.1).

The equation of motion for the ship hull can be written as:

$$\sum_{r=0}^{N}[a_{rs}\ddot{p}_r(t)+b_{rs}\dot{p}_r(t)+c_{rs}\ddot{p}_r(t)]=\int_L F_s(x,t)w_s dx\,,\ \text{s = 0, 1, 2, …, N} \quad (2.5)$$

where, $a_{rs,}$ b_{rs}*and* c_{rs} denote the generalised mass, damping and stiffness, respectively, given by (Bishop and Price 1979)

$$a_{rs}=\int_L(\mu w_r w_s+I_y\theta_r\theta_s)dx \quad (2.6)$$

$$b_{rs}=(\alpha_{rs}+\beta_{rs})=\int_L \alpha kAG\gamma_r\gamma_s dx+\int_L \beta EI\theta_r'\theta_s' dx \quad (2.7)$$

$$c_{rs}=\int_L[EI\theta_r'\theta_s'+kAG\gamma_r\gamma_s]dx\,. \quad (2.8)$$

Structure damping, as expressed by Equation 2.7, is difficult to estimate. Bishop and Price (1979) adopted a more simplified and practical way for inclusion of structure damping, namely

$$b_{rr}=2\nu_r\omega_r a_{rr},\quad r=2,3,\ldots N. \quad (2.9)$$

The modal bending moment is expressed:

$$M_r(x)=EI(x)\theta_r' \quad (2.10)$$

and the modal shearing force is:

$$V_r(x)=kAG(x)\gamma_r\,. \quad (2.11)$$

The generalized force F_s in Equation 2.5 comprises the hull weight due to gravity, the hydrostatic force and the hydrodynamic force. The hydrostatic force in still water is not considered because this force is equal to the weight of the ship and acts in the opposite direction. In order to estimate the hydrodynamic forces, there are various methods and assumptions. This study focusses on the vertical forces based on the strip theory and the nonlinearities due to large amplitude motions.

Having found the principal coordinates, the shear force V(x,t) and the bending moment M(x,t) can be obtained, using modal superposition, as:

$$V(x,t)=\sum_{r=2}^{N}V_r(x)p_r(t) \quad (2.12)$$

$$M(x,t) = \sum_{r=2}^{N} M_r(x) p_r(t) . \tag{2.13}$$

2.2 Strip theory

The present method mainly focusses on the loads which are important in the hull girder structural analysis for mono-hulled vessels so that strip theory formulation for vertical ship motion is applied. Conventionally the hydrodynamic force is divided into two terms. One is the Froude-Krylov force, which is based on integration of the undisturbed wave-induced pressure over the wetted hull surface. The second term is the interaction between the hull surface and the fluid, which is named the hydrodynamic force in the broad sense (i.e. diffraction and radiation force).

The linear part of the present theory follows conventional linear strip theory (Salvesen, Tuck and Faltinsen, 1970) and the nonlinear effects are incorporated into the linear system in the time domain analysis, as described in Section 2.3.

2.2.1 Velocity potential and wave theory

For the ideal fluid, a velocity potential ϕ is defined. Assuming the disturbance of the steady fluid field by the ship can be ignored and the incident wave and the resulting motions are small, the velocity potential can be decomposed in the form

$$\phi = \phi_I + \phi_D + \sum_{j=1}^{6} \phi_j e^{i\omega_e t} \tag{2.14}$$

where ϕ_I is the incident wave potential, ϕ_D is the diffraction potential and ϕ_j is the contribution to the velocity potential from the jth mode of ship motion. Each velocity potential satisfies Laplace's equation and the radiation condition at infinity.

Assuming that the wave elevation is sufficiently small and ignoring the second order terms in the fluid velocity, the linearised free surface conditions for the velocity potential is written as:

$$\frac{\partial^2 \phi}{\partial t^2} + g\frac{\partial \phi}{\partial z} = 0 \text{, on } \; z = 0 . \tag{2.15}$$

The global coordinates XYZ are fixed so that Z is the vertical coordinate (positive out of water) and XY plane is in the mean waterline (X is positive to bow and Y is positive to port). Considering two-dimensional (long-crested) waves traveling in the X-direction in infinite water depth, the velocity potential becomes (Jensen 2001)

$$\phi_I(X,Z,t) = -\frac{iga}{\omega} e^{kZ} e^{i(kX-\omega t)} \tag{2.16}$$

and the corresponding wave elevation is

$$\zeta(X,Z,t) = ae^{i(kX-\omega t)} \tag{2.17}$$

where *a* is the wave amplitude.

The pressure is obtained using Bernoulli's equation. Omitting the higher order terms in Bernoulli's equation, the first order pressure is

$$p(X,Z,t) = p_a - \rho gZ - \rho\frac{\partial \phi_I}{\partial t} = p_a - \rho gZ + \rho gae^{kZ} e^{i(kX-\omega t)} \; .$$

$$= p_a - \rho gZ + \rho g e^{kZ}\zeta(X,Z,t) \tag{2.18}$$

2.2.2 Hydrostatic Froude-Krylov force

When a ship moves ahead with a steady velocity U in the direction of the global coordinate axis X, the wave elevation of Equation 2.17 can be represented in the equilibrium coordinate system as (Bishop and Price 1979)

$$\zeta = ae^{i(kx\cos\chi + ky\sin\chi - \omega_e t)}, \quad \text{for} \;\; \chi = 180°, \;\; \zeta(x,t) = ae^{-i(kx+\omega_e t)} \tag{2.19}$$

where χ is heading angle, the wave number $k = \omega^2 / g$ and the encounter frequency $\omega_e = \omega - kU\cos\chi$.

Ignoring the interaction between the hull surface and the waves, the hydrodynamic force on the ship can be obtained by integration of the undisturbed pressure p in the incident waves over the instantaneous wetted surface *S* as

$$F_I = -\iint_S p\vec{n}dS \tag{2.20}$$

where the pressure p is defined by Equation 2.18 and $\vec{n}$ is the vector normal to the hull surface.

The sectional force due to the dynamic pressure is obtained in the equilibrium coordinate system as (Jensen 2001, see Appendix 1 for the details)

$$F_I = \rho g \int_0^{\zeta - w} B(x,z)dz - \rho g k \zeta \int_{-T}^{\zeta - w} e^{k(z+w)} B(x,z)dz\,. \tag{2.21}$$

Assuming that the wave elevation and hull displacement are small and the breadth does not vary near a mean draught, the linear sectional force can be approximated as:

$$\begin{aligned} F_{I,lin} &= \rho g B_o(x)(\zeta - w) - \rho g k \zeta \int_{-T}^{0} e^{kz} B(x,z)dz \\ &= -\rho g B_o(x) w + \rho g B_o(x)\zeta \left(1 - k\int_{-T}^{0} e^{kz}\frac{B(x,z)}{B_o(x)}dz\right) \\ &= -\rho g B_o(x) w + \rho g B_o(x)\kappa\zeta\,, \end{aligned} \tag{2.22}$$

where $B_o(x)$ is the breadth at the mean draught and κ is the Smith correction factor defined as:

$$\kappa = 1 - k\int_{-T}^{0} e^{kz}\frac{B(x,z)}{B_o(x)}dz\,. \tag{2.23}$$

Here the first term of Equation 2.22 is called the fluid restoring force, and the second term is the linear Froude-Krylov force.

It is convenient to express the linear Froude-Krylov force using the equivalent draught for Smith correction, simplifying the calculation without the integration of the exponential function (Bishop and Price 1979). That is

$$F_{FK} = \rho g B_o(x)\kappa\zeta = \rho g B_o(x)\bar{\zeta} = \rho g B_o(x)e^{-k\bar{T}}\zeta \tag{2.24}$$

where $\bar{\zeta}(x,t)$ is the wave elevation with the Smith correction and the equivalent draught for Smith correction ($\bar{T}$) is defined as:

$$\bar{T} = \frac{1}{k}\ln(\kappa) = \frac{1}{k}\ln\left(1 - k\int_{-T}^{0} e^{kz}\frac{B(x,z)}{B_o(x)}dz\right). \tag{2.25}$$

The nonlinear Froude-Krylov and fluid restoring force (F_4) associated with the instantaneous wetted hull surface is defined by subtracting the linear Froude-Krylov force in Equation 2.22 from Equation 2.21 as:

$$\begin{aligned} F_4 &= F_I - F_{I,lin} \\ &= \rho g\int_{0}^{\zeta-w} B(x,z)dz - \rho g k\zeta\int_{-T}^{\zeta-w} e^{k(z+w)}B(x,z)dz + \rho g B_o(x)(w-\bar{\zeta}) \end{aligned}. \tag{2.26}$$

2.2.3 Hydrodynamic force

The relative motion between the ship and wave surface is used in strip theory and the relative displacement is expressed as:

$$z_{rel}(x,t) = w(x,t) - \bar{\zeta}(x,t) \tag{2.27}$$

where *w(x,t)* is the upward displacement of the section of the hull and $\bar{\zeta}$ is the equivalent wave elevation including the Smith correction.

As described in Equations 2.19 and 2.24, the wave elevation with the Smith correction is presented as

$$\bar{\zeta}(x,t) = ae^{k\bar{T}}e^{-i(kx+\omega_e t)}. \tag{2.28}$$

When the relative motion concept with the Smith correction is introduced, the body boundary condition of the diffraction potential can be treated as that of a radiation potential, using the total derivatives of the equivalent wave elevation, $D\bar{\zeta}/Dt$. Then the diffraction field can be solved together with the radiation field as a disturbance field with the velocity of the ship section (Wu 1994).

The vertical hydrodynamic force per unit length using the linear strip theory (Salvesen et al. 1970) can be expressed in the form (Bishop and Price 1979)

$$F(x,\omega_e) = -\frac{D}{Dt}\left[\left\{m(x,\omega_e) + \frac{i}{\omega_e}N(x,\omega_e)\right\}\frac{Dz_{rel}}{Dt}\right] \tag{2.29}$$

In this expression, $m(x,\omega_e)$ is the sectional added mass, $N(x,\omega_e)$ is the sectional fluid damping and the operator D/Dt is the total derivative with respect to time: that is

$$\frac{D}{Dt} = \frac{\partial}{\partial t} + \frac{\partial}{\partial x}\frac{dx}{dt} = \frac{\partial}{\partial t} - U\frac{\partial}{\partial x}. \tag{2.30}$$

2.3 Hydroelastic equation for large amplitude motion

The Froude-Krylov force, the fluid restoring force and the hydrodynamic force (i.e. the radiation and diffraction force) were defined in Section 2.2. The Froude-Krylov force was derived at the instantaneous draught as shown in Equation 2.21. However, the radiation and diffraction force in Equation 2.29 were derived under the assumption of linear strip theory using the mean draught. In order to consider the nonlinearities, such as the effects of flared sections, bottom slamming, or green water on deck, a simplified two-dimensional method for the nonlinear hydroelastic response of a ship experiencing large amplitude motions is suggested with the following assumptions:

- The nonlinearities arise from the large ship motions of heave and pitch.

- Structural deformation remains small; namely the structure behaviour is in the range of linear stress-strain relations, so that the linear hydroelastic theory, with Timoshenko beam model, is applicable.
- Incident waves can be described sufficiently by linear wave theory
- The memory effect of free surface is treated through a linear method.

Figure 2.1 shows the relevant characteristics of travelling waves over a sea bottom. According to this figure, in deep sea, sinusoidal waves may be used only when the wave height-length ratio (H/λ) are less than 0.01. Linear wave theory is adopted to represent wave motion in this study, because the responses to irregular waves are expressed by superposition of many different components of sinusoidal waves of differing frequencies without interaction between them. However, a higher order wave model, such as Stokes' waves, may be worth considering for application in motion and wave load analysis in one wave.

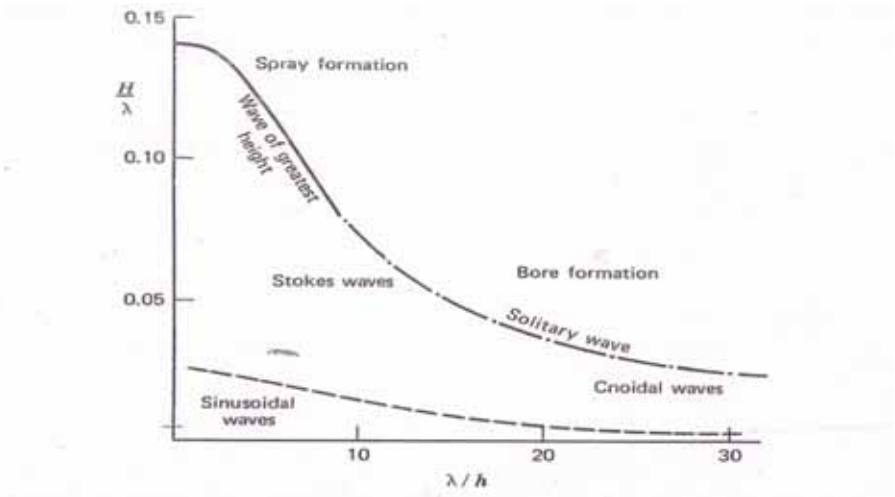

Figure 2.1 Schematic indication of periodic waves travelling over a horizontal sea bottom; h is water depth; H is wave height; λ is wave length (Hooft, J.P, 1982)

When a ship motion is of large amplitude, added mass and damping coefficients are dependent on the wetted hull surface and vary according to instantaneous draught. In the method presented in the thesis, hydrodynamic forces are calculated using the strip

theory, which includes nonlinearities considering the variation of the hydrodynamic coefficients in the time domain. The coordinate system is the same as in the linear analysis.

Considering the time variation of the ship's wetted surface, including that of hydrodynamic coefficients, total vertical fluid force acting on a strip can be written as in Equations 2.21 (non-linear Froude-Krylov and hydrostatic) and 2.29 (linear hydrodynamic)

$$F(x,t) = -\frac{D}{Dt}\left[\left\{m(x,\omega_e,t) + \frac{i}{\omega_e}N(x,\omega_e,t)\right\}\frac{Dz_{rel}}{Dt}\right] + \rho g \int_0^{\zeta - w} B(x,z)dz - \rho g k \zeta \int_{-T}^{\zeta - w} e^{k(z+w)} B(x,z)dz \tag{2.31}$$

where now the hydrodynamic coefficients have time dependence and the relative displacement z_{rel} is defined in Equation 2.35.

The hydrodynamic coefficients are decomposed into linear and nonlinear parts as:

$$m(x,\omega_e,t) = m_o(x,\omega_e) + m_{nl}(z_{rel};x,\omega_e,t) \tag{2.32}$$

$$N(x,\omega_e,t) = N_o(x,\omega_e) + N_{nl}(z_{rel};x,,\omega_e t) \tag{2.33}$$

where the index "o" denotes the coefficients at mean water line and the index "nl" the influence of nonlinearities.

Decomposing the total vertical displacement $w(t)$ also into linear and non-linear parts,

$$w(t) = w_l(t) + w_{nl}(t), \tag{2.34}$$

then the relative vertical displacement of the ship becomes

$$z_{rel}(x,t) = z_{ro}(x,t) + w_{nl}(x,t), \quad z_{ro}(x,t) = w_l - \overline{\zeta}. \tag{2.35}$$

It can be seen that z_{ro} is the same expression as the linear relative displacement given by Equation 2.27.

Substituting Equations 2.32 to 2.35 into Equation 2.31, the vertical fluid force on the hull section is obtained as

$$F(x,t) = F_l(x,t) + H_{nl}(x,t) + F_{nl}(x,t) \tag{2.36}$$

where

$$F_l(x,t) = -\frac{D}{Dt}\left[\left\{m_o(x,\omega_e) + \frac{i}{\omega_e}N_o(x,\omega_e)\right\}\frac{Dz_{ro}}{Dt}\right] - \rho g B_o z_{ro}\,, \tag{2.37}$$

$$H_{nl}(x,t) = -\frac{D}{Dt}\left[\left\{m_o(x,\omega_e) + \frac{i}{\omega_e}N_o(x,\omega_e)\right\}\frac{Dw_{nl}}{Dt}\right] - \rho g B_o w_{nl}\,, \tag{2.38}$$

and

$$F_{nl}(x,t) = -\frac{D}{Dt}\left[\left\{m_{nl}(z_{rel};x,\omega_e,t) + \frac{i}{\omega_e}N_{nl}(z_{rel};x,\omega_e,t)\right\}\frac{Dz_r}{Dt}\right] + \rho g\int_0^{\zeta-w} B(x,z)dz - \rho g k\zeta\int_{-T}^{\zeta-w} e^{k(z+w)}B(x,z)dz + \rho g B_o z_{rel}\,. \tag{2.39}$$

As can be seen the linear force, defined by Equation 2.44, is the same as the forces given in the previous section for linear Froude-Krylov and hydrostatic (Equation 2.22) and linear hydrodynamic forces (Equation 2.29).

In the same manner, decomposing the principal coordinates $p(t)$ into linear and non-linear parts

$$p(t) = p_l(t) + p_{nl}(t)\,. \tag{2.40}$$

From Equations 2.5 and 2.36, the governing equation of nonlinear hydroelasticity is composed of linear and nonlinear parts in matrix form:

$$[a]\{\ddot{p}_l(t)\} + [b]\{\dot{p}_l(t)\} + [c]\{p_l(t)\} = \{F_l(t)\} \tag{2.41}$$

$$[a]\{\ddot{p}_{nl}(t)\} + [b]\{\dot{p}_{nl}(t)\} + [c]\{p_{nl}(t)\} = \{H_{nl}(t)\} + \{F_{nl}(t)\}\,. \tag{2.42}$$

Here, Equation 2.41 describes the equation of motion for linear analysis, while Equation 2.42 is the equation of motion for the nonlinear contributions. The

generalised force is obtained by multiplying the mode shapes and integrating along the ship length (Bishop and Price 1979). That is to say:

$$F(t) = \int_L w_r(x) F(x,t) dx \tag{2.43}$$

When the radiation force and fluid restoring force in Equations 2.41 and 2.42 are moved to the left hand side, the linear and nonlinear hydroelastic equations of motion can be expressed by: (see Appendix 2 for the details)

$$\left[a + A(\omega_e)\right]\left\{\ddot{p}_l(t)\right\} + \left[b + B(\omega_e)\right]\left\{\dot{p}_l(t)\right\} + \left[c + C\right]\left\{p_l(t)\right\} = \left\{F_w(t)\right\} \tag{2.44}$$

$$\left[a + A(\omega_e)\right]\left\{\ddot{p}_{nl}(t)\right\} + \left[b + B(\omega_e)\right]\left\{\dot{p}_{nl}(t)\right\} + \left[c + C\right]\left\{p_{nl}(t)\right\} = \left\{F_{nl}(t)\right\} \tag{2.45}$$

where $\left[A(\omega_e)\right]$, $\left[B(\omega_e)\right]$and $\left[C\right]$ represent the generalized linear fluid added mass, damping and restoring coefficients matrix. $\left[A(\omega_e)\right]$ and $\left[B(\omega_e)\right]$ are frequency dependent coefficients and represent the hydrodynamic pressure over the mean wetted surface of the hull section.

The sectional nonlinear force discussed in Equation 2.39 is composed of four force components as: (see Appendix 3 for the details)

$$F_{nl}(x,t) = F_1(x,t) + F_2(x,t) + F_3(x,t) + F_4(x,t) \tag{2.46}$$

where

$$F_1(x,t) = -\frac{\partial m_{nl}(z_{rel}; x, \omega_e, t)}{\partial t}\frac{Dz_{rel}}{Dt} - \frac{i}{\omega_e}\frac{\partial N_{nl}(z_{rel}; x, \omega_e, t)}{\partial t}\frac{Dz_{rel}(x,t)}{Dt} \tag{2.47}$$

$$F_2(x,t) = -m_{nl}(z_{rel}; x, \omega_e, t)\frac{D^2 z_{rel}(x,t)}{Dt^2} + U\frac{\partial m_{nl}(z_{rel}; x, \omega_e, t)}{\partial x}\frac{Dz_{rel}(x,t)}{Dt} \tag{2.48}$$

$$F_3(x,t) = -\frac{i}{\omega_e} N_{nl}(z_{rel}; x, \omega_e, t)\frac{D^2 z_{rel}}{Dt^2} + \frac{i}{\omega_e} U\frac{\partial N_{nl}(z_{rel}; x, \omega_e, t)}{\partial x}\frac{Dz_{rel}}{Dt} \tag{2.49}$$

$$F_4(x,t) = \rho g \int_0^{\zeta - w} B(x,z) dz - \rho g k \zeta \int_{-T}^{\zeta - w} e^{k(z+w)} B(x,z) dz + \rho g B_o(x) z_{rel} \tag{2.50}$$

Here F_1 is the so-called flare slamming force, which is the time rate of added mass and is widely used in nonlinear modifications (Belik et al 1980, Xia et al. 1998). F_4 is the nonlinear modification in the Froude-Krylov force and hydrostatic restoring forces (Domnisoru and Domnisoru 1997), which is usually included (Wu et al. 2002), Gu et al. 2003) in the form of.

$$F_4(x,t) = \rho g \left\{ A(x,t) - A_o(x) \right\} + \rho g B_o(x) z_{rel}(x,t) \tag{2.51}$$

where A and A_o are the submerged areas at the instantaneous and mean draughts respectively.

F_2 and F_3 are the nonlinear modifications in the radiation and diffraction forces corresponding to added mass and damping, respectively, which are not considered in many cases. For example, Domnisoru and Domnisoru (1997) included the damping terms, while Wu et al. (2002) consider only the added mass at infinite frequency.

The flare slamming force (F_1) in Equation 2.47 only acts during downward motion (i.e. when $Dz_{rel}(x,t)/Dt < 0$) and caters well for so-called bow flare slamming, which is dominant in ships with a large bow flare. In such cases, the fluid will be accelerated in a very short period (proportional to the square of the section's relative velocity) and the added mass and its derivatives can be determined at $\omega_e \to \infty$. This mechanism can also be applied to the second term of Equation 2.47, the rate of damping coefficient. It can be determined at $\omega_e \to \infty$ but will be omitted (Gu et al, 2003).

The following equations are satisfied for the instantaneous draft T(x,t)

$$T(x,t) = T_o(x) - z_{rel}(x,t) \quad \text{and} \quad \frac{\partial T(x,t)}{\partial t} = -\frac{\partial z_{rel}(x,t)}{\partial t}, \tag{2.52}$$

where *To(x)* is mean draught of sections, and

$$\frac{\partial m_{nl}(x,t)}{\partial t}\frac{Dz_{rel}(x,t)}{Dt} = -\frac{\partial m_{nl}(x,t)}{\partial T}\frac{\partial z_{rel}(x,t)}{\partial t}\frac{Dz_{rel}(x,t)}{Dt}. \tag{2.53}$$

Then, the flare slamming force of Equation 2.47 can be expressed as

$$F_1(x,t) = \frac{\partial m_{nl}(z_r;x,\infty)}{\partial T}\frac{\partial z_{rel}(x,t)}{\partial t}\frac{Dz_{rel}(x,t)}{Dt}. \tag{2.54}$$

The flare slamming force is suitable for the entire slamming process from the bottom to the weather deck of the ship. A differentiation method is used to calculate $\partial m/\partial T$. Bottom flatness with small deadrise angle make it difficult to accurately calculate the hydrodynamic coefficient and its variation with draught, $\partial m/\partial T$. Actually, when a hull section with a nearly flat bottom impinges the compressibility of fluid, consideration of the effects of air cushion and pile-up of water may be necessary. This is a very complicated problem. So, an empirical formula is widely used for bottom slamming (see Section 2.4.2). In the present study, the slamming forces are separated into bottom impact slamming and flare slamming. Bottom impact slamming is assumed to be dominant in the range between the hull bottom to 0.1 draught while flare slamming works above 0.1 draught.

The total derivatives in Equations 2.47 to 2.49 can be written in terms of the estimated responses (principal coordinate and its derivatives) as

$$z_{rel} = \sum_{r=0}^{N} w_r(x)\,p_r(t) - \bar{\zeta}(x,t), \tag{2.55}$$

$$\frac{Dz_{rel}}{Dt} = \sum_{r=0}^{N} w_r(x)\,\dot{p}_r(t) - \dot{\bar{\zeta}}(x,t) - U\left[\sum_{r=0}^{N} w_r'(x)\,p_r(t) - \bar{\zeta}'(x,t)\right], \tag{2.56}$$

$$\frac{D^2 z_{rel}}{Dt^2} = \sum_{r=0}^{N} w_r(x)\,\ddot{p}_r(t) - \ddot{\bar{\zeta}}(x,t) - 2U\left[\sum_{r=0}^{N} w_r'(x)\,\dot{p}_r(t) - \dot{\bar{\zeta}}'(x,t)\right] + U^2\left[w_r''(x)\,p_r(t) - \bar{\zeta}''(x,t)\right]. \tag{2.57}$$

On the other hand, assuming the hydrodynamic force is defined to be harmonic, i.e. $p(t) = pe^{-i\omega_e t}$, the expressions in Equations 2.56 and 2.57 can be written (Gu et al. 2003) as:

$$\frac{i}{\omega_e}\frac{Dz_{rel}}{Dt} = \sum_{r=0}^{N} w_r(x)p_r(t) + U\sum_{r=0}^{N} w_r'(x)\frac{\dot{p}_r(t)}{\omega_e^2} - \frac{\omega}{\omega_e}\bar{\zeta}(x,t), \tag{2.58}$$

$$\frac{i}{\omega_e}\frac{D^2 z_{rel}}{Dt^2} = \sum_{r=0}^{N} w_r(x)\dot{p}(t) - 2U\sum_{r=0}^{N} w_r'(x)p_r(t) - U^2\sum_{r=0}^{N} w_r''(x)\frac{\dot{p}_r(t)}{\omega_e^2} - \frac{\omega^2}{\omega_e^2}\bar{\zeta}(x,t). \tag{2.59}$$

2.4 Transient loads

2.4.1 Green water

When the incident water surface exceeds the moving deck level at any section, green water related hydrodynamic forces may also contribute. When water surges on deck, fluid will flow from bow to amidships rapidly, like the dam breaking problem (Buchner 1995). At the next stage, most of the kinetic energy of the water jet has been expanded and a quasi-static load applies on the deck. The high velocity water shooting over the deck lasts for a very short period and acts on a comparatively small area. Although the instantaneous impact pressures on that area may be large, the resulting hydrodynamic force on the ship is comparatively small. In this investigation, the water jet event is omitted and the quasi-static load is added into F_{nl} of Equation 2.46 in order to obtain global response due to green water.

The green water load (F_5) is obtained by simply including a term proportional to the change of the momentum of the water on deck. The hydrodynamic force of fluid on deck per unit length of the ship can be expressed as (Buchner 1995).

$$F_5(x,t) = -m_g(x,t)\cdot g - \frac{D}{Dt}\left(m_g(x,t)\frac{Dw(x,t)}{Dt} \right), \tag{2.60}$$

where

$m_g(x,t) = \rho B_{deck}(x) h_g(x)$ is the mass of fluid above the deck level

$h_g(x) = \zeta(x,t) - w(x,t) - h_{deck}(x)$ is instantaneous water height above the deck

$h_{deck}(x)$ and $B_{deck}(x)$ are the free board of the hull and breadth at deck level.

Equation 2.60 can also be rewritten

$$\begin{aligned} F_5(x,t) &= -m_g(x,t)g - \frac{D}{Dt} m_g(x,t) - m_g(x,t)\frac{D^2 w(x,t)}{Dt^2} \\ &= -\rho B_{deck} h_g g - \rho B_{deck}\frac{Dh_g}{Dt}\frac{Dw(x,t)}{Dt} - \rho B_{deck} h_g \frac{D^2 w(x,t)}{Dt^2}. \end{aligned} \tag{2.61}$$

In this equation, the first term is the weight of the fluid itself (F_{51}) and the second (F_{52}) and third terms (F_{53}) are induced by the rate of change of water height on deck and the inertia of fluid due to the vertical absolute acceleration of the ship, respectively. The rate of water height on the deck has an important effect on the maximum deck pressure. If the water height increases rapidly in the time the deck has an upward velocity, large pressures are found.

2.4.2 Bottom slamming

The slam-induced impulsive force is experienced when the hull emerges above the wave surface and impinges on the water. Many methods for analyzing impact loads are based on semi-empirical methods. The impulse force per unit length due to the sudden increase of pressure around the bottom of the hull can be represented as a function of the maximum pressure at the keel and its distribution along the hull

section and time variation. It was represented by Ochi and Motter (1971) as:

$$F_6(x,t) = p_{\max}(x)G(x)\,f(t) \tag{2.62}$$

where $p_{max}(x)$ is the maximum impact slamming pressure at the keel, G(x) is the integration shape factor which defines a linear distribution of the impact pressure around the bottom (see Appendix 3 for the details) and *f(t)* defines the time variation of the impact pressure. The maximum slamming pressure is given by the section geometry factor and the square of the body velocity as

$$p_{\max} = \frac{1}{2}k\rho v^2 \tag{2.63}$$

where k is a non-dimensional factor depending on section geometry. Stavovy and Chuang (1976) proposed a method to obtain the k-factor by regression analysis of experimental data. That is

$$p_{\max}(x) = \frac{1}{2}v_{ns}^2(x)\left[2\rho k_1 \cos^2\{\xi(x,t)\} + \rho \sin^2\{\xi(x,t)\}\right] \tag{2.64}$$

where v_{ns} is the relative velocity and $\xi(x,t)$ is the effective impact angle as a function of the local hull effective impact angle. The effective impact angle is defined as a function of the deadrise angle, the effective impact angle in the horizontal longitudinal plane and vertical transverse plane. To simplify the problem, only deadrise angle at each section was estimated in the present study and used when calculating $\xi(x,t)$, for substituting for the pressure in Equation 2.62.

The vertical distribution of slamming pressure is assumed to be linear with the maximum value at the bottom and zero value at 1/10 of the design draught (Ochi and Motter 1973). Kawakami et al. (1977) proposed a formula, based on their experimental work, to represent the bottom slamming force as a function of time as follows:

$$f(t) = \frac{t}{T_o}\left[\exp\left(1 - \frac{1}{T_o}\right)\right] \tag{2.65}$$

where T_o is the time when the maximum pressure is reached, which is suggested as: $T_o = 0.00088\sqrt{L}$, where L is the ship length.

The bottom slamming force per unit length in Equation 2.62, thus, can be re-written

$$F_6(x,t) = \delta_{bs}(x,t)\frac{1}{2}\rho k(x)G(x)\frac{t}{T_o}e^{(1-t/T_o)}\left[\frac{Dw_{rel}(x,t)}{Dt}\right]^2 \qquad (2.66)$$

where $\delta_{bs}(x,t) = \begin{cases} 1, & T(x) < -z_r < 0.9T(x) \\ 0, & -z_r > 0.9T(x) \end{cases}$ and $w_{rel}(x,t) = w(x,t) - \zeta(x,t)$

The total load at each section of the ship is the sum of the wave-frequency loads and the high frequency loads caused by impact.

The use of Equation 2.63, with the time dependence as per Equation 2.65 and the maximum pressure as per Equation 2.64 will be hitherto referred to as the method by Stavovy and Chuang (1976).

Chapter 3

Linear Solution

The linear dynamic responses of beam-fluid model are calculated for the S175 container ship. In the frequency domain analysis, the motions and wave loads for symmetry motions and distortions with regular head waves are calculated as a function of frequency. The hydrodynamic coefficients are estimated at mean draught. Heave and pitch transfer function and wave bending moment are obtained for three ship speeds. The transient responses for a unit impulse load are calculated in time domain simulations. Numerical methods (convolution integral and direct integration) are applied and discussed. Time domain simulation in a regular head wave shows the consistency of these numerical methods.

3.1 Ship characteristics

The calculations were performed for the S175 container ship, for which a number of good experimental and numerical results are available, thus providing guidance for investigating the reliability of the methods and the accuracy of the calculations (ISSC 1997, 2000; Watanabe et al. 1989; Chen et al. 1999). The ship has a large flare angle so that the nonlinear effects due to large amplitude of motions can be easily identified (see Chapter 4).

The principal particulars and the body lines of the ship used in the calculation are shown in Table 3.1 and Figure 3.1.

Table 3.1 Principal particulars of S175

Description	Value,unit
Length between perpendiculars (L)	175.0 m
Beam amidships	25.4 m
Draught amidships	9.5 m
Displacement	24742.0 tonnes
Longitudinal centre of gravity aft of amidships	2.34 m
Vertical centre of gravity above base line	9.52 m

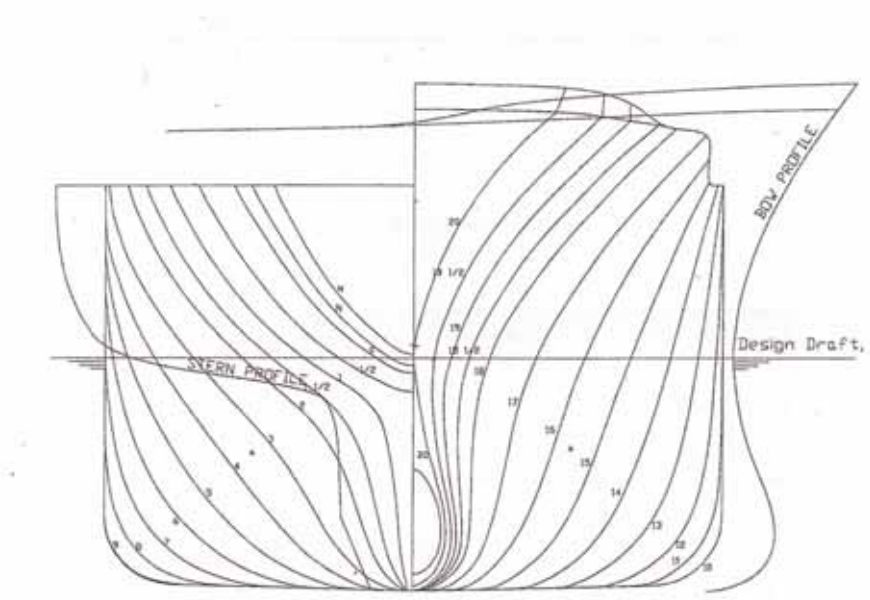

Fig. 3.1 The body plan of S175 (Wu and Hermundstad, 2002)

The distributions of the sectional properties for the Timoshenko beam model, such as mass per unit length of the ship (μ), flexural rigidity (EI), shear rigidity (kAG) and rotary inertia (I_y) are shown in Figures 3.2 to 3.4. The mass distribution of the model ship is obtained by referring the Wu and Hermundstad (2002).

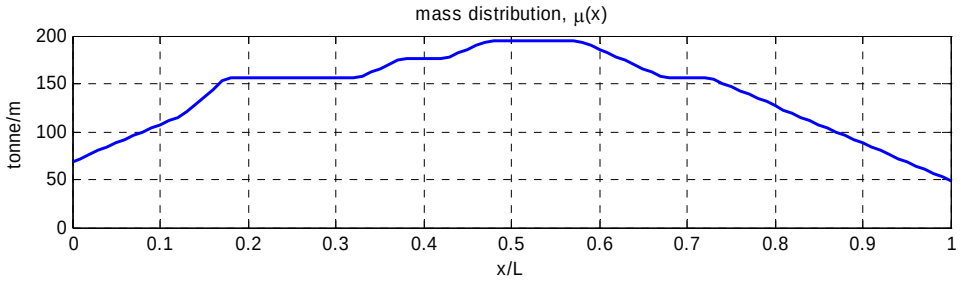

Figure 3.2 Distribution of sectional mass (μ) of S175

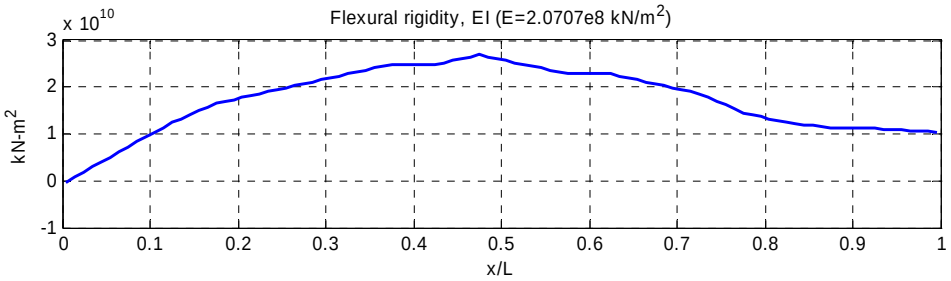

Figure 3.3(a) Distribution of flexural rigidity (EI) of S175

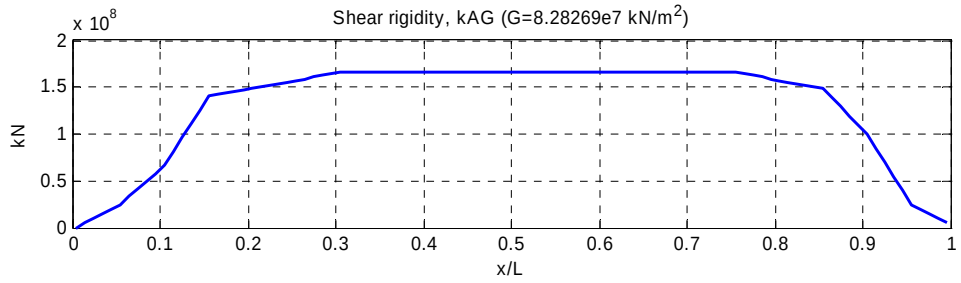

Figure 3.3(b) Distribution of shear rigidity (kAG) of S175

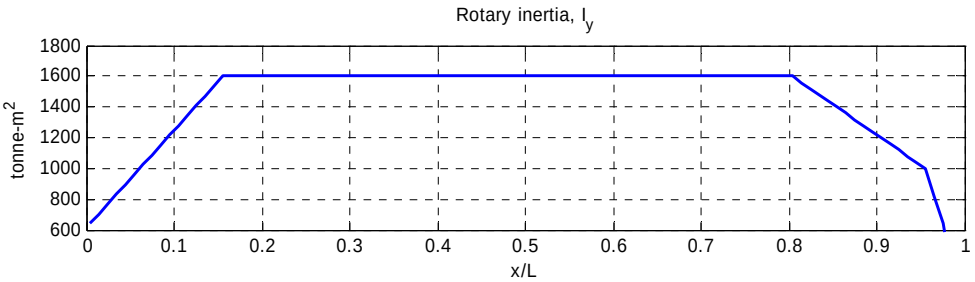

Figure 3.4 Distribution of rotary inertia (I_y) of S175

3.2 Dry analysis

The ship is modelled using 100 sections which is more than sufficient number of segments to represent the vibration characteristics of the dry hull up to the 3rd flexural mode. The sensitivity analysis for the number of sections is shown in Table 3.2. It shows that the number of segments has negligible effect for the first three flexible modes. However in order to estimate the hydrodynamic force properly, a large number of sections (e.g. 100) may be better.

Estimating the structural damping of a ship is one of the most difficult problems in hull vibration studies because damping factors in ships are complicated by the complexity of the structure itself, the various types of cargo, bunkering, amount of machinery, etc. Some effective methods have been developed and the concept of modal damping is easy to apply. Modal damping estimates are based on Kumai's (1958) method in the present investigation.

Table 3.2 Natural frequencies for the "dry" hull of S175

Flexural mode	Natural frequency (rad/s) using 100 sections	Natural frequency using 20 sections
1st	10.005	10.038
2nd	22.645	22.669
3rd	37.287	37.008

The ship is treated as a Timoshenko beam and the natural frequencies and mode shapes are calculated using Prohl-Myklestad's finite difference method (Myklestad 1944, Bishop and Price 1979). The mode shapes are scaled to 1 m deflection at the stern. Two rigid body modes (r=0,1) and the first three flexible modes (r=2,3,4) are considered when estimating the dynamic response of the hull. For the rigid body dry

modes, the mode shapes are defined by

$$w_o = 1 \quad for \quad r = 0$$

$$w_1 = 1 - \frac{x}{\bar{x}} \quad for \quad r = 1.$$

These two modes correspond to the heave and pitch motions of the hull, where $\bar{x}$ is the longitudinal position of the mass centre measured from the stern. The mode shapes w_r of the hull girder vibration are shown in Figure 3.5. Whether N = 4 is adequate to ensure convergence in the modal superposition will be discussed later (see Section 3.4.1). The corresponding bending moment (M_r) and shear force (V_r) modal functions of these three dry modes are presented in Figures 3.6 and 3.7, respectively. Note that M_r=0=V_r for r=0 and 1. The calculation for 'Dry mode' was carried out following the analysis by Bishop et al. (1977).

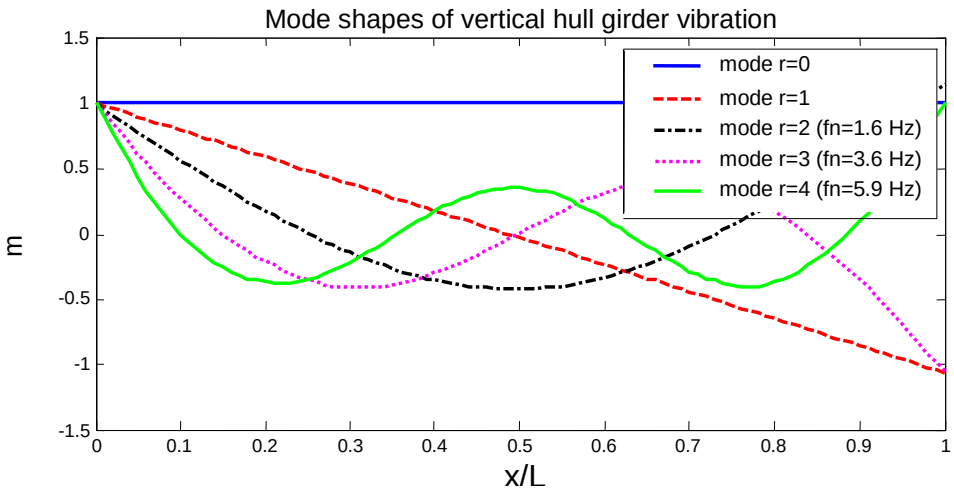

Figure 3.5 Mode shapes of vertical hull girder vibration in the 'Dry mode' for S175

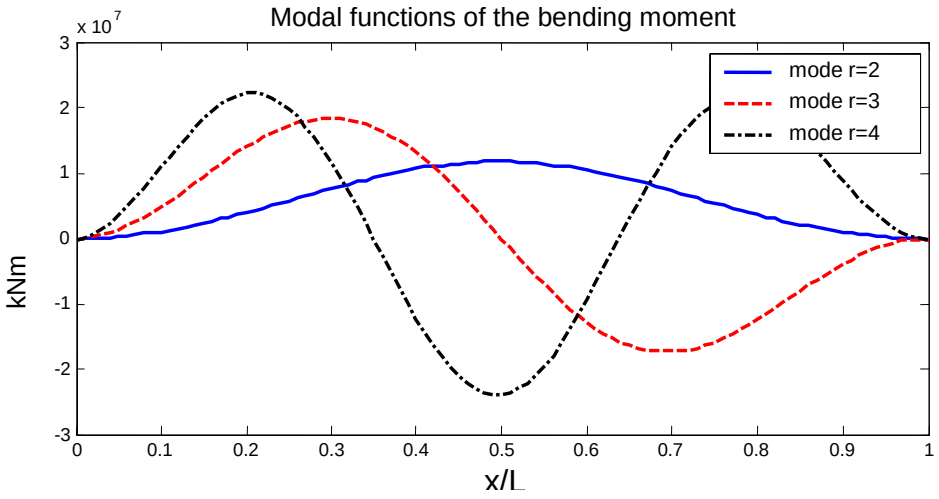

Figure 3.6 Modal functions of bending moment of S175

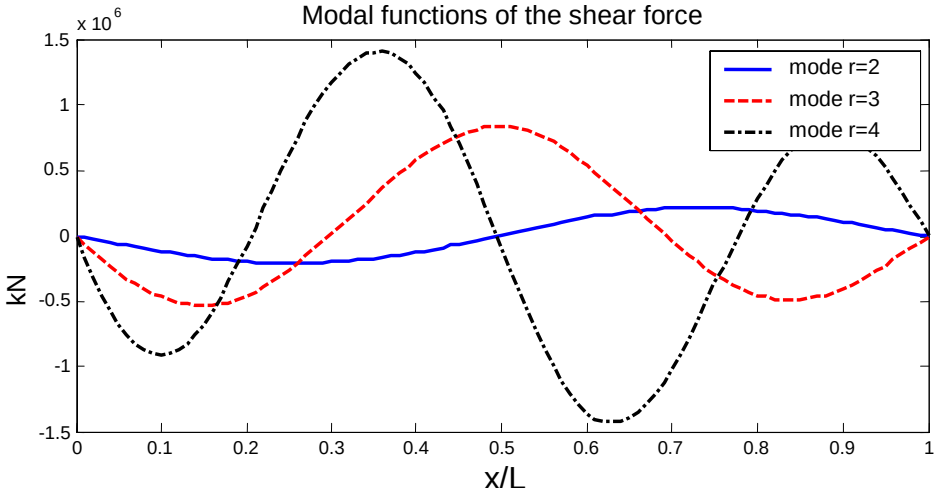

Figure 3.7 Modal functions of shear force of S175

3.3 Fluid forces

The sectional added mass coefficients and fluid damping coefficients are calculated by assuming Lewis form sections. Figures 3.8 and 3.9 show the sectional added mass, $m(x,\omega)$, and damping coefficients, $N(x,\omega)$, of some sections (STN=0, 5, 10, 15 and 20) according to wave encounter frequency (ω_e) where STN 0 denotes the AP

and STN 20 is the FP. Asymptotic values of sectional added mass at infinite frequency are presented in Table 3.3. The sectional damping coefficients decrease to zero at a higher frequency range.

Table 3.3 Asymptotic values of added mass at infinite frequency at mean draught

station number	0	5	10	15	20
added mass (tonne/m)	3.42	209.9	331.8	125.4	1.11

The Lewis form sections are presented and compared with the original ship sections in Figures 3.10. Lewis form sections follow the original shape well for most sections; however for fine or bulbous sections at bow and stern, the Lewis conformal transformation does not map the hull sections as accurately. The hull section contour can be defined more accurately using the multi-parameter conformal transformation technique (Bishop et al. 1978c). The hydrodynamic coefficients for some sections at mean draught are shown in Figures 3.11 and 3.12, comparing the Lewis form formulation to the multi-parameter conformal transformation technique. 4, 6 and 8 parameter conformal transformations are used. The added mass coefficients are close to each other whether using the Lewis or multi-parameter mapping as shown in Figure 3.11. Figure 3.12 shows that the fluid damping coefficients differ slightly between the Lewis form and the multi-parameter mapping at stations 2 and 18, while for other sections the fluid damping coefficients estimated by the Lewis form are close to those using multi-parameter mapping. The Lewis form formulation was employed in the present study considering the benefit of its simplicity.

The reduction of added mass due to three-dimensional flow effect is applied using Townsin's (1969) formulation. This factor is only applicable to the lower modes of vibration and to the diagonal terms of the generalised added mass matrix (Bishop and Price 1979). Table 3.4 presents the wet resonance frequencies of the hull vibration

(r=2, 3, 4) with and without three-dimensional reduction. The table shows that three-dimensional reduction increases resonance frequencies. Hence forth the reduced added mass is used in the analysis.

Table 3.4 'Wet' resonance frequency of hull girder vibration with/without 3-D correction (wave encounter frequency)

mode	Wet natural frequency without 3-D reduction (rad/s)	Wet natural frequency with 3-D reduction (rad/s)
2-node (r=2)	7.9	8.4
3-node (r=3)	17.1	18.7
4-node (r=4)	28.0	32.2

For the vertical deflection of the hull, the generalized fluid forces due to hull motion and distortion can be expressed by the matrix $[A]$ and $[B]$, as described in Equations 2.44 (see also Appendix 2). By contrast to the generalised structural mass, damping and stiffness coefficients in the dry hull, a_{rs}, b_{rs} and c_{rs} of the diagonal matrices in Equation 2.5, $[A]$ and $[B]$ do not form a symmetric array. The matrices $[A]$ and $[B]$ are neither symmetric nor positive definite, and are dependent on encounter frequency and speed. The off-diagonal terms are not small enough to be negligible.

Table 3.5 illustrates the magnitude of the structural damping, based on the method by Kumai (1958) and diagonal hydrodynamic fluid damping terms at various frequencies. Structural damping becomes more dominant by comparison with fluid damping as the mode number increases. The stiffness terms, $[C]$ of Equation 2.44, correspond to purely hydrostatic effects and are independent of frequency.

Table 3.5 Generalised structural damping (b_{rr}) and fluid damping (B_{rr}) for various modes (kN ms)

Mode, r	Structural damping	Fluid damping at ω_e=0.883	Fluid damping at ω_e=8.4	Fluid damping at ω_e=18.7
0	-	1.125e4	36.90	27.8
1	-	2.910e3	30.40	24.9
2	3.9546e2	1.716e3	28.60	25.2
3	1.2009e3	2.380e3	23.00	29.6
4	2.5574e3	2.952e3	28.2	25.9

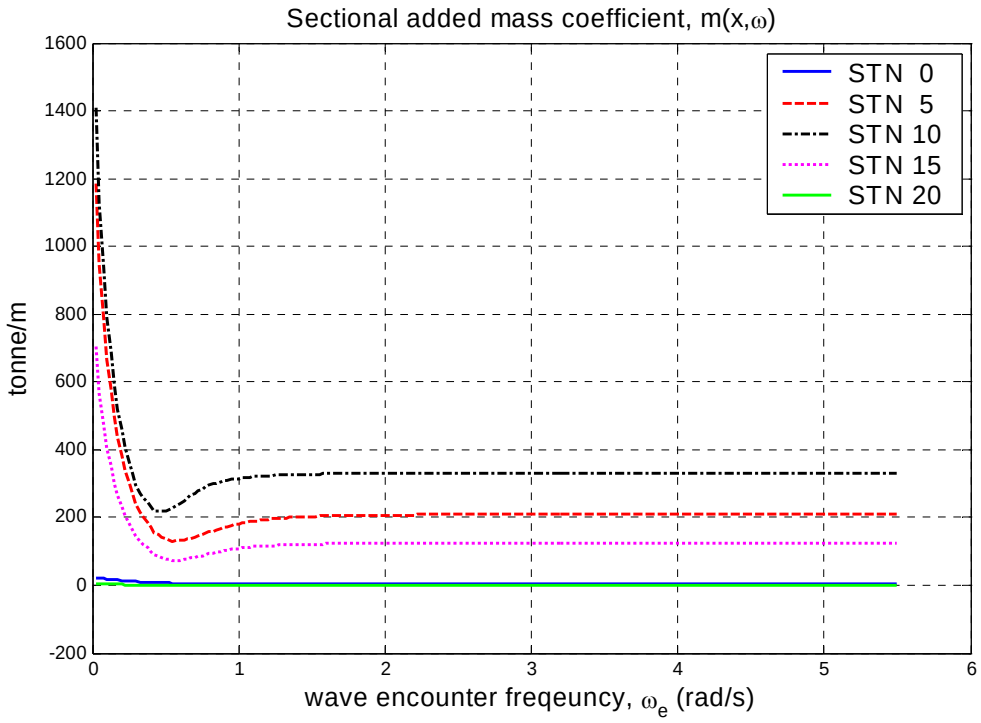

Figure 3.8 Added mass $m(x,\omega)$ as a function of wave encounter frequency

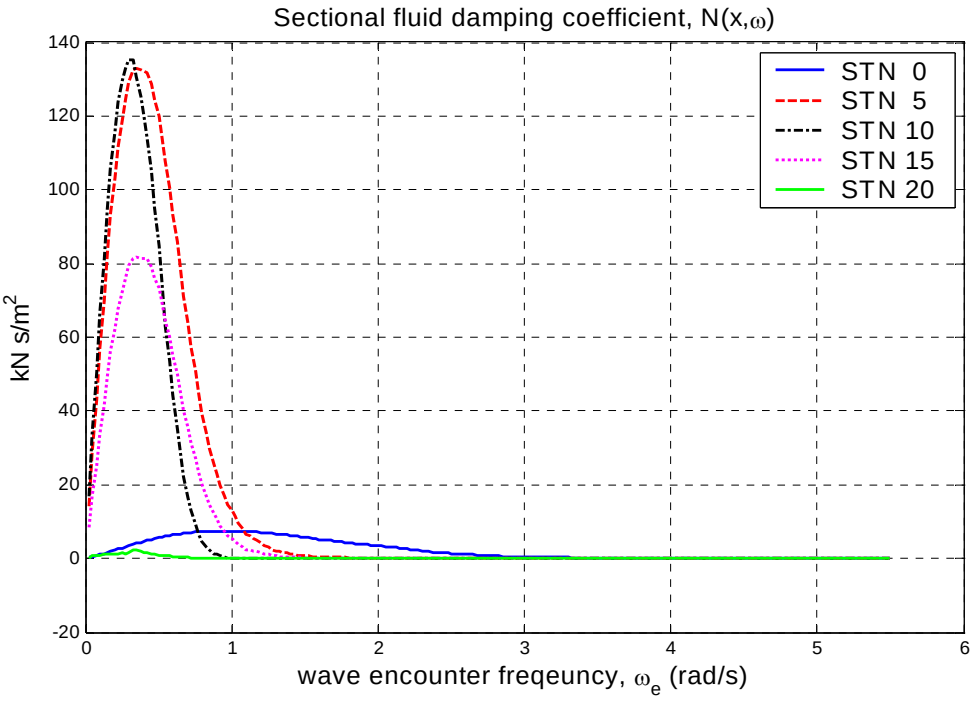

Figure 3.9 Fluid damping coefficient $N(x,\omega)$ as a function of wave encounter frequency

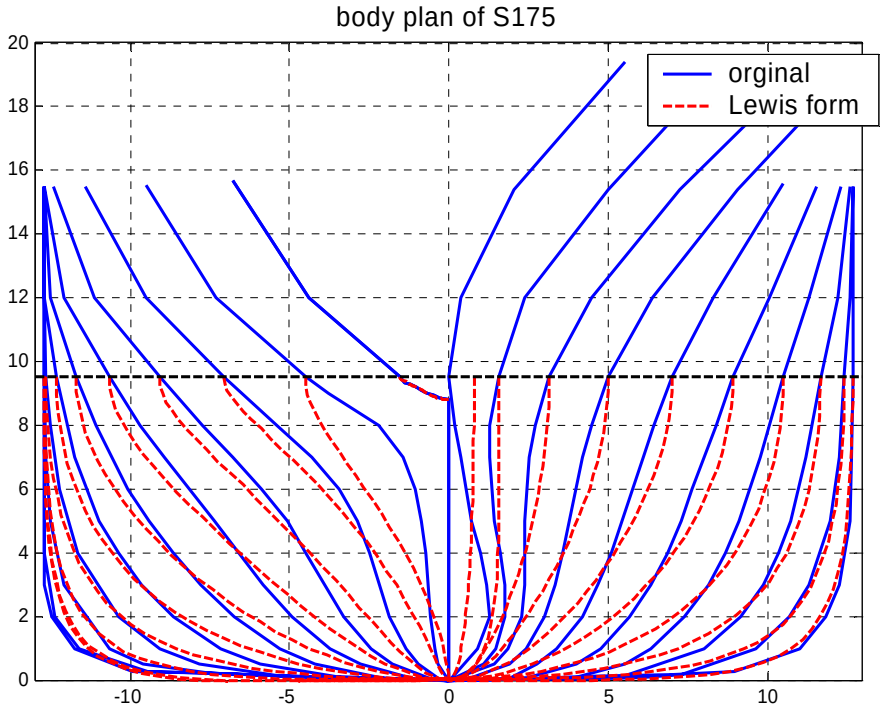

Figure 3.10 The body plan of S175 container ship (original and Lewis form)

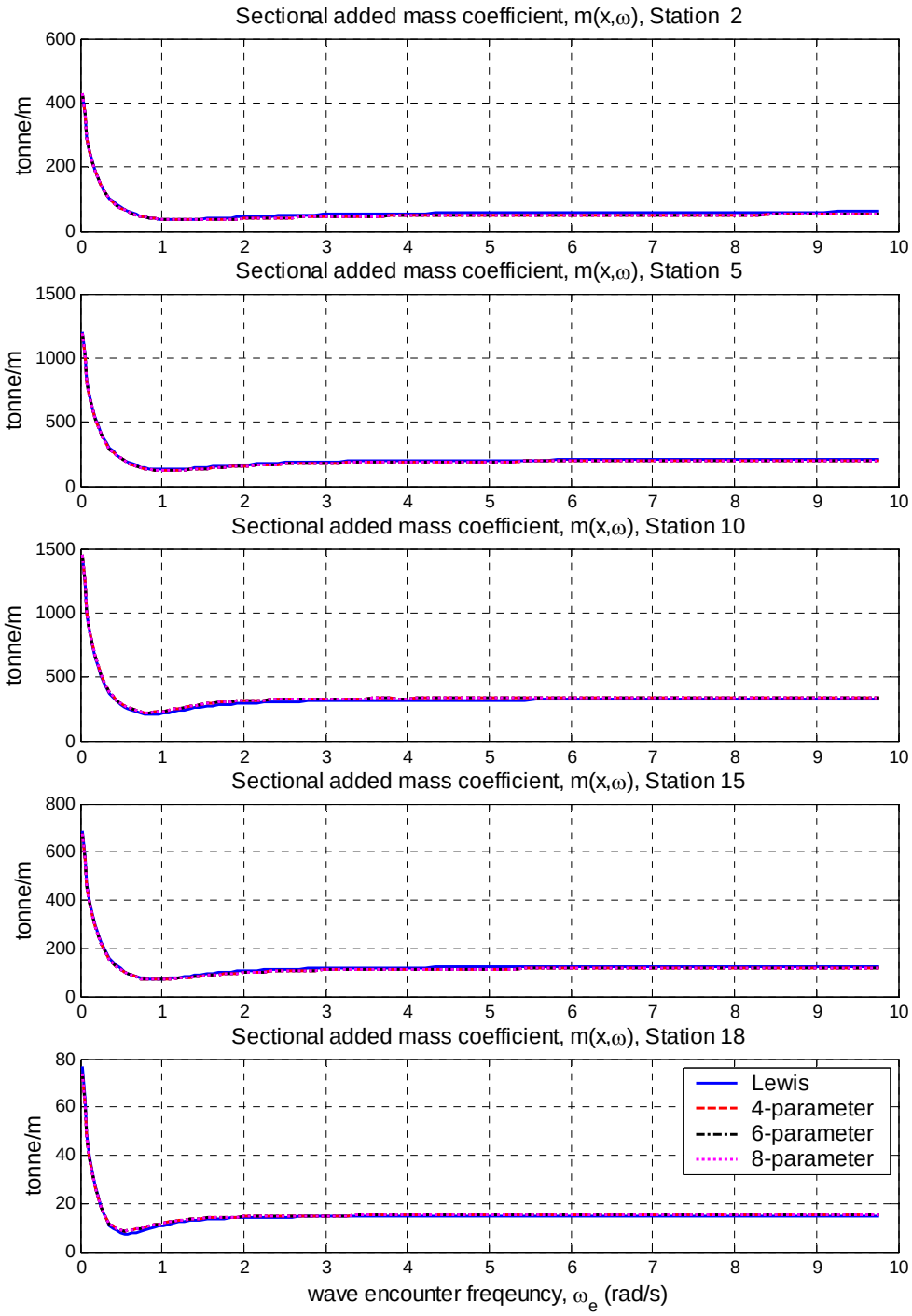

Figure 3.11 Added mass $m(x,\omega)$ evaluated using multi-parameter conformal mapping technique

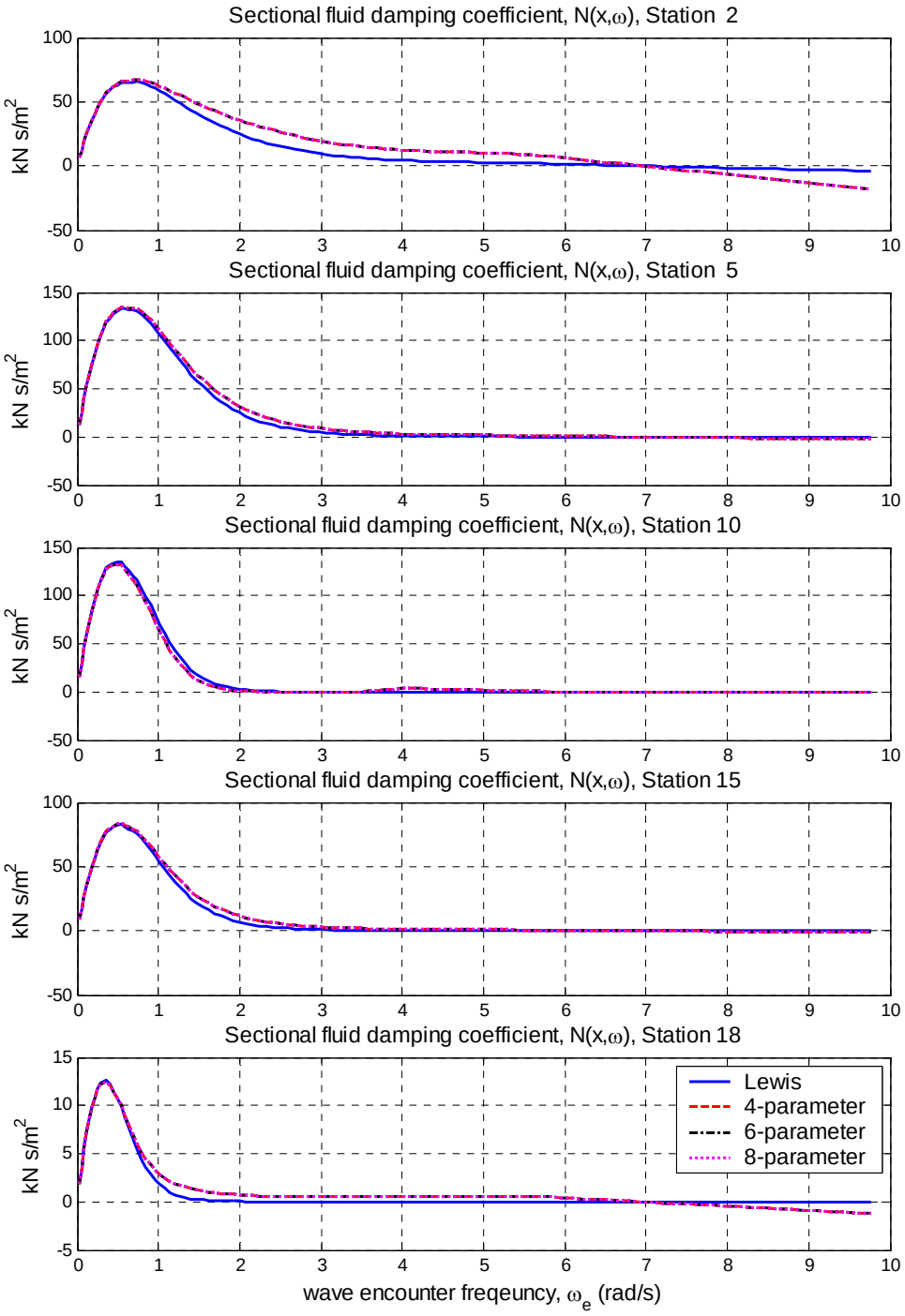

Figure 3.12 Fluid damping coefficient $N(x,\omega)$ evaluated using multi-parameter conformal mapping

3.4 Solution of equations of motion

The linear equation of motion, Equation 2.44, is solved in both the frequency and time domains in regular head waves of unit amplitude. The responses in frequency domain analysis, i.e. the steady state response, are compared to the responses in linear time domain analysis using various numerical simulation methods, namely convolution integral and direct integration, in order to check the accuracy of these numerical methods. The transient response for a unit impulse force is also presented using a convolution integral method and a direct numerical integral method.

3.4.1 Frequency domain analysis

Considering exponential decay in wave pressures according to water depth in calculating the hydrodynamic forces (Equations 2.21 and 2.29), it was shown in Section 2.2 that it is convenient to introduce the concept of Smith correction. Figure 3.13 shows that the Smith correction factor κ decreases as kT (wave number multiplied by draught) increases, at five sections along the hull. The Smith correction factor decreases to zero as the wave number becomes high (i.e. shorter wave length).

As previously discussed in Section 2.3, the principal coordinate responses for a harmonic excitation in frequency domain are obtained:

$$\{p(\omega_e)\} = [H(\omega_e)]\{F_w(\omega_e)\} \tag{3.1}$$

where, $[H(\omega_e)]$ is the complex frequency response function defined as

$$[H(\omega_e)] = \left\{-\omega_e^2[a + A(\omega_e)] - i\omega_e[b + B(\omega_e)] + [c + C]\right\}^{-1} \tag{3.2}$$

The system being linear, a sinusoidal input (a regular wave) produces a steady sinusoidal output of the same frequency. By definition, the frequency response function, $H(\omega_e)$ in Equation 3.2, is the complex response to waves of unit amplitude and the diagonal elements of $|H(\omega_e)|$ are shown in Figure 3.14 as a function of wave encounter frequency. It can be seen that the diagonal elements show peak at the appropriate resonance (i.e. at 0.883 rad/s for $r = s = 0,1$ and at the wet resonance frequencies shown in Table 3.4 for $r = s \geq 2$).

The magnitudes of the linear wave excitation force (diffraction and Froude-Krylov force) due to unit amplitude regular head wave are presented in Figure 3.15. In the high encounter frequency range (say above 5.0 rad/s), the wave excitation force is very small for all modes.

Figure 3.16 shows the amplitudes of the first five principal coordinates for three different Froude numbers (Fn = 0.20, 0.25 and 0.275). It can be pointed out that the peaks correspond to the maxima of $|H(\omega_e)|$ and each generalised coordinate has distinct dominant peaks at the same encounter frequencies. The peaks of p_2, p_3 and p_4 correspond to the resonance frequencies for the wet modes, r=2, 3 and 4, respectively show are shown in Table 3.4. It can be seen that the resonance characteristic of the system do not depend on the speed of the ship. As the speed increases the magnitude of the principal coordinates increase. The coupling between rigid and distortions is apparent as all principal coordinates display a substantial peak at ω_e=0.883 rad/s, corresponding to the pitch/heave resonance. The peaks of the two principal coordinates (p_0 and p_1, respectively) are likely to occur at very low encounter frequencies. Physically, modes 0 and 1 represent the heave and pitch modes, respectively. Figure 3.17 shows the heave and pitch as a function of non-dimensionalized frequency. The heave transfer function has a peak response, even

though it only looks like a small hump around $\omega_e\sqrt{L/g}$ =2.24 at Fn=0.275, where the corresponding wave/hull length ratio (λ/L) is around 1.2, by contrast, the pitch transfer function has a flatter peak response. The amplitudes of the heave transfer function increase as the ship speed increases (Fn=0.2, 0.25 and 0.275, respectively).

The frequency responses of midship bending moment for these different Froude numbers is depicted in Figure 3.18 with the wave encounter frequency range up to 40 rad/s. The first big peak occurs around the wave encounter frequency of 0.883 rad/s. This peak comes from the resonances in heave motion, i.e. at $\lambda/L \approx 1.2$. Another peak corresponds to the wave encounter frequency of 8.4 rad/s, which results from the first flexural mode of hull vibration in wet condition. This frequency may be resonant with the high frequency wave excitation (i.e. the so-called springing response), however it does not always imply that the response of the ship in a seaway is affected severely because of wave energy distribution. At the high frequency range, wave energy is small.

Damping is a crucial factor for the resonance response. The damping consists of hydrodynamic damping and structural damping. Figure 3.19 shows the bending moment amidships at Froude number of 0.275, when the structural damping is omitted. It shows that the structural damping is dominant compared with the hydrodynamic damping for the first flexural mode.

In order to estimate whether N=4 is adequate to ensure convergence in the modal superposition, a sensitivity study on the influence of higher modes is carried out. Figure 3.20 shows the vertical bending moments at three different locations along the hull, in which the maximum number of modes in the summation (see Equation 2.13) is varied (N=2, 3, 4 and 5). For the midship bending moment, the higher mode

effects (above N=5) are negligible. Bending moments at 1/4 L and 3/4 L appear to be affected at corresponding resonance frequency regions. However the difference is so small as to be negligible. It can thus be concluded that the first three flexural modes (r=2, 3 and 4) is adequate to ensure convergence. Through the sensitivity study, it can also be pointed out that the two-node mode (r=2) is completely dominant for the wave bending moment.

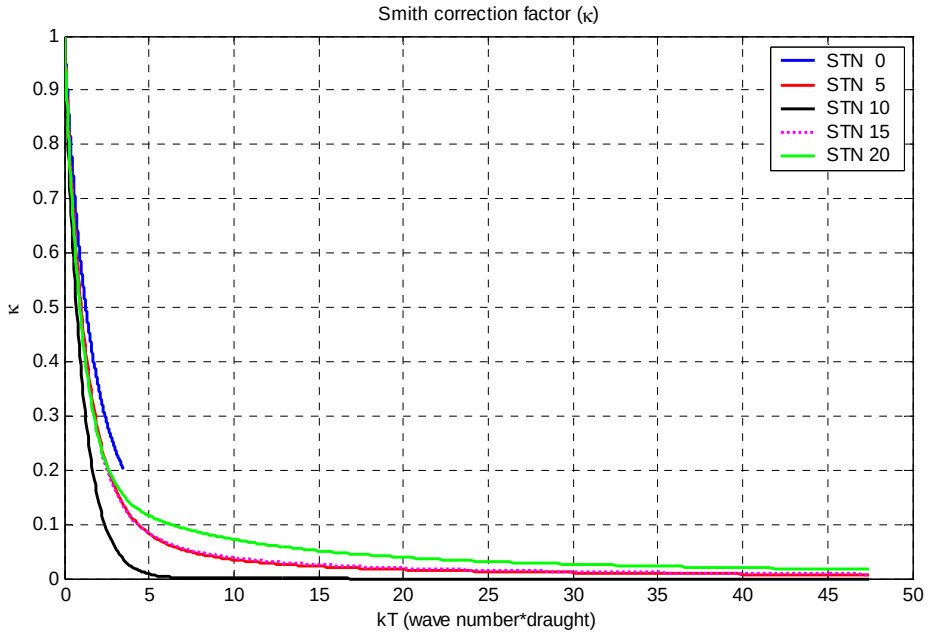

Figure 3.13 Smith correction factor at mean draught as a function of kT

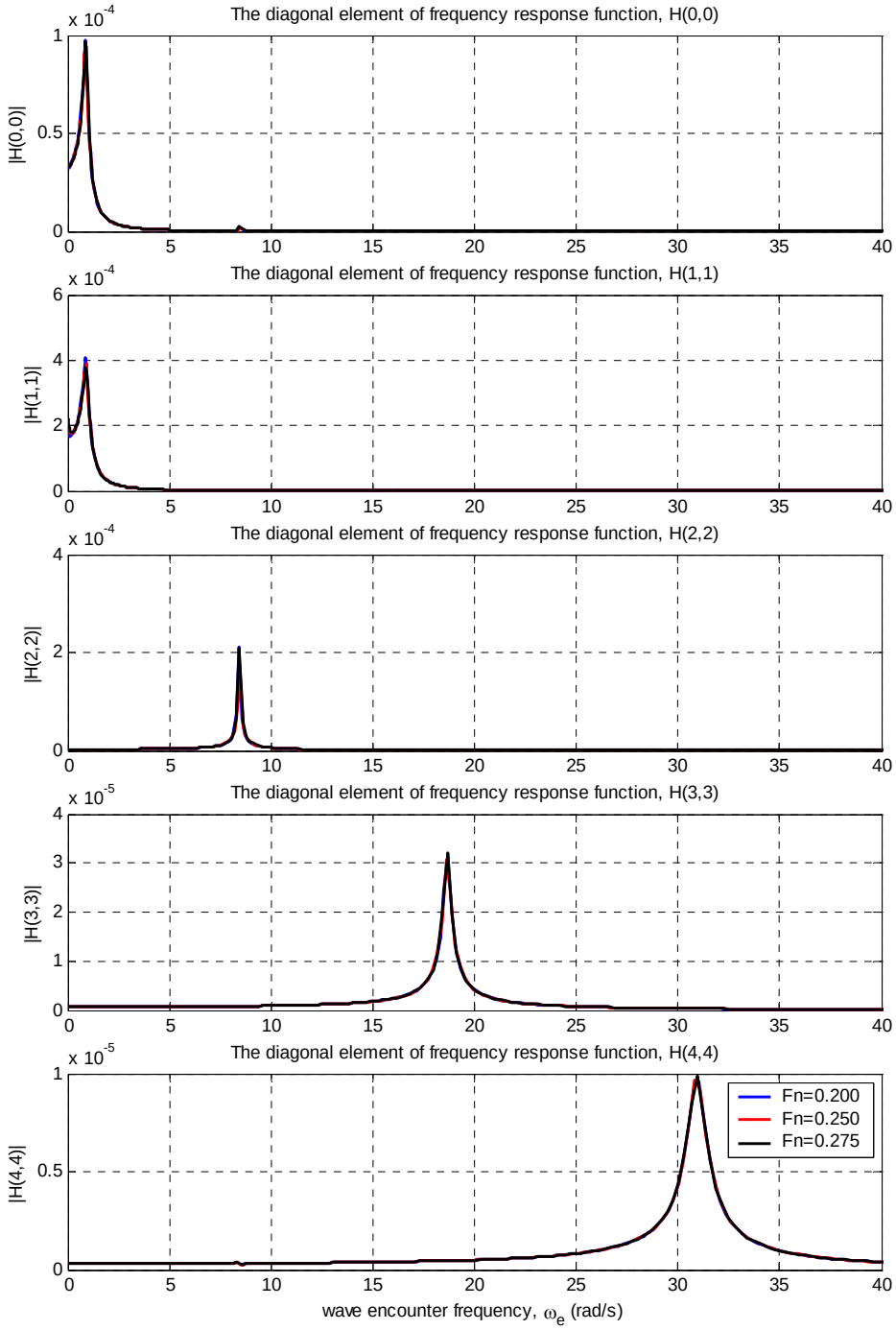

Figure 3.14 Diagonal elements of frequency response function of Equation 3.2 [units: $(Nm)^{-1}$]

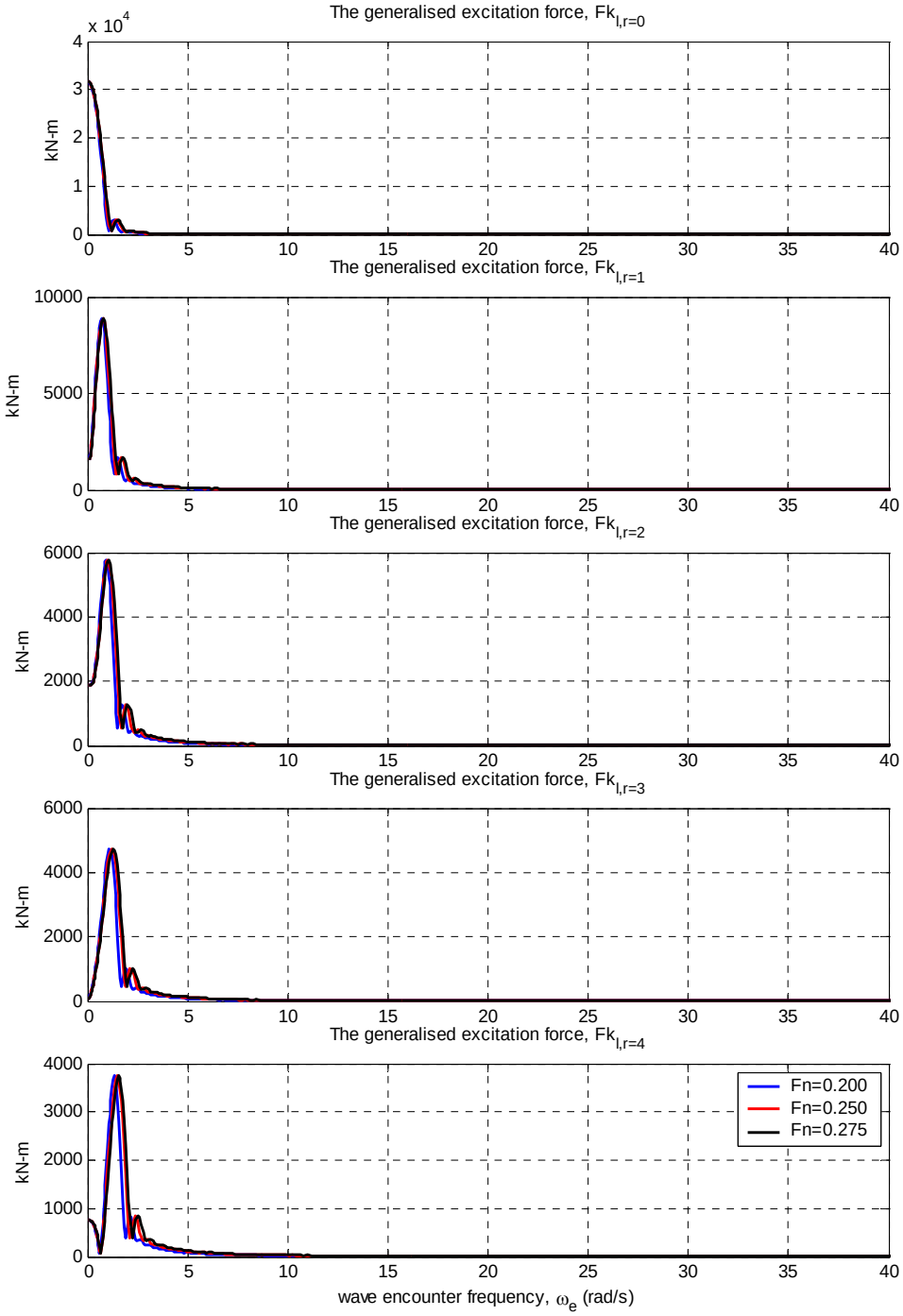

Figure 3.15 The generalised excitation forces in regular waves

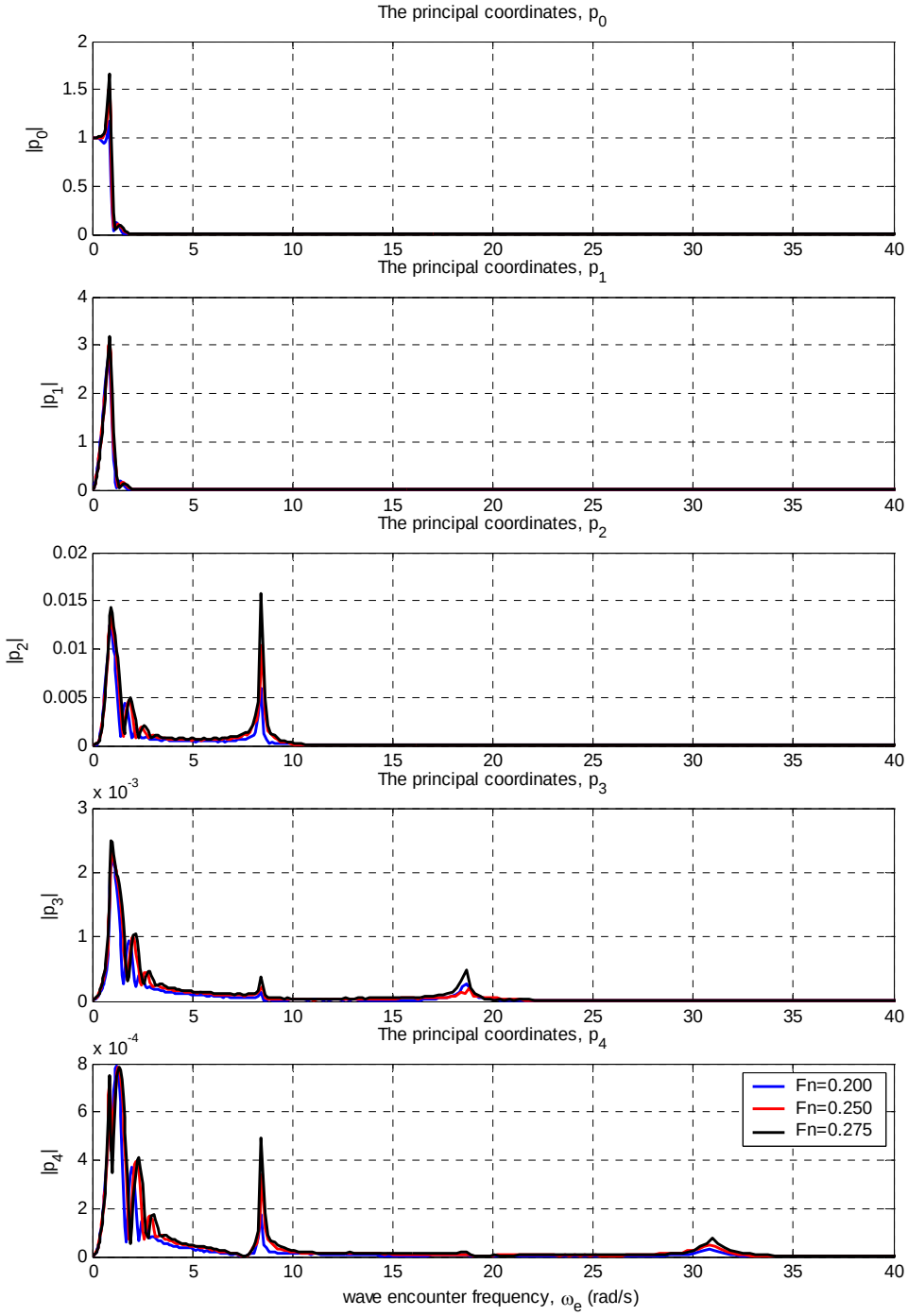

Figure 3.16 Variation of principal coordinate amplitudes with encounter frequency at three different speeds

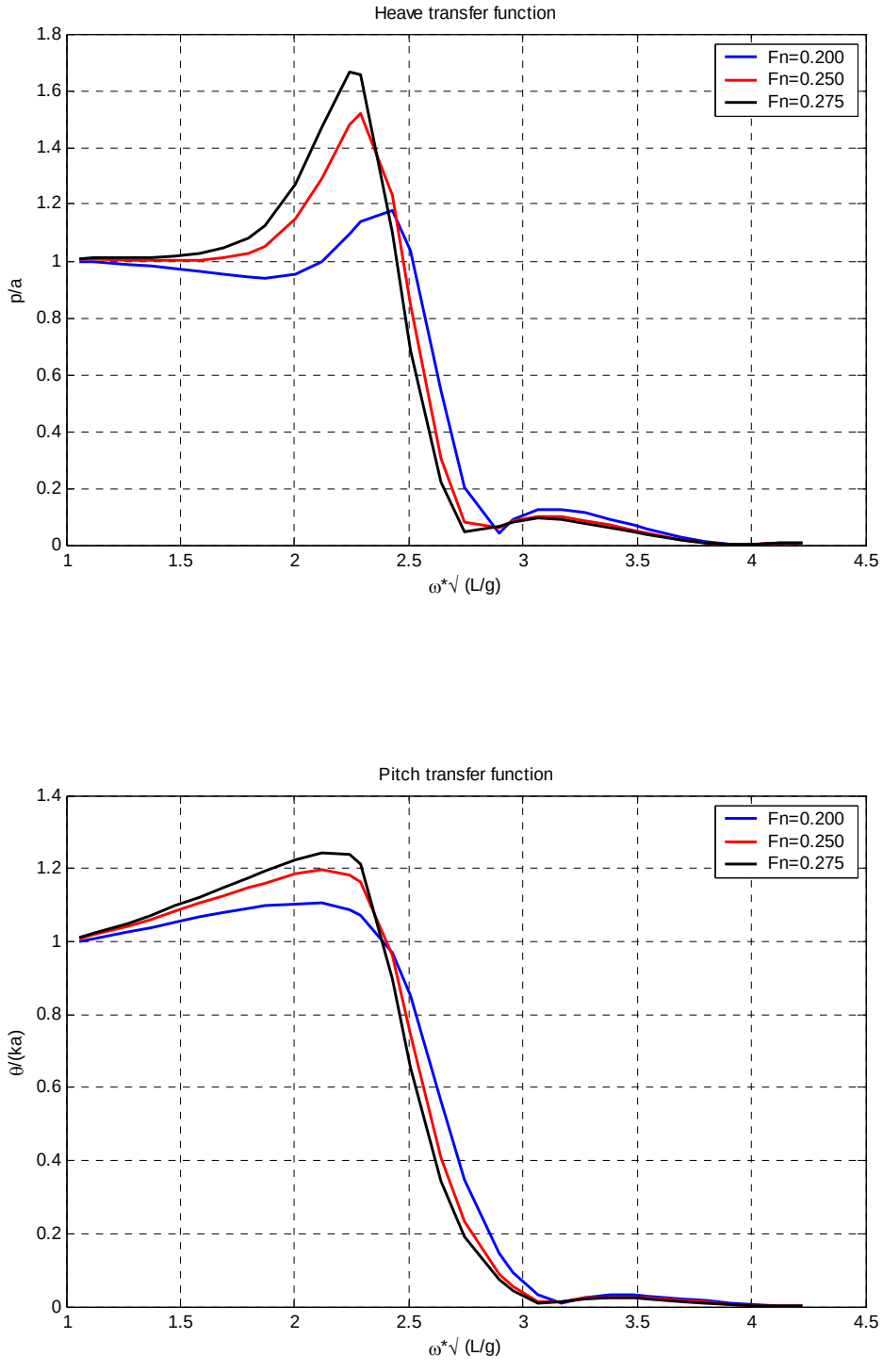

Figure 3.17 Heave and pitch transfer functions as a function of $\omega_e\sqrt{L/g}$

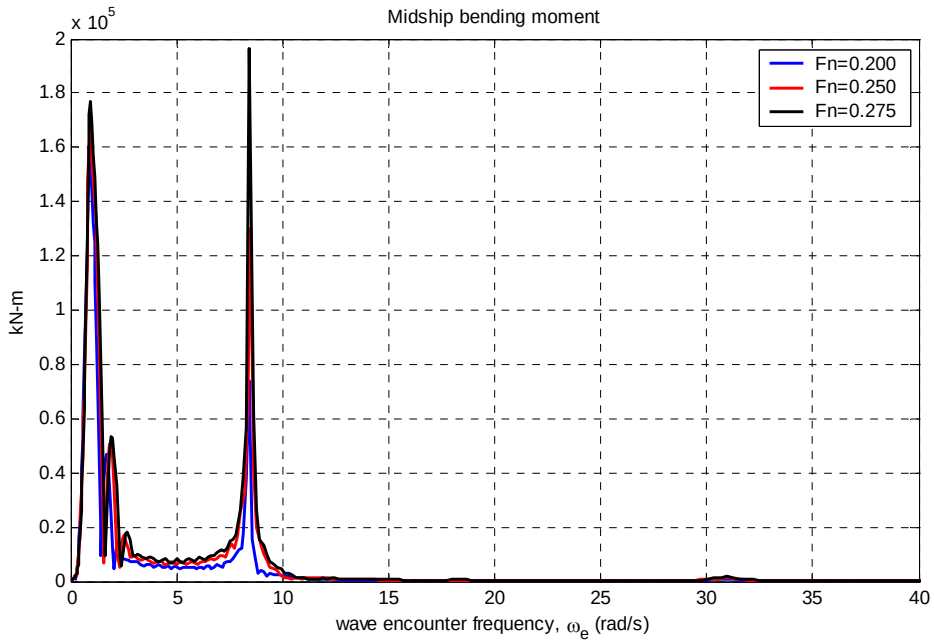

Figure 3.18 Midship bending moment at three different ship speeds

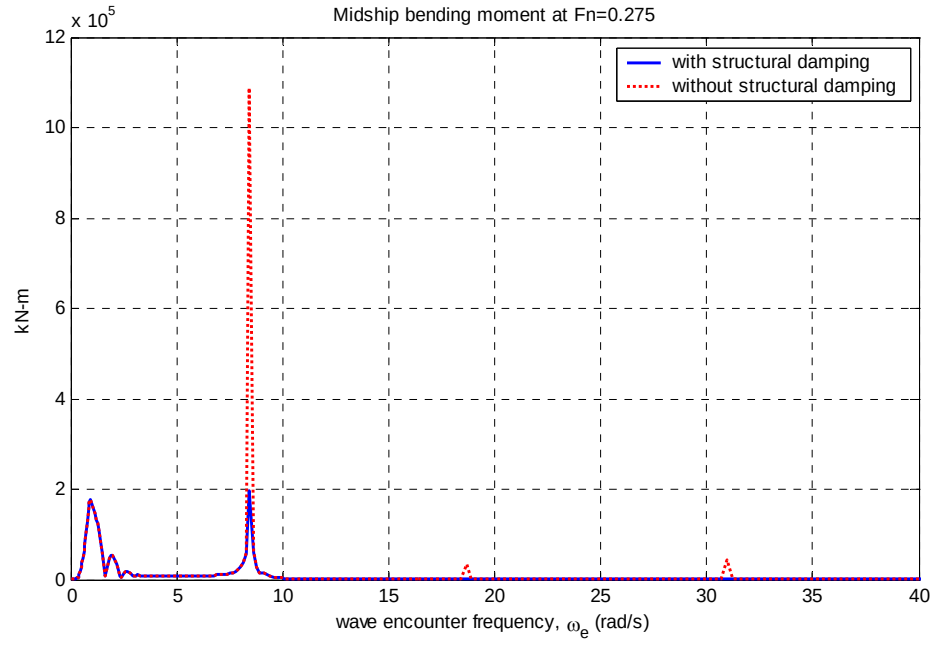

Figure 3.19 Midship bending moment with/without structural damping

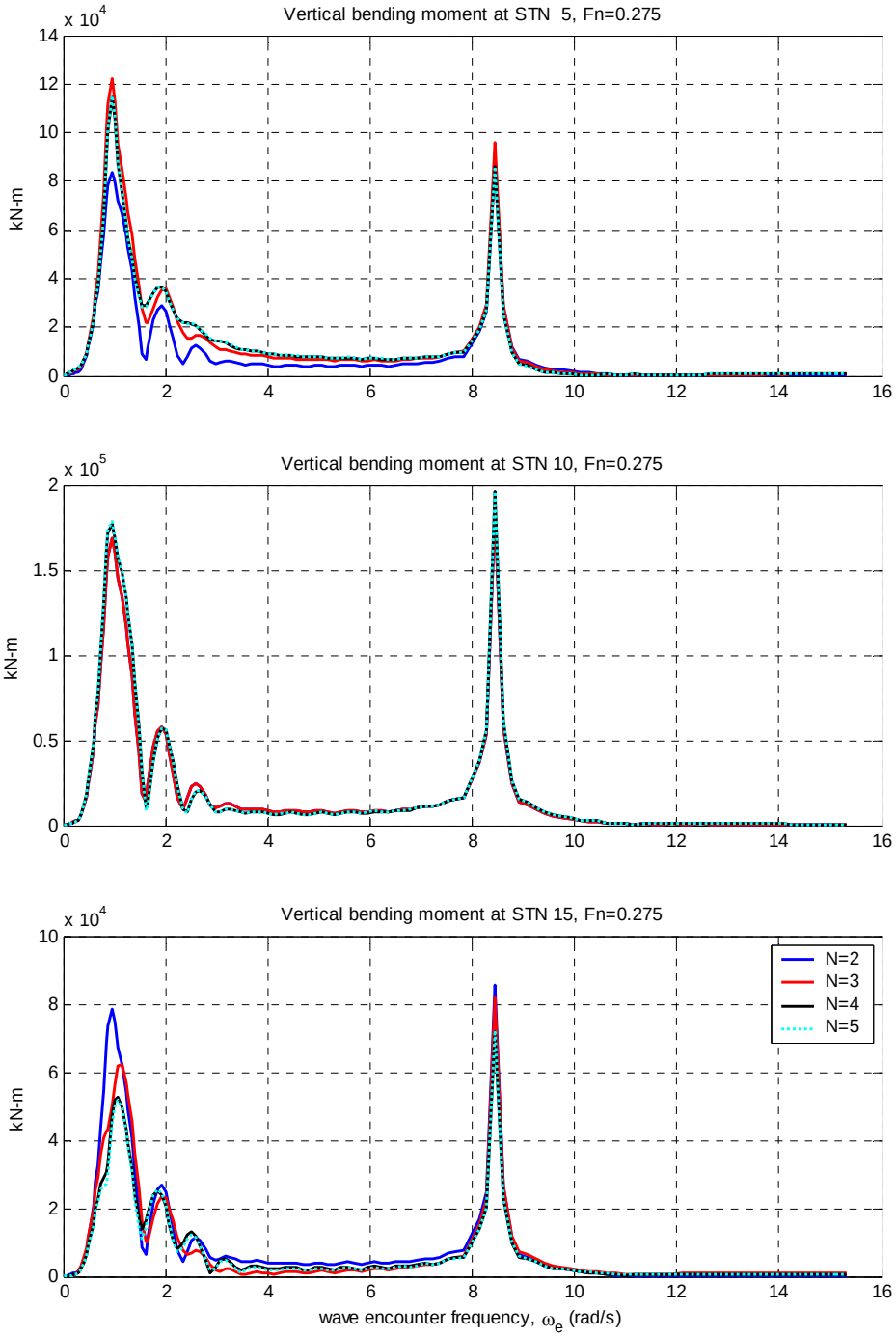

Figure 3.20 Sensitivity of modal summation on bending moments

3.4.2 Numerical methods for time domain analysis

The ship responses are assumed to be harmonic due to harmonic excitation. Under this assumption, the added mass and damping coefficients are determined in the frequency domain and the equation of motion in the frequency domain can be transformed to the time domain, as explained in sections 3.4.2.1. and 3.4.2.2. It implies that the responses in the time domain at each time step display oscillatory steady state behaviour and the equations of motions cannot be applied directly to a general time dependent excitation.

Two time domain simulation methods are introduced in this section: one is the convolution integral method and the other is the direct numerical integral method.

3.4.2.1 Convolution integral method

The total response of a linear system having a number of inputs can be computed by determining the response to each input considered separately and then summing the individual responses. The impulse response function, *h(t)*, of a time-invariant system denotes the output time function which results when the input signal is a unit impulse accruing at t=0. It is assumed that the output was zero before the application of the impulse and would have remained zero if the impulse had not been applied. When the impulse is set as $x(\tau)\delta(t-\tau)$ in the mathematical expression, where $\delta(t)$ is the Dirac delta function, the response to each impulsive input is obtained by multiplying the impulse response function *h(t)* by the strength of the impulse. That is the convolution integral expressed as:

$$y(t) = \int_{-\infty}^{\infty} h(\tau)x(t-\tau)d\tau \quad . \tag{3.3}$$

As impulse response function is the response of the system to a unit impulse at time t=0, so that there can be no response before the input is applied, the lower limit of the integral in Equation 3.3 may be replaced by 0 without change of value of *y(t)* (Ballard et al. 2003). Furthermore, the condition imposed allows the upper limit in Equation 3.3 to be replaced by the arbitrary time *t*.

The linear hydroelastic equation of motion (Equation 2.44) was given as:

$$[a+A]\{\ddot{p}_l(t)\}+[b+B]\{\dot{p}_l(t)\}+[c+C]\{p_l(t)\}=\{F_w(t)\}. \tag{3.4}$$

The linear responses are obtained by applying convolution integral formulation, as:

$$\{p_l(t)\} = \int_{o}^{t} [h(\tau)]\{F_w(t-\tau)\}\, d\tau \,. \tag{3.5}$$

Here, $[h(\tau)]$ is the impulse response function matrix, which can be estimated using the linear system coefficients.

Using the inverse Fourier transformation of the frequency response function, the impulse response function $[h(\tau)]$ is defined by adopting the new variable $\omega = -\omega_e$ (Bishop and Price 1979):

$$[h(t)] = \frac{1}{2\pi}\int_{-\infty}^{\infty} [H(\omega)]\, e^{i\omega t} d\omega \tag{3.6}$$

where

$$[H(\omega)] = \left\{-\omega^2[a+A(\omega)]+i\omega[b+B(\omega)]+[c+C]\right\}^{-1} = \int_{-\infty}^{\infty} h(\tau)e^{-i\omega t}d\tau$$

and h(t) and H(ω) form a Fourier transform pair.

If the integrand is assumed to be symmetric, Equation 3.6 may be written as (Ballard et al. 2003):

$$[h(t)] = \frac{1}{\pi}\int_0^{\infty} [H(\omega)]\, e^{i\omega t} d\omega \tag{3.7}$$

The impulse response function of velocity, $h_v(t)$, and acceleration, $h_a(t)$, can be obtained by differentiating Equation 3.7. That is (Wu et al. 1996):

$$[h_v(t)] = \frac{1}{\pi}\int_0^{\infty} i\omega [H(\omega)] e^{i\omega t} d\omega \tag{3.8}$$

$$[h_a(t)] = \frac{1}{\pi}\int_0^{\infty} -\omega^2 [H(\omega)] e^{i\omega t} d\omega \tag{3.9}$$

Then, the velocity and acceleration responses can be obtained using the convolution integral as:

$$\{\dot{p}_l(t)\} = \int_0^t [h_v(\tau)]\{F_l(t-\tau)\} d\tau \tag{3.10}$$

$$\{\ddot{p}_l(t)\} = \int_0^t [h_a(\tau)]\{F_l(t-\tau)\} d\tau \tag{3.11}$$

The alternative method to find the impulse response function of *h(t)* is called the Hamiltonian method (Bishop and Price 1979). Equation 3.4 can be transformed to the Hamiltonian form such that

$$[I]\{\dot{y}(t)\} + [G]\{y(t)\} = \{E(t)\} \tag{3.12}$$

where, $\{y_r(t)\} = \{\dot{p}_r(t)\}$ $(r = 0,1,\ldots,N)$

$$\{y_r(t)\} = \{p_{r-N-1}(t)\} \ (r = N+1, N+1, \ldots, 2N+1)$$

$[I]$ is a unit matrix and the matrices $[G]$ and $\{E(t)\}$ are derived from the matrices, $[a+A]$, $[b+B]$, $[c+C]$ and $\{F(t)\}$.

The solution of Equation 3.12 is

$$y = \int_0^t Y\Lambda(\tau)Y^{-1}E(t-\tau)d\tau \tag{3.13}$$

where $[Y]$ contains the eigenvectors and $\Lambda(t)$ is the diagonal matrix related eigenvalues.

Comparing Equation 3.5 to Equation 3.13, the impulse response functions for the principal coordinates are given as (Bishop and Price 1979) :

$$h(t) = [0 \ \mathrm{I}]Y\Lambda(t)Y^{-1}\begin{bmatrix}[a+A]^{-1}\\ 0\end{bmatrix} \quad for \quad t \geq 0, \ = 0 \quad for \quad t < 0. \tag{3.14}$$

3.4.2.2 Direct numerical integral method

The direct integral method is also a widely used method in the time domain simulation. The implicit Newmark-beta method is suitable for nonlinear systems by using iteration. Using the Newmark-beta method scheme, the velocity and displacement at time t+Δt are given by (Weaver et al. 1987):

$$\dot{x}_{t+\Delta t} = \dot{x}_t + \{(1-\gamma)\ddot{x}_t + \gamma\ddot{x}_{t+\Delta t}\}\Delta t \tag{3.15}$$

$$x_{t+\Delta t} = x_t + \dot{x}_t\Delta t + \{(0.5-\beta)\ddot{x}_t + \beta\ddot{x}_{t+\Delta t}\}(\Delta t)^2 \tag{3.16}$$

where, β and γ are selected as 1/4 and 1/2 respectively, as suitable values for this investigation.

A step-by-step procedure with iteration is used, because the force (linear or nonlinear) depends on the response together with its derivatives. To start the iteration in the jth time step, the velocity is provided in terms of the previous displacement value and velocity (explicit predictor). An improved value for velocity (corrector) is obtained after an estimation of acceleration by the Newmark-beta method. The iteration at the j^{th} time step will stop when a criterion of convergence is reached such as:

$$\frac{\max\left|p_r^{(k+1)}(t) - p_r^{(k)}(t)\right|}{\max\left|p_r^{(k)}(t)\right|} \le \varepsilon = 0.001, \text{ for } k^{th} \text{ iteration step,}$$

where p_r is the principal coordinates.

3.4.3 Time domain analysis – Linear system

3.4.3.1 Response to a unit impulse

When a unit impulse applies at 0.85L from F.P. (station 17), the time histories of the principal coordinates, shear force and bending moments are calculated. Both the convolution integral method and the Newmark-beta method are applied. As discussed in Section 3.4.2, the impulse response function is estimated using two methods, i.e. inverse Fourier transform and the Hamiltonian method.

The diagonal terms of the complex frequency response function $H(\omega)$ are shown in Figure 3.21. The corresponding diagonal terms of the impulse response function matrix (IRF 1) derived by inverse Fourier transform is shown in Figure 3.22 for a duration of 20 or 10 seconds. By contrast to Fourier transform, the impulse response

function calculated by the Hamiltonian method requires a frequency to be specified, as the matrices involved are frequency dependent. Usually a sufficiently large frequency is used. In this investigation, the IRF was estimated at two frequencies: one is the wave encounter frequency of 0.883 rad/s (IRF 2, in the region of heave/pitch resonance frequency) and the other is 8.445 rad/s (IRF 3, 1st flexural resonance frequency). These impulse response functions are presented in Figure 3.22 together with those from inverse Fourier transform. In this figure, the impulse response function of IRF 1 is close to that of IRF 2 for rigid body mode (r=0,1) while IRF 1 is close to IRF 3 for the flexural modes (r=2,3,4). It is obvious that in the impulse response function of IRF 1, the frequency effects, both low and high frequencies, are well reflected.

Principal coordinates applying a unit impulse at station 17, calculated by the convolution integral method with three different impulse response functions of IRF1, IRF2 and IRF3, are shown in Figure 3.23. The same trends observed in the IRFs can be seen in the corresponding principal coordinates in Figure 3.23. Heave and pitch motion (p_0 and p_1), estimated by IRF 1 and IRF 2, decay faster. However, the estimated heave and pitch motion by IRF 3 decays very slowly, because there is no structural damping for modes r=0,1 and the fluid damping estimated at high frequency ($\omega_e = 8.445$ rad/s) is small. For the higher modes, the results of IRF 1 are close to those of IRF 3. The results from the Newmark-beta method are also shown in Figure 3.23, with two different system matrices of $[a+A]$, $[b+B]$, $[c+C]$: estimated at $\omega_e = 0.883$ rad/s (Newmark 1) and 8.445 rad/s (Newmark 2). Principal coordinates by Newmark 1 are close to those of IRF 2 and Newmark 2 is close to IRF 3 as expected. Figures 3.24 and 3.25 show velocity and acceleration responses due to a unit impulse respectively. These figures show similar trends to the displacement response in Figure 3.23, according to the calculation method used.

Velocity and acceleration of IRF 1 contains high frequency oscillation in modes r=0,1.

The time history of the midship bending moment is shown in Figure 3.26, and the corresponding Fourier transform in Figure 3.27. The estimated midship bending moment by IRF1, IRF3 and Newmark 2 are close to each other at the first mode wet resonance frequency of 8.445 rad/s. Figures 3.26 and 3.27 show that the contribution of $p_2(t)$ with a dominant frequency of 8.445 rad/s is large, while the contributions of $p_3(t)$ and $p_4(t)$ are small. The curves in Figure 3.26 show that the components of high frequency die out rapidly. The curve of the Fourier transform in Figure 3.27 shows two small peaks at high frequency around 18.7 rad/s and 32.2 rad/s (3 and 4-node wet resonance frequencies). However, it should be noted that the response at high frequencies decays fast, such that the Fourier transform may not be accurately carried out.

From Figures 3.23 to 3.27, it is concluded that the convolution integral method using the impulse response function estimated by the inverse Fourier transform may give correct results in the whole frequency range of excitation, while the system matrix for the Hamiltonian method and the Newmark-beta method need to be modified for the rigid body in order to calculate the transient response. For example, Domnisoru and Domnisoru (1977) calculated the hydrodynamic coefficients separately: the hydrodynamic terms of rigid modes are calculated using the ship oscillation frequency (i.e. heave/pitch resonance) and those of flexural modes are calculated at the first flexural mode frequency.

3.4.3.2 Response to a sinusoidal excitation

The principal coordinates and bending moments are calculated in the time domain for the ship travelling with Fn=0.275 in a regular head wave of unit amplitude encountered with frequencies ω_e=0.883 rad/s (i.e near heave/pitch resonance) and ω_e=8.445 rad/s (i.e. 2-node wet resonance). This is carried out in order to verify the consistency of the numerical methods used. The steady-state responses (frequency domain response) were evaluated using an existing methodology (Bishop et al. 1977). With the linear system, the steady-state response (SSR) is sinusoidal with the corresponding excitation frequency. The results calculated by the numerical methods of the previous section are compared with the steady state responses in the time domain. Figures 3.28 and 3.29 show the principal coordinates. Figure 3.28 shows that the principal coordinate estimated by SSR as well as IRF 1, IRF 2 and Newmark 1 are very close to the steady state response, in which the Hamiltonian method (IRF 2) and the Newmark method (Newmark 1) use the system matrix at one particular frequency (in this case, 0.883 rad/s). Those using IRF 3 are not particularly good as they increase with time, due to the system matrix being at a high frequency. In Figure 3.29, the principal coordinates of IRF 1, IRF 3 and Newmark 2 are close, for the higher modes, to the steady state response with the regular wave at an encounter frequency of $\omega_e = 8.445$ rad/s. Naturally those for IRF 2, using the Hamiltonian for a frequency of 0.883 rad/s show, by and large, different and smaller amplitudes.

It can be concluded that by and large the convolution integral methods and Newmark-beta method, provided the system matrices at the relevant ω_e are used, do not make much difference for a regular wave (single sinusoidal excitation). Furthermore use of the inverse Fourier transform method to obtain IRF is better for transient arbitrary excitation.

One other issue should be noted, with reference to **initial condition**. The motion is initiated from the steady state response of the frequency domain solution instead of being initiated from rest i.e. $p_o(t = t_o = 0) = \mathrm{Re}\left[p_o e^{i\omega_e t_o} \right]$, an approach followed by others (i.e. Fonseca and Guedes Soares 1998). For the Hamiltonian method, the complementary solution of the ordinary differential equation of motion is calculated according to the initial condition and added to particular integral solutions (Bishop and Price 1979). These complementary solutions by initial condition and homogeneous solution are shown in Figure 3.30. The fluctuation of these two responses may be cancelled out, so that total responses (black line) seem to be sinusoidal at the initial stage of the simulation, and this allows observation of a periodic response in the initial stage of simulation.

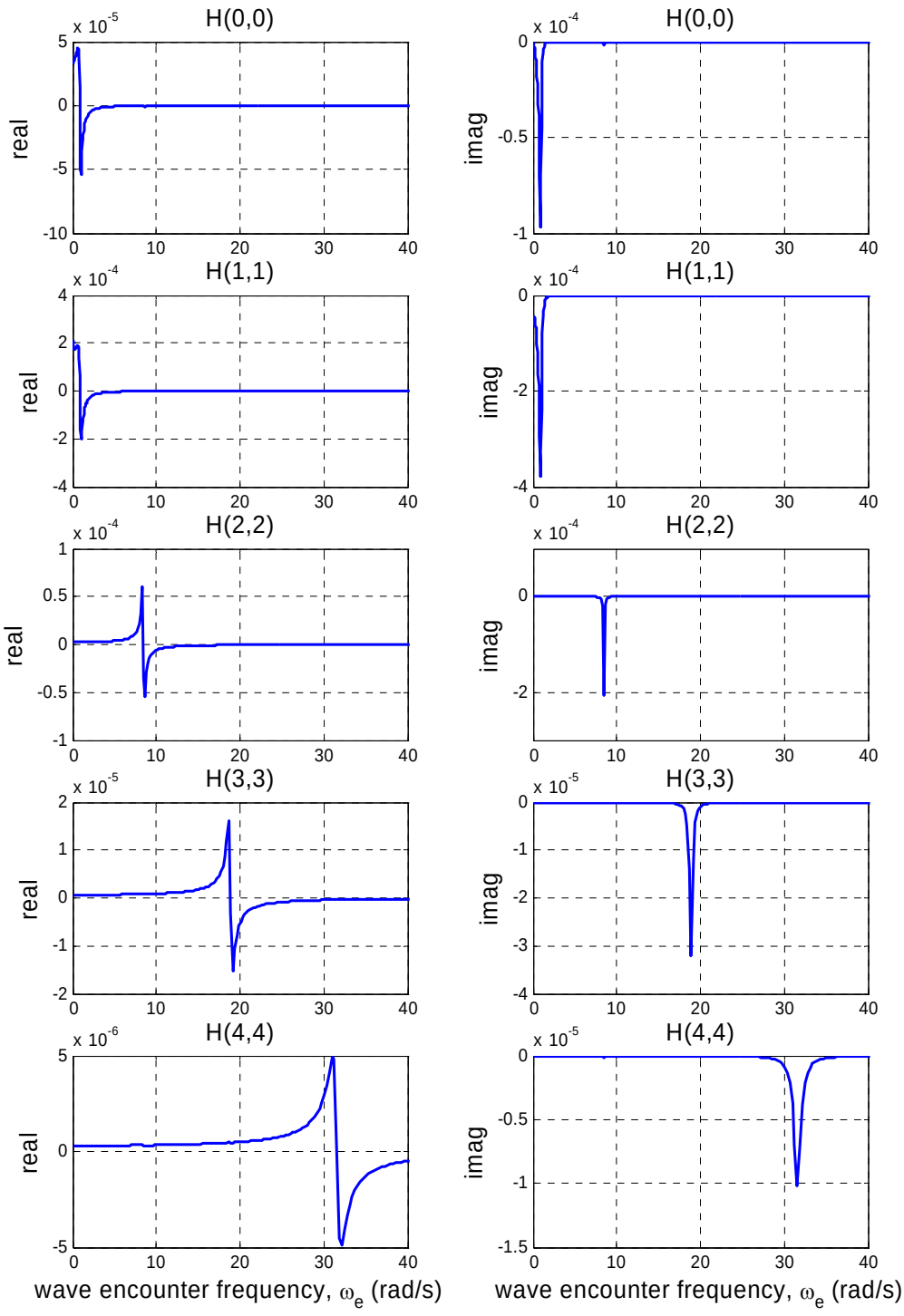

Figure 3.21 Diagonal terms of the complex frequency response function $H(\omega)$

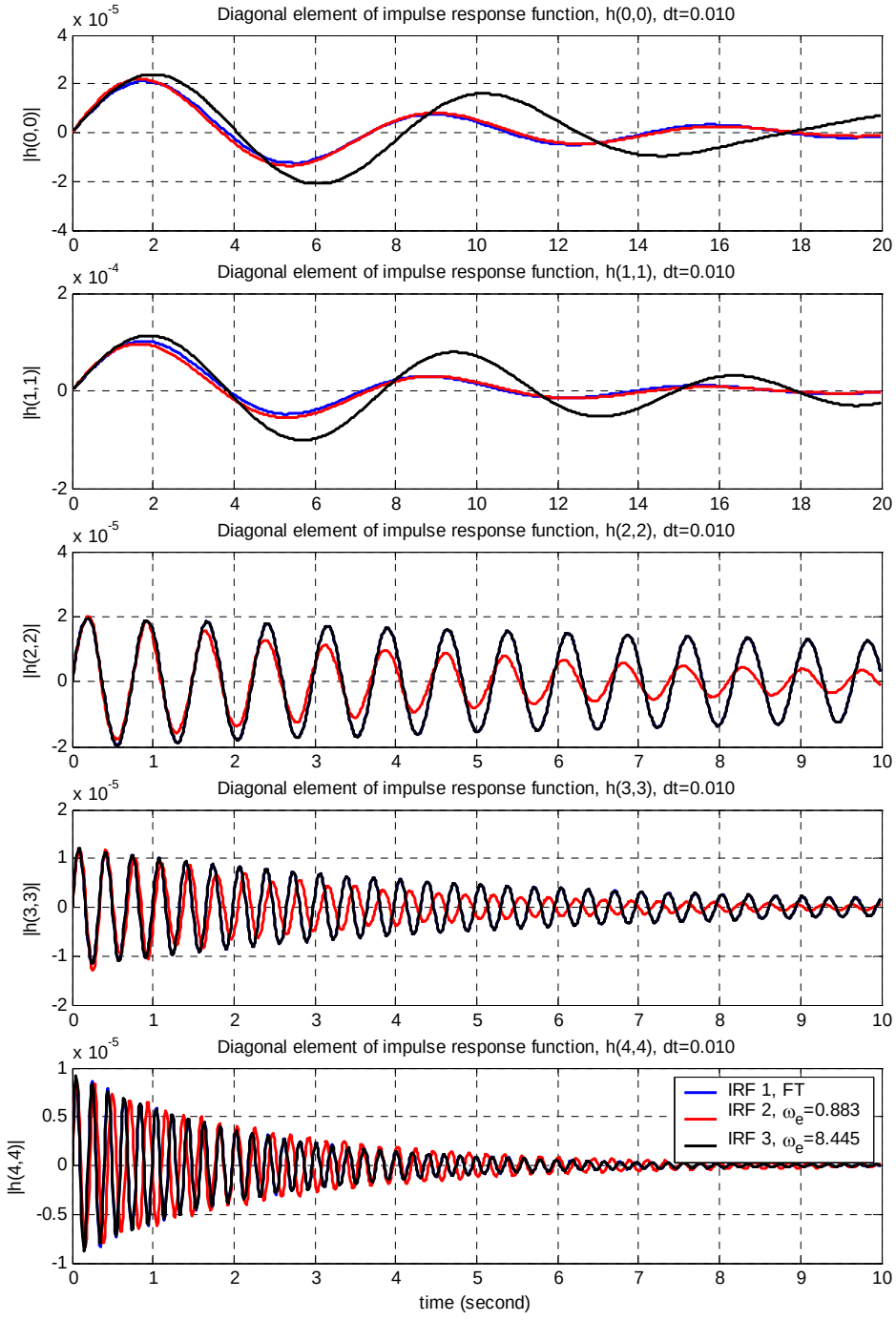

Figure 3.22 Diagonal elements of impulse response function h(t)

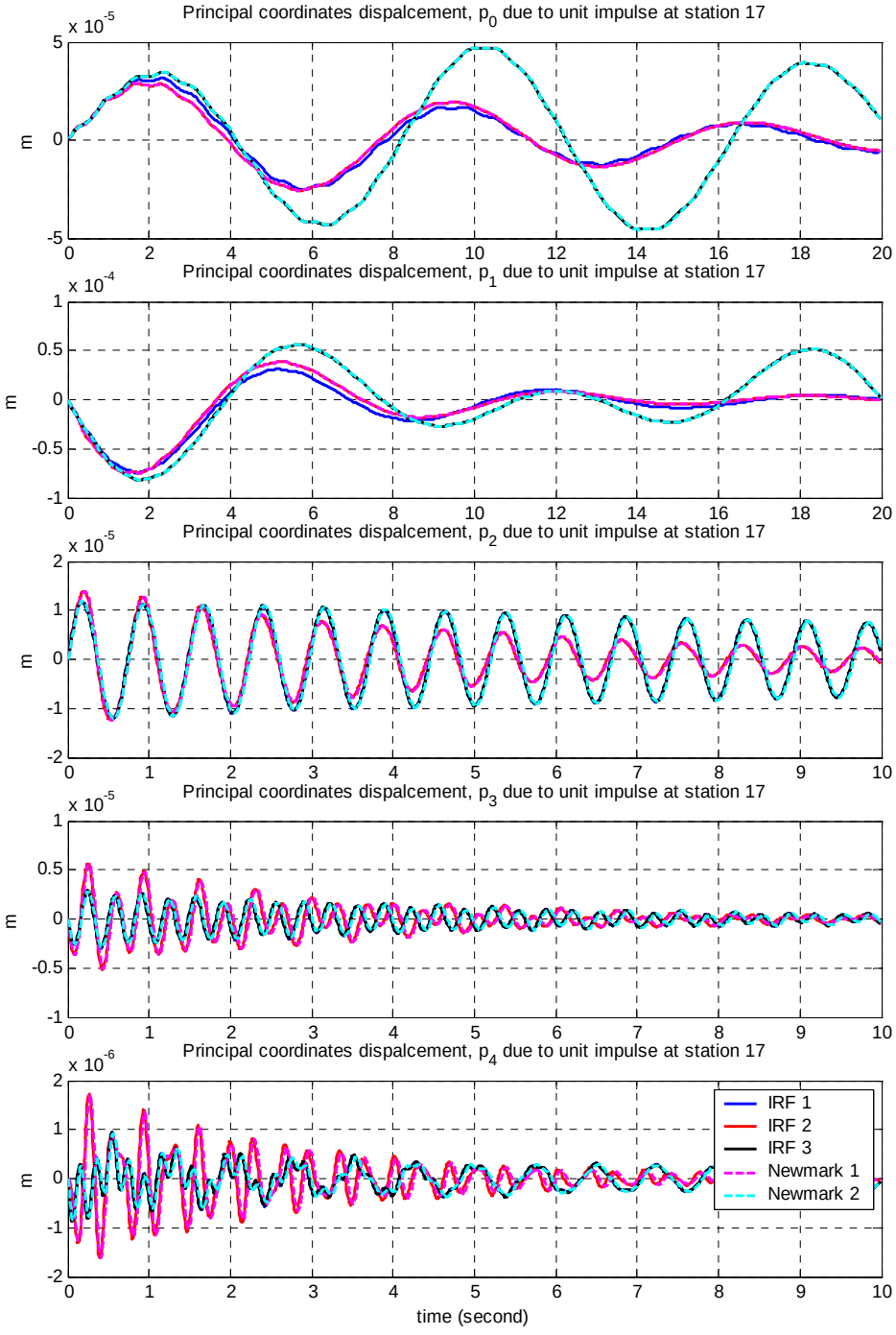

Figure 3.23 Principal coordinate due to unit impulse at station 17

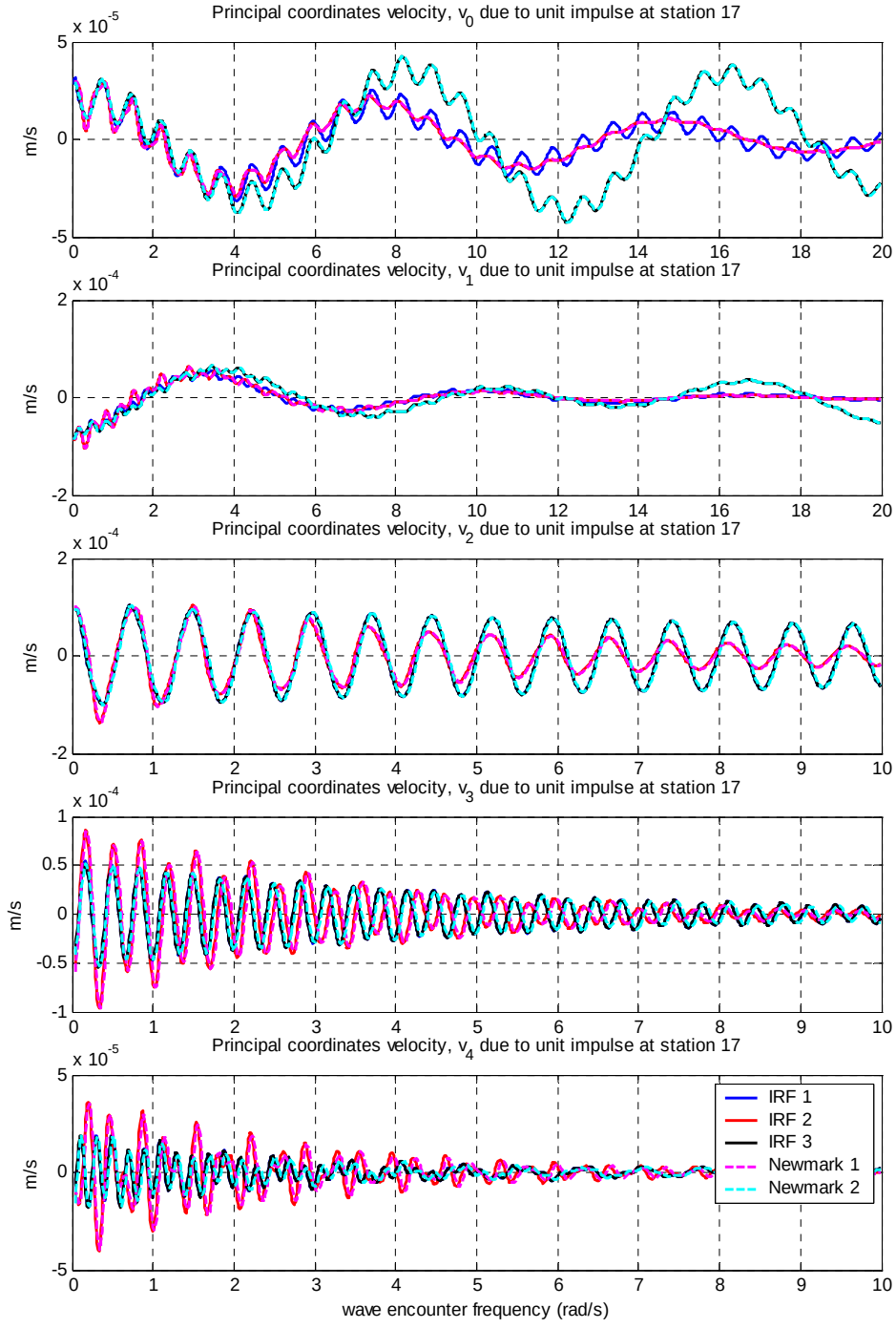

Figure 3.24 Velocity due to unit impulse at station 17

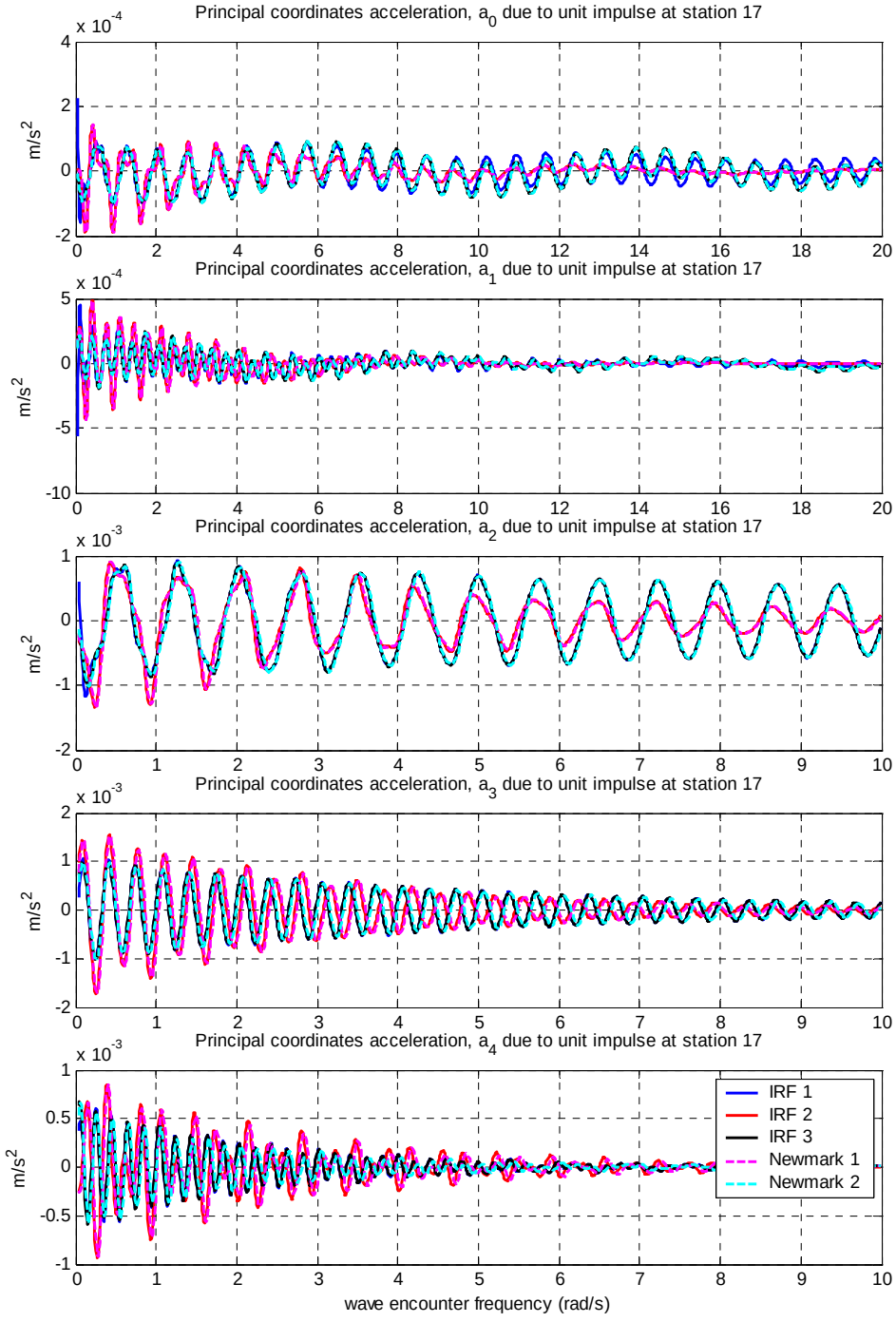

Figure 3.25 Acceleration due to unit impulse at station 17

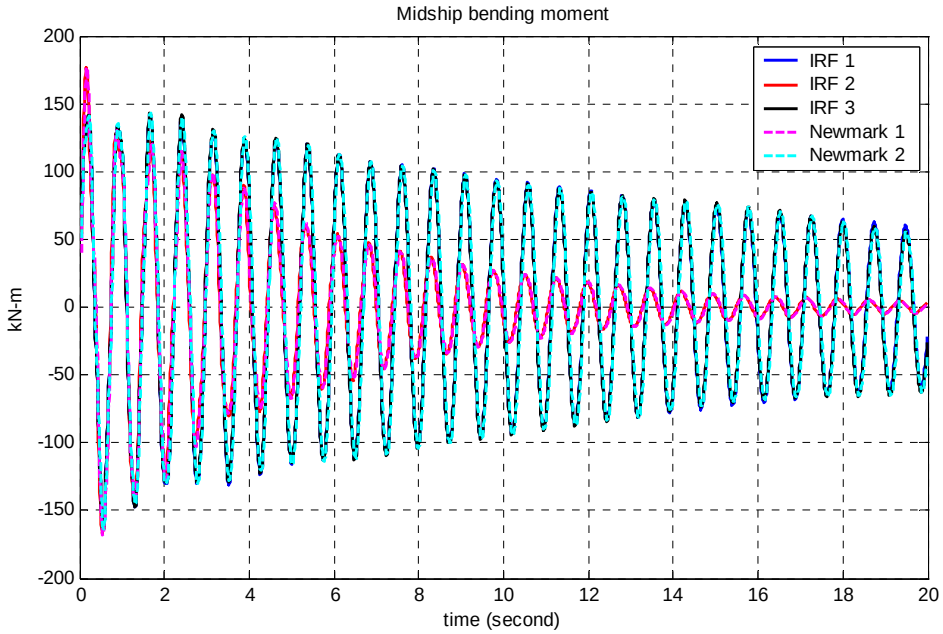

Figure 3.26 Time history of midship bending moment due to unit impulse

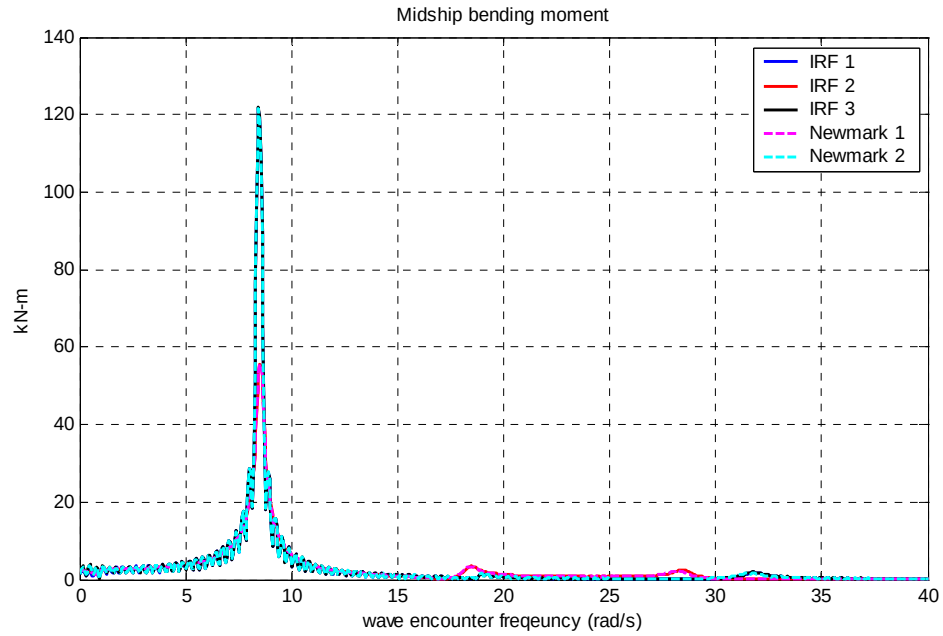

Figure 3.27 Fourier transform of midship bending moment

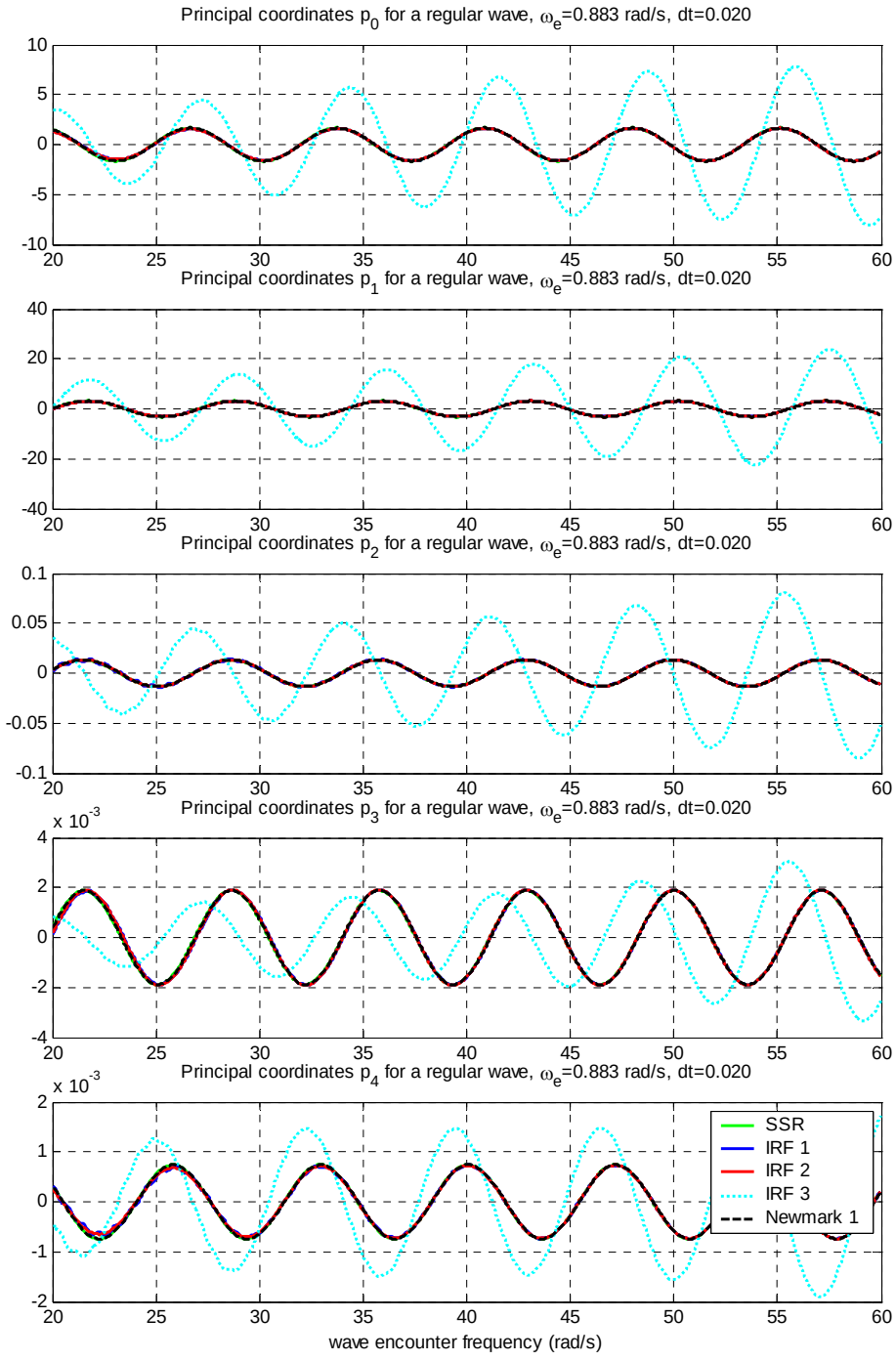

Figure 3.28 Principal coordinate amplitudes for a regular wave encountered with $\omega_e = 0.883$ rad/s

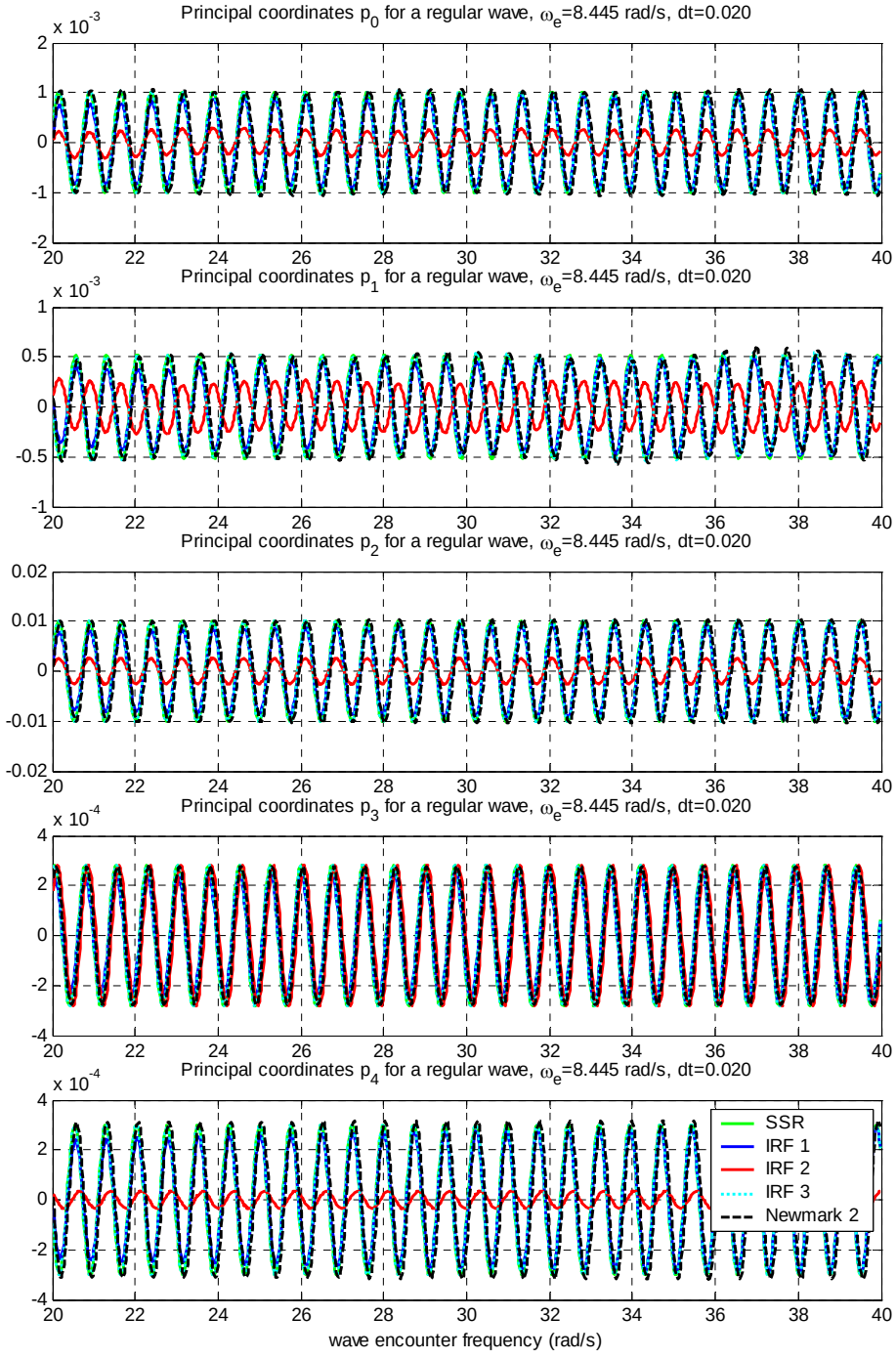

Figure 3.29 Principal coordinate amplitude for a regular wave encountered with $\omega_e = 8.445$ rad/s

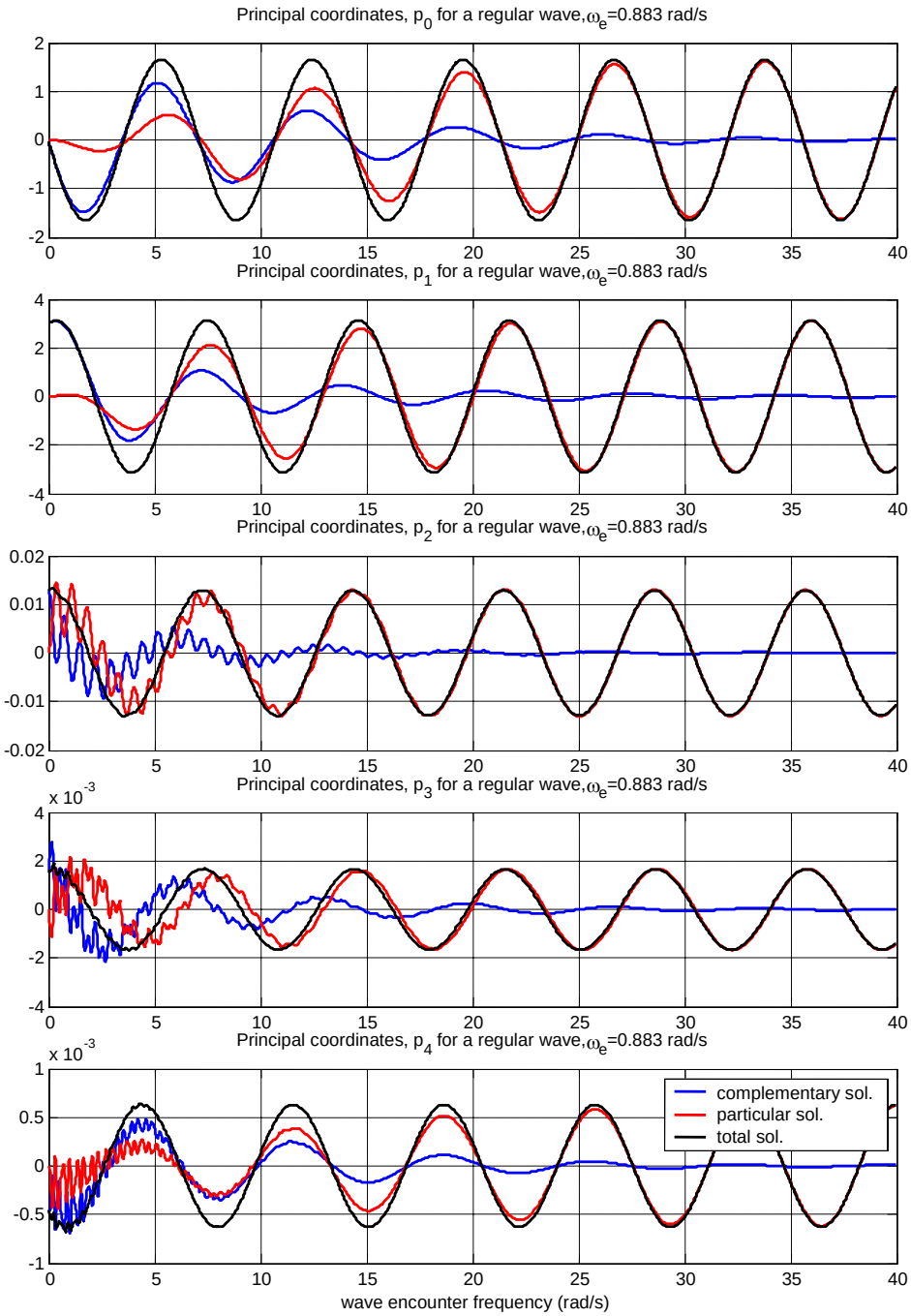

Figure 3.30 Principal coordinate amplitudes estimated by convolution integral method (IRF2) with the impulse response estimated by Hamiltonian method in considering initial condition at t=0

3.5 Conclusive remarks

1. The rigid body motion is only affected by a small amount due the number of modes in the modal summations. The vertical bending moment and shear force on the other hand are more sensitive, depending on position along the hull. Influence of the five modes (N=0, 1, 2, 3 and 4) are adequate to ensure convergence.

2. The convolution integral method using the impulse response function estimated by the inverse Fourier transformation may give correct results by comparison with steady state sinusoidal response for the whole frequency range of excitation while the system matrix for the Hamiltonian method and the Newmark beta direct integration method need to be modified, i.e. have the relevant wave encounter frequency properties in order to calculate transient response.

3. The added mass coefficients at mean draught are close to each other, whether using the Lewis form transformation or multi-parameter conformal transformation. The fluid damping coefficients differ slightly between the Lewis form and the multi-parameter mapping at bow and aft body sections. The Lewis form formulation is acceptable for its simplicity, however it is not accurate enough and may not describe well enough fluid forces, especially nonlinear effects considered in thenext section.

Chapter 4

Nonlinear Solution

4.1 Introduction

In the linear solution discussed in Chapter 3, time domain responses to a unit impulse response and a sinusoidal excitation due to a regular wave obtained. In the linear solution, the hydrodynamic coefficients were estimated at mean draught and assumed to be independent of time. That assumption is based on the small amplitude of motion and the wall-sided section profile. When a ship with large flare sections travels in large amplitude waves, the forces have to be estimated at instantaneous draught in a time domain simulation.

A ship travelling in a seaway moves up and down (only vertical motion is considered in the present study) and may regularly emerge and immerse from/into the water surface. The emergence and immersion conditions of the hull are considered as follows: When the ship (ship's keel) emerges from the water and re-enters, bottom slamming will occur (F_6). When the wave surface exceeds one-tenth of still water draught, the so called "flare slamming" force (F_1) comes into operation. When the wave surface exceeds deck level, green water (F_5) takes place. The bottom slamming (F_6) starts at bottom when the hull impinges into water surface and continues up to one-tenth of still water draught. The flare slamming (F_1) is applied above one-tenth of the draught until the hull moves upward again. Furthermore the modification of hydrodynamic force (F_2, F_3), Froude-Krylov and restoring forces (F_4) are applied during the whole procedure.

The equations of motion for large amplitude sinusoidal/regular waves (Equations

2.44 and 2.45) divided the nonlinear forces into six components, which allows estimation of the contribution of each force to the response. Parametric studies on these force components are performed and discussed. In summary, the following nonlinear forces and their combination, caused by hull geometry changes, are considered:

F_1: flare slamming force

F_2: nonlinear modification due to added mass variation

F_3: nonlinear modification due to fluid damping variation

F_4: nonlinear modification to hydrostatic restoring and Froude-Krylov force

F_5: green water effects

F_6: impact slamming force

During time domain simulation, the instantaneous draught is determined using the linear and the nonlinear responses. The linear responses of displacement, velocity and acceleration, given by in Equation 2.44, are calculated using the frequency domain solution for a given regular wave, and obtaining the time domain variation for this simple harmonic motion, rather than using any of the time domain solutions discussed in Chapter 3. Then, the total motion of the hull is determined by adding the current linear hull motion and the nonlinear hull motion at the previous time step. The instantaneous draught is obtained by subtracting the vertical displacement from the current wave elevation at any position along the hull. The nonlinear forces (F_i, i=1, … 6) are then calculated at the instantaneous draught using the relative motion and its derivatives for each section. As mentioned before, the reason for separating the linear and nonlinear parts in the equation of motion is to use linear (or mean draught) radiation and diffraction force in estimating the impulse response function as defined by Equation 3.7. It also means that the nonlinear effect of these radiation and diffraction forces is modified though the F_2 and F_3 force components. The

numerical convolution integral method is applied in calculating nonlinear responses in time domain simulations.

The ship is flexible so that structural dynamic effects of the flexural modes may contribute to wave loads, four flexible modes, N=4, were included in the analysis

4.2 Time domain simulation of nonlinear responses

The nonlinear responses are calculated in a linear manner; the nonlinear equation of motion from Equation 2.45 is presented as

$$[a+A]\{\ddot{p}_{nl}(t)\}+[b+B]\{\dot{p}_{nl}(t)\}+[c+C]\{p_{nl}(t)\}=\{F_{nl}(t)\} \tag{4.1}$$

and the nonlinear principal coordinates can also be calculated as

$$\{p_{nl}(t)\}=\int_0^t [h(\tau)]\{F_{nl}(t-\tau)\}\,d\tau \tag{4.2}$$

$$\{\dot{p}_{nl}(t)\}=\int_0^t [h_v(\tau)]\{F_{nl}(t-\tau)\}\,d\tau \tag{4.3}$$

$$\{\ddot{p}_{nl}(t)\}=\int_0^t [h_a(\tau)]\{F_{nl}(t-\tau)\}\,d\tau \tag{4.4}$$

where the impulse response functions $h(t)$ $h_v(t)$ and $h_a(t)$ are defined in Equations 3.7, 3.8 and 3.9 respectively.

Time domain simulations are carried out using the present method for the S175 container ship (see Chapter 3 for properties) travelling in regular head waves at a number of speeds, encounter frequencies and wave amplitudes investigated in the experiments by O'Dea et al. (1986), Watanabe et al. (1989), Chen et al. (1999). The nonlinear effects are illustrated in the form of various combinations of the separate forces in order to observe their influence.

Hydrodynamic coefficients are dependent on wave encounter frequency and the shape of the wetted section. The variation of sectional added mass and fluid damping coefficients with draught was calculated using 0.5 m intervals (-9.5 m denotes the keel line), as shown in Figures 4.1 and 4.2 for some sections (Stations 0, 5, 10, 15, 20, where 0 is A.P. and 20 is F.P.). Added mass, as shown in Figure 4.1, increases in general as draught increases, while the fluid damping does not. Fluid damping coefficients of midship section decrease as draught increases, because the beam-draught ratio becomes larger. The hydrodynamic coefficients are dependent on the beam-draught ratio and sectional area coefficient in the Lewis form formulation used. It should be noted that use of multi-parameter conformal mapping to describe all relevant hydrodynamic coefficients provide an improvement in accuracy, due to improved description of section shape (See Fig. 3.10). During the time simulation accounting for non-linear effects (F_1, F_2 and F_3), hydrodynamic coefficients at the appropriate instantaneous draught value along the ship are obtained by interpolation. When the wave elevation come over the deck (e.g. 10 m at station 20), the hydrodynamic coefficients (m, N) are assumed to be constant with those estimated at the deck level. Fluid actions above deck (green water) are included in the nonlinear force F_5.

In Chapter 2, the formulation of the hydrodynamic force was developed based on relative motions with Smith correction. When the draught changes, the Smith correction factor varies so that the new Smith correction factor needs to be calculated at the new draught. The Smith correction factor is dependent on sectional geometry and wave number, hence pre-calculation of the Smith correction factor was made at several wave heights for the given wave number of a regular wave (similar to Figure 3.13). The exact values of the Smith correction factor are obtained by interpolation at the instantaneous draught value along the ship.

The flare slamming force (F_1) has a coefficient, $\partial m_{nl}/\partial T$ in Equation (2.54) where m is added mass and T is draught. Figure 4.3 shows the coefficient, $\partial m_{nl}/\partial T$ at several forward sections. As the draught rises, especially for a bow section (Station 19) with a relatively large flare, $\partial m_{nl}/\partial T$ increases. Bottom flatness gives a large variation in $\partial m_{nl}/\partial T$ (e.g. station 10), which might be reflected in the evaluation of the influence of bottom slamming. However this effect is dominant at midship sections where bottom emergence rarely occurs, if it occurs at all. In the present calculation, the bottom impact force will be calculated using the empirical formula described in Chapter 2.4.2 and force F_1 is not included below 0.1 of the mean draught.

Figure 4.4 shows the deviation of added mass estimated at the mean draught from that estimated at instantaneous draught (m_{nl}), which is a coefficient for the nonlinear modification of the hydrodynamic force. Figure 4.5 shows the deviation in fluid damping in Equation 2.49, levels of which are comparable to the added mass. the effect of flare can be easily seen in these figures, through the large variations observed in the foremost station, when the instantaneous draught is far above the mean draught.

The instantaneous wave profile along the ship is important. Figure 4.6 shows two examples for vertical motion of the ship and the relative vertical motion, in the form of the instantaneous draught at two time instants, t=12 and t=15.5 seconds, for λ/L=1.2 and wave amplitude a=L/60, with Fn=0.275. The deck and bottom are also shown for convenience. In this calculation, five nonlinear forces (F_1, F_2, F_3, F_4 and F_5) are considered. From this figure, the relative vertical motion can be found and the occurrence of deck wetness can be ascertained if the freeboard is known. Figure

4.6 also shows whether the ship bottom emerges and, subsequently, impinges on the wave surface or not. The solid blue line indicates instantaneous draught based on linear analysis alone, while the dashed red line indicates those by including nonlinear analysis. Figure 4.6 shows that the hull emerges from bow to station 16 ($x/L=0.8$) in a linear response while the nonlinear response shows that the hull emerges up to around station 18 ($x/L=0.9$). Similar differences can be observed regarding the deck wetness. The differences indicate that it is important to consider the effects of non-linearities when evaluating the instantaneous draught and forces, F_i, i=1,…,6.

The time history of instantaneous draught at F.P. (station 20) is shown in Figure 4.7 for small and large wave amplitudes a=L/120, and a=L/60 with Fn=0.275, and λ/L=1.2. In this figure, the solid blue line (linear) indicates the overestimates compared with the dashed red line (nonlinear). It can also be seen that for the large amplitude wave, the nonlinear effects are more emphasized. The figures show that an increase in wave amplitude may cause bow emersion or deck wetness, but over predicted by linear analysis.

Figures 4.8 and 4.9 show heave and pitch motions, bow acceleration at 0.85L, bending moment and shear force at forward quarter for two wave amplitudes of a=L/120 and a=L/60 respectively, for the ship travelling at Fn=0.275 in regular head waves of length λ=1.2L. The nonlinear forces of F_1, F_2, F_3, F_4 and F_5 are considered. The heave and pitch motions in Figures 4.8 and 4.9 are close to a simple harmonic for the sinusoidal wave; however the amplitudes decrease in comparison with linear response, showing the nonlinear effects. The reduction in motions for higher amplitude waves (a=L/60 in Figure 4.9) are larger than those for lower amplitude waves (a=L/120 in Figure 4.8). The vertical bending moments and shear forces in both Figures 4.8 and 4.9 are not simple harmonic and the positive and negative peaks are not symmetric by comparison with linear solutions. By definition, the positive

and negative bending moments indicate the sagging and hogging moments, respectively. The nonlinear hogging moment does not change much compared with the linear one in both Figures 4.8 and 4.9. Sagging moments in Figures 4.8 and 4.9 show a large peak and some fluctuations. The fluctuation of the signal comes from the distortion responses of the hull vibration, mainly 2-node hull girder vibration, because of flare slamming. It is generally known that sagging moment is larger than hogging moment. In a sagging condition, the wave profile is high at the fore and after parts of the ship and low at amidships. In this condition, the large flare at the bow sections (and after body) creates a large buoyancy force, which increases the bending moment and the shear force. This cannot be considered to occur in the linear solution. On the contrary, in the hogging condition, the bending moment may decrease compared to the linear solution; however the deviation is not large compared with those for sagging moment because a flared section does not vary much below the still water line. In Figures 4.8 and 4.9, the shear forces, including the nonlinear effects in the sagging condition, are larger than those estimated by linear theory.

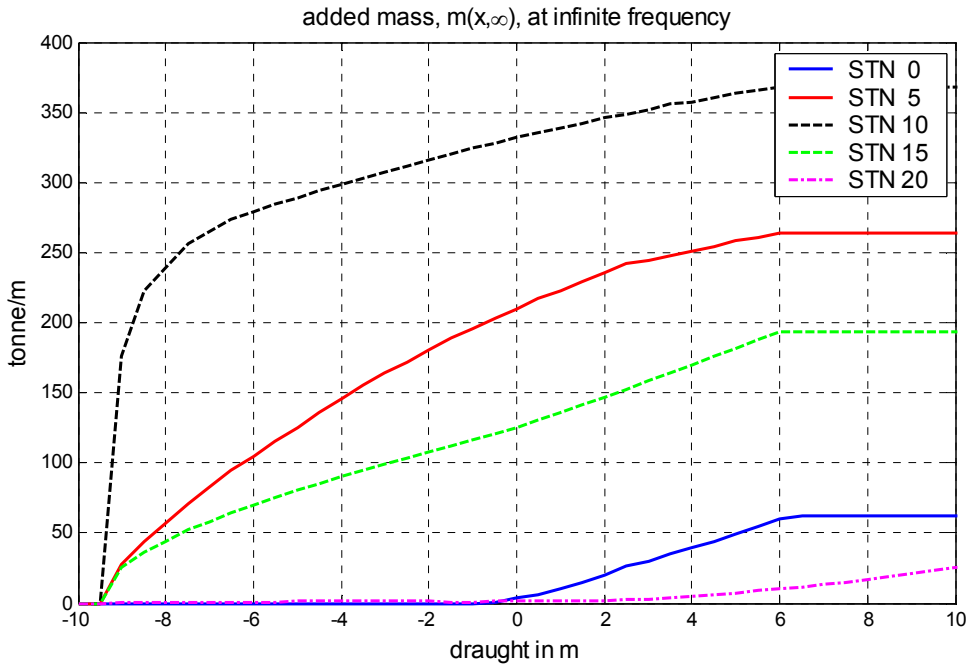

Figure 4.1 Variation of added mass according to draught at infinite frequency (in practice ω_e=37.5 rad/s was used), 0 denotes still water line

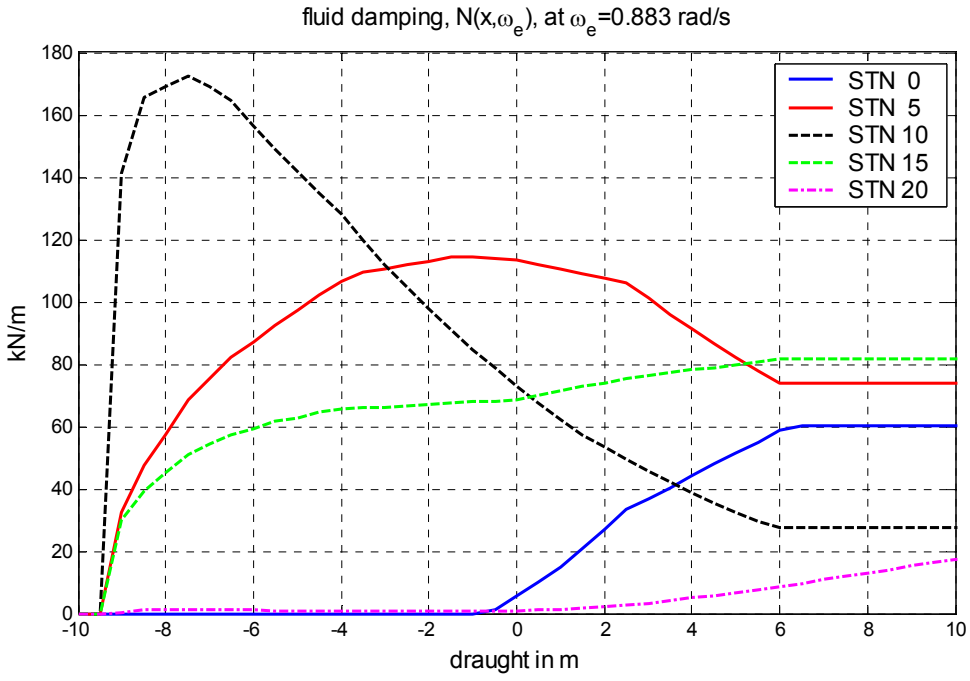

Figure 4.2 Variation of fluid damping according to the draught at $\omega_e = 0.883$ rad/s, 0 denotes still water line

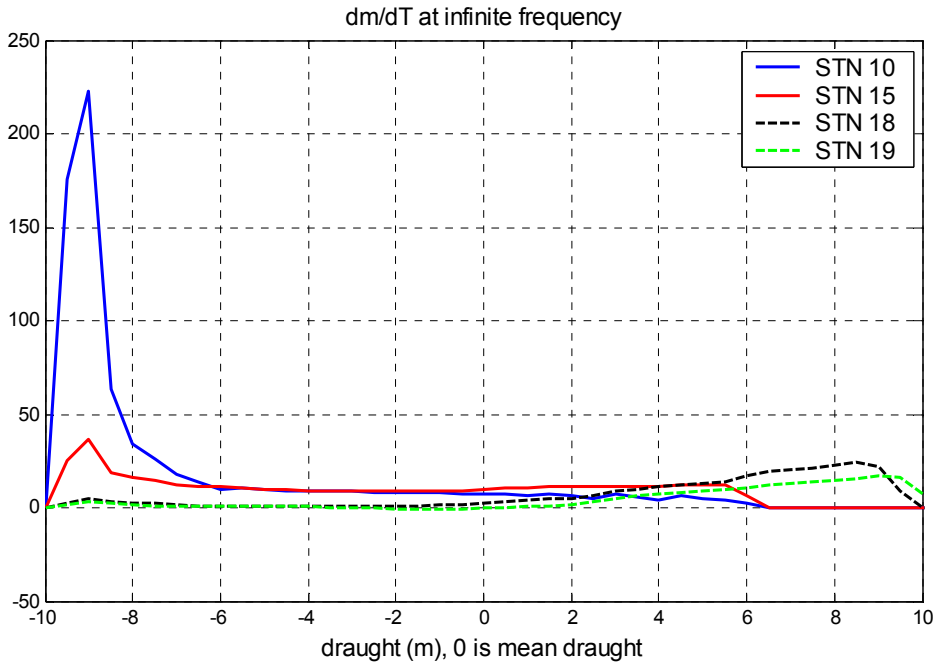

Figure 4.3 Variation of dm/dT with draught, involved in F_1 (flare slamming force)

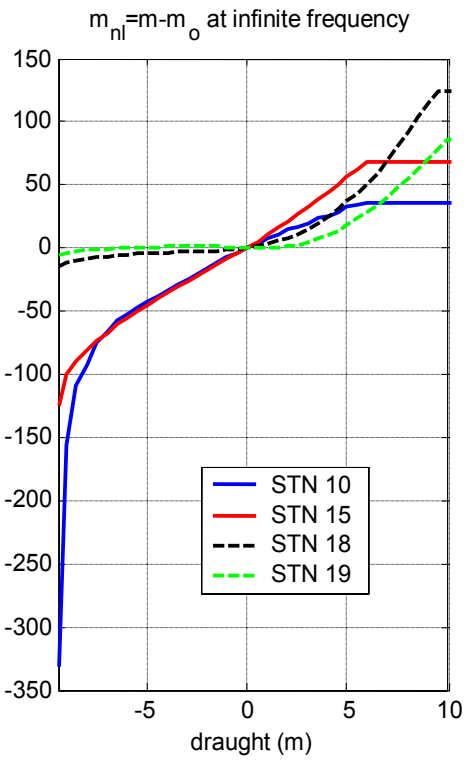

Figure 4.4 Added mass coefficient according to draught [units: tonne/m]

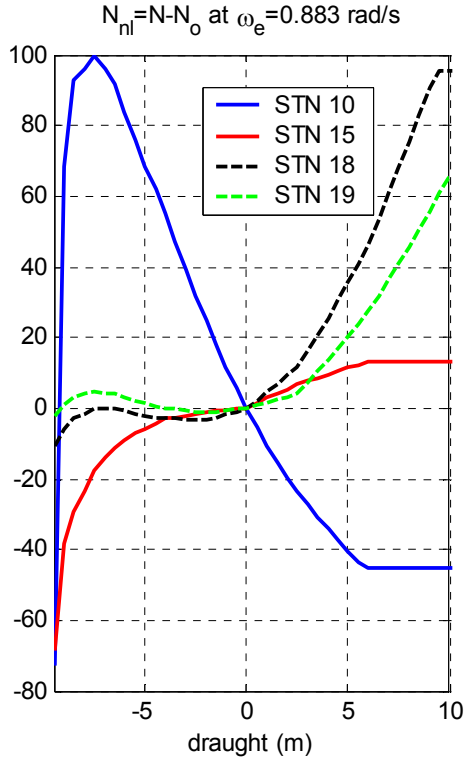

Figure 4.5 Damping coefficient according to draught [units: kN m/s^2]

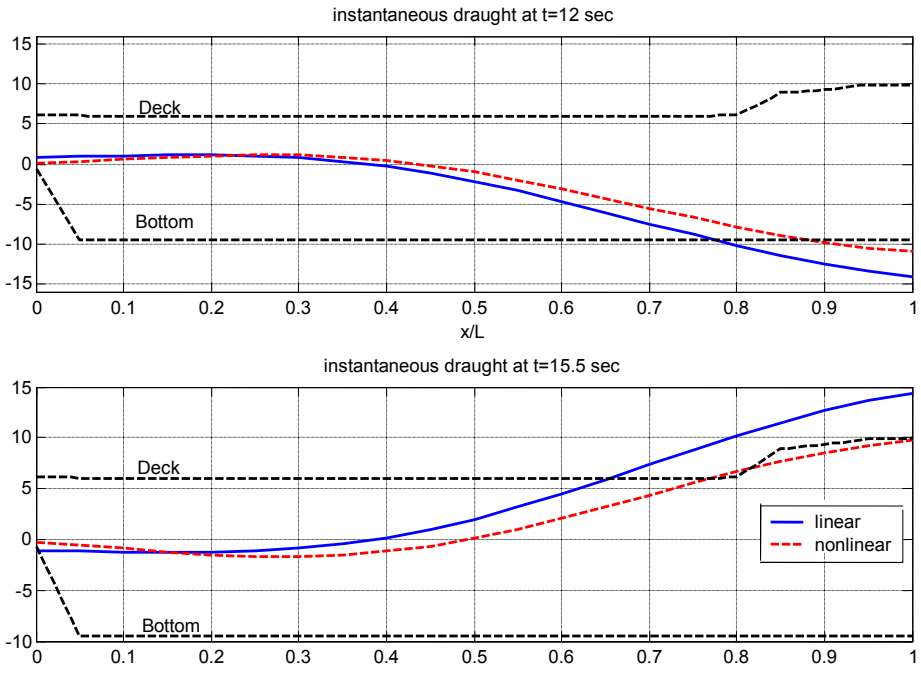

Figure 4.6 Instantaneous draught, λ/L=1.2, a=L/60, Fn=0.275

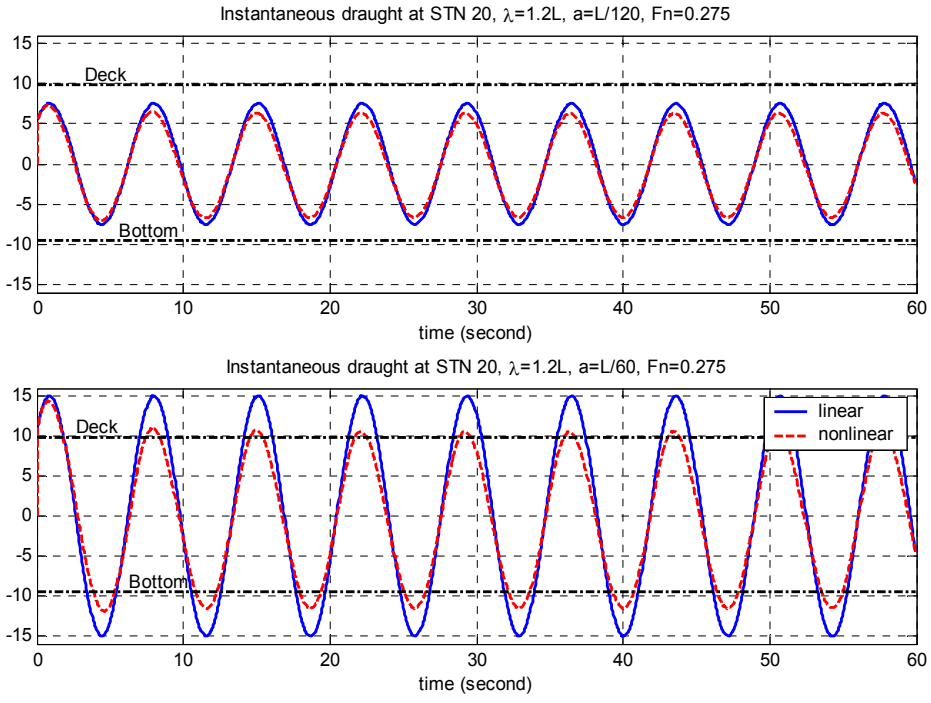

Figure 4.7 Instantaneous draught at station 20 (F.P), λ/L=1.2, a=L/120 and L/60, Fn=0.275

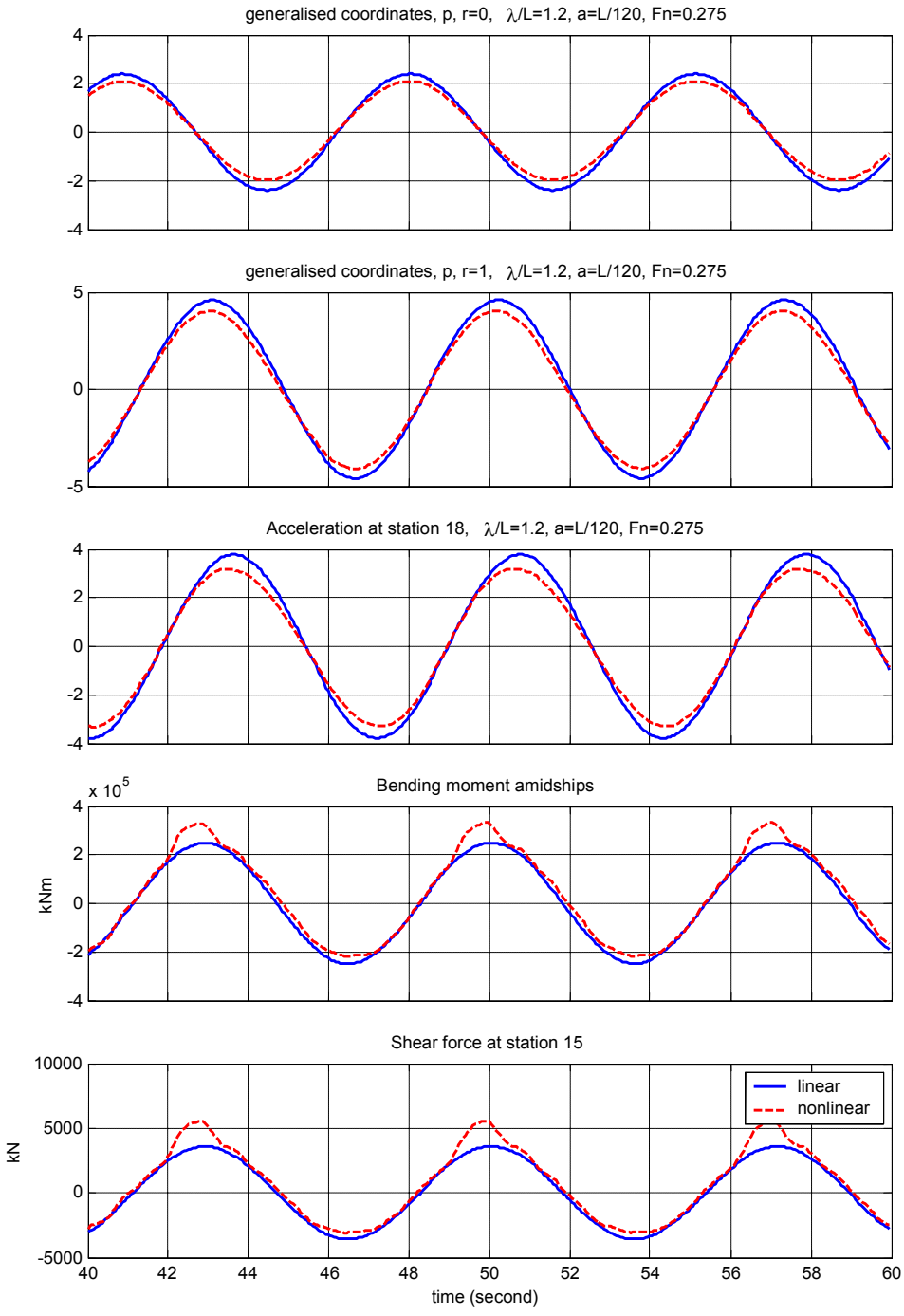

Figure 4.8 Time simulation of heave and pitch motions, bow acceleration at 0.85L, bending moment and shear force at 0.75L, λ/L=1.2, a=L/120, Fn=0.275

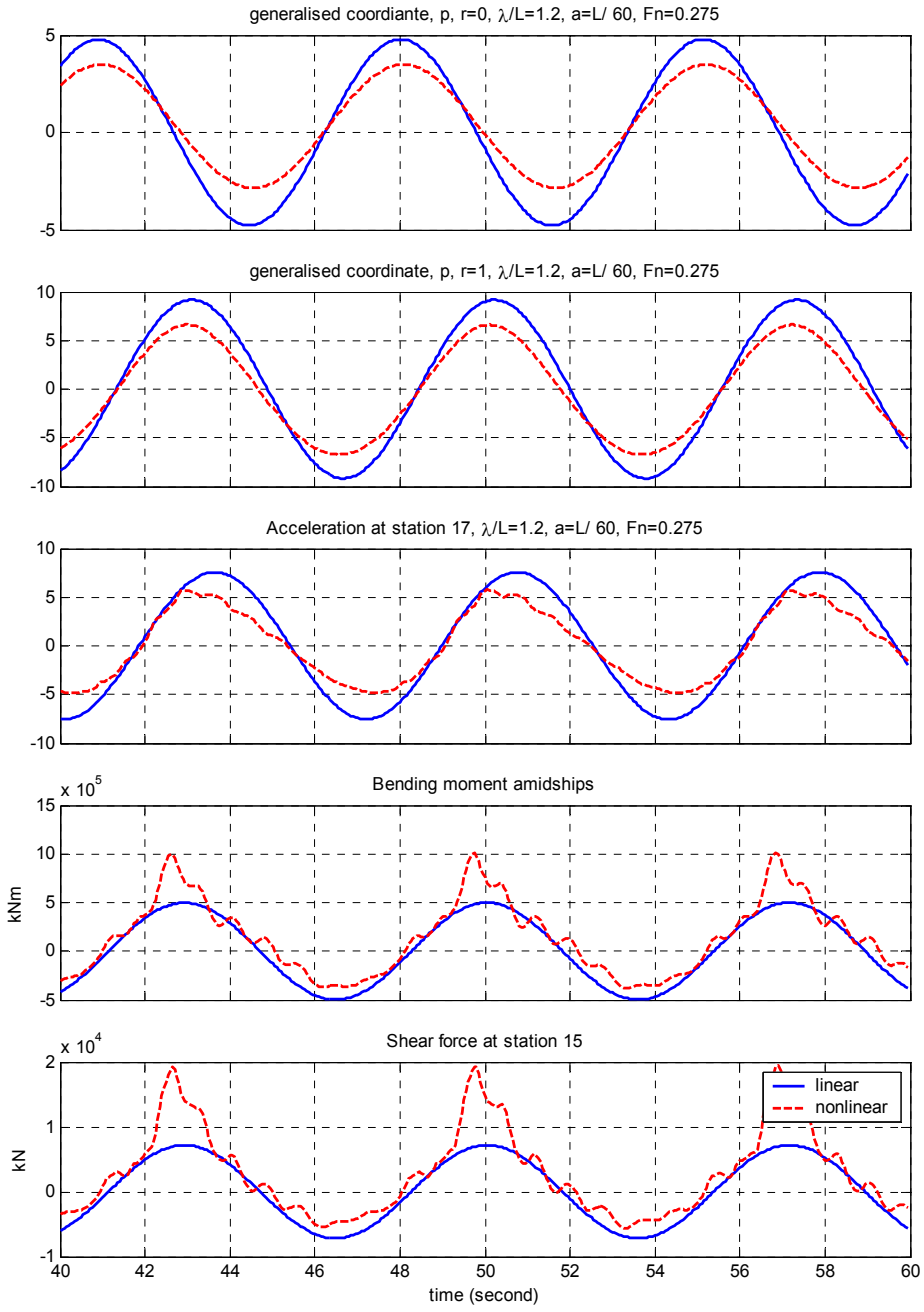

Figure 4.9 Time simulation of heave and pitch motions, bow acceleration at 0.85L, bending moment and shear forces at 0.75L, λ/L=1.2, a=L/60, Fn=0.275

4.3 Variation and Influence of nonlinear force components on the response

Figures 4.10 to 4.14 represent the time histories of the instantaneous draught and each nonlinear force (F_1, F_2, F_3, F_4 and F_5) at a number of sections along the ship for a regular head wave of λ/L=1.2, a=L/120 and a=L/60 at Froude number Fn=0.275. The solid blue line and solid red line indicate the nonlinear forces for a=L/120 and a=L/60, respectively, and the dashed blue line and dashed red line indicate corresponding instantaneous draughts for a=L/120 and a=L/60, respectively. The deck and bottom lines for each section are also presented in black. Although the time histories and components of each individual force component as shown separately, the instantaneous draught is calculated using all components.

F_1 in Figure 4.10 occurs only during negative relative motion (hull immersing) because when the hull is emerging, F_1 cannot pull the hull (i.e. F_1 is negative), hence it has an intermittent appearance. F_1 is assumed to continue until the instantaneous draught rises up to deck, so the duration time of one cycle flare slamming force is about 3~4 seconds for a regular wave of λ/L=1.2 (wave period is 7.1 seconds). The flare slamming force is the force due to the rate of change of the added mass with time (see Equation 2.47). The first and second graphs (at station 20 and 18) in Figure 4.10 show double peaks. As shown in Figure 3.10, the bow sections under using Lewis form mapping cannot reflect the bulbous shape properly. The change of added mass (i.e. $\partial m/\partial T$) is small for such a Lewis form, which may make double peaks. A multi-parameter mapping technique or a panel method can be used, in order to estimate more accurately hydrodynamic forces for such complex section shapes. When the hull re-enters the water, a large amplitude F_1 force occurs, because of the

rapid change of added mass (see Figure 4.3). In Section 2.3, it was noted that flare slamming is assumed to have an effect above 0.1 mean section draught, so the F_1 force between hull bottom to 0.1 draught will be omitted and instead the estimated bottom slamming force will be considered. In Figure 4.10, the maximum magnitude (350 kN/m) of F_1 due to a regular wave of a=L/60 occurs at station 18 and it is much larger than that of a=L/120, 80 kN/m. The magnitude of force F_1 decays around amidships and increases again as approaching A.P. The ninth graph (station 0) in Figure 4.10 shows that stern slamming occurs, for example, at 43.7 seconds and then the F_1 force rises to 210 kN/m. At the instant of 42.4 seconds, the bow section immerses below the water surface, as shown in the first graph in Figure 4.10. This is an indication that the method can be observed by looking at the instantaneous draughts.

The nonlinear modifications of radiation and diffraction force are shown in Figures 4.11 (a,b) and 4.12 (a,b). In Equations 2.48 and 2.49, those forces were divided into added mass force (F_2, Figure 4.11) and damping force (F_3, Figure 4.12). Both figures are estimated for two regular wave amplitudes of a=L/120 and a=L/60 with λ/L=1.2, Fn=0.275. The magnitude of F_2 force in Figure 4.11a becomes large (negative) when the instantaneous draught reaches its peaks and begins to decreases in the fore part of the ship. The excitation force may increase as draught rise. When the draught is below still water line, for example, from 45 seconds to 49 seconds, there is a small magnitude F_2 force at stations 20 and 17 (the first and second graphs in Figure 4.11a) compared with sections in the vicinity of amidships (the third and fourth graphs). This is because the added mass of the fore sections of the ship below the still water line do not vary significantly with draught, as was shown in Figure 4.4. The trend of the first graph (station 20) is somewhat different to the other graphs in Figure 4.11a, because the dominant term in F_2 (see Equation 2.48, F_{21} force is the first term and F_{22} is the second term in Equation 2.48) at the bow section is the speed dependent term

(F_{22}), while acceleration term (F_{21}) is dominant at other sections as illustrated in Figure 4.11b. The magnitude of F_2 force (with a=L/60) is two to three times that obtained with a=L/120.

The first graph in Figure 4.12a shows that F_3 force at station 20 is relatively large, and it is positive when draught increases so that it magnifies the total hydrodynamic force at the bow section. The speed dependent term F_{32} (the second term in Equation 2.49) is dominant at fore sections, as shown in the first to third graphs in Figure 4.12b. The sectional fluid damping coefficients are affected by the shape of the wetted area, i.e. area-beam ratio and beam-draught ratio in the Lewis form formulation, so the deviation of fluid damping coefficients is not simply dependent on variation with draught. In Figure 4.2, the damping coefficients amidships decrease as draught rises, which is the opposite trend to the other sections. The fourth graph in Figure 4.12a shows that F_3 force is mainly positive at the midship section compared with negative values at other sections.

The time history of the nonlinear restoring and Froude-Krylov force (F_4) at λ/L=1.2 and Fn=0.275 is shown in Figure 4.13a. According to the definition of F_4 in Equation 2.50, it is noted that this nonlinear Froude-Krylov force is the difference between the linear Froude-Krylov force together with the fluid restoring force and the direct integral of dynamic pressure on the wetted hull at instantaneous draught. In Figure 4.13b, these two linear and nonlinear forces, respectively, are plotted separately for a wave with a=L/60. The last term in Equation 2.50 is defined as F_{40}, with remaining nonlinear terms denoted F_{41}. Figure 4.13a shows that the nonlinear force at the bow sections increases much more in comparison with that of the midship section, thus confirming that the nonlinear effects increase with larger flare. When green water occurs at station 20, nonlinear F_{41} stays nearly constant (see Figure 4.13b). This means that there is no additional hydrostatic Froude-Krylov force. On the other hand,

the linear Froude-Krylov force cannot reflect this effect. Figure 4.13b shows that F_{41} force is much larger at the bow section, when the deck gets immersed, compared with F_{40}. For other sections, the magnitude between F_{40} and F_{41} shows little difference.

Figure 4.14 shows the time history of the green water force (F_5 in Equation 2.61) using the quasi-static approach for $\lambda/L=1.2$, $a=L/60$ and $Fn=0.275$. F_{51}, F_{52} and F_{53} denote the fluid weight, the rate of change of water height and the inertia of fluid, first, second and third terms respectively. The inertia of fluid (F_{53}) is the main component of total green water force and it is negative (push on the deck), together with fluid weight (F_{51}), while green water occurs. On the other hand, the force due to the rate of change of water height (F_{52}) is positive (pull on the deck), acting as the modification of total force on deck. The resultant F_5 force would be positive when the green water leaves the deck, but physically impossible, and is always negative (Wang et al. 1998). In the current application, the impact force induced by a water-jet event which may be negative, is not considered. When the incident wave height is $a=L/120$, deck immersion does not happen at all, as shown in Figure 4.7.

The generalised forces of F_1, F_2, F_3, F_4 and F_5 are shown in Figures 4.15 and 4.16, with regular waves of $a=L/120$ and $a=L/60$, respectively, at $Fn=0.275$, respectively. Figure 4.17 presents the generalised force for $a=L/60$ at $Fn=0.2$. Figure 4.15 shows that the generalised forces of F_3 and F_4 are the most influential for all modes. F_1 and F_2 are a little smaller. The nonlinear generalised forces become larger as wave height increases (Figure 4.16, compared with Figure 4.15). F_1 is larger at the first mode (heave) and F_3 is large at the fifth mode (r=4). When the wave height rises to $a=L/60$ in Figure 4.16, F_1 and F_3 become dominant. F_4 is important in both cases. The linear forces (F_{lin}) shows diffraction and Froude-Krylov forces estimated at mean draught. The generalised force when the ship speed reduce to $Fn=0.2$ is shown in Figure 4.17.

F_4 force is dominant for all modes, and is a little smaller at low speed (Fn=0.2). From Figures 4.15 to 4.17, it may be said that F_4 is the most influential for all of the case simulation and F_2 is also large with generally an opposite sign to F_4. F_3 is larger at higher modes, especially the fifth mode. F_5 is shown as being magnified 100 times in Figures 4.16 to 4.17 and is relatively small compared to other components. In general, the amplitudes of nonlinear wave excitation forces F_1, F_2, F_3 and F_4 are not so different as to indicate a dominant force among them.

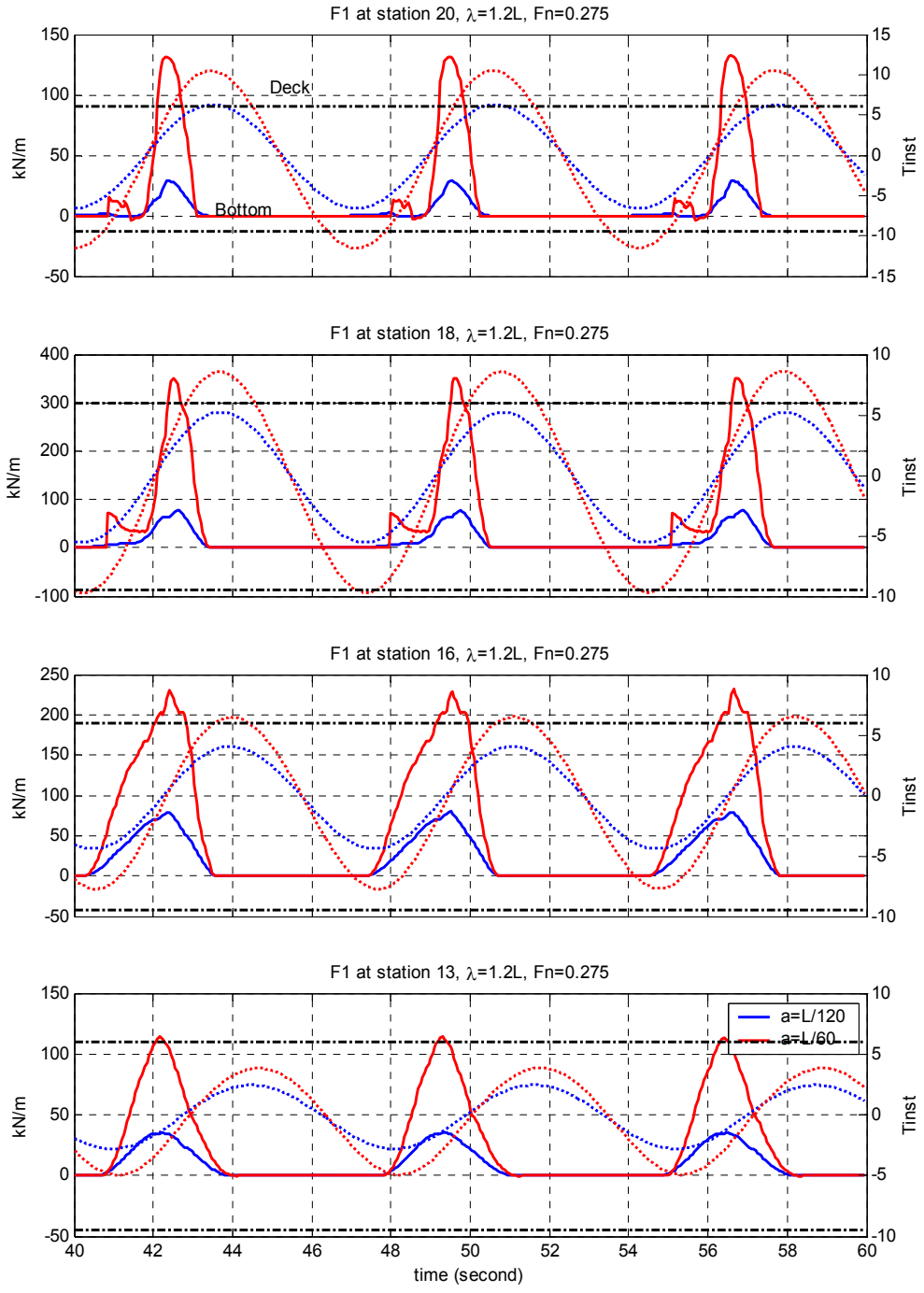

Figure 4.10 Flare slamming force (F_1), λ/L=1.2, Fn=0.275 (STN 20~13) (continued)

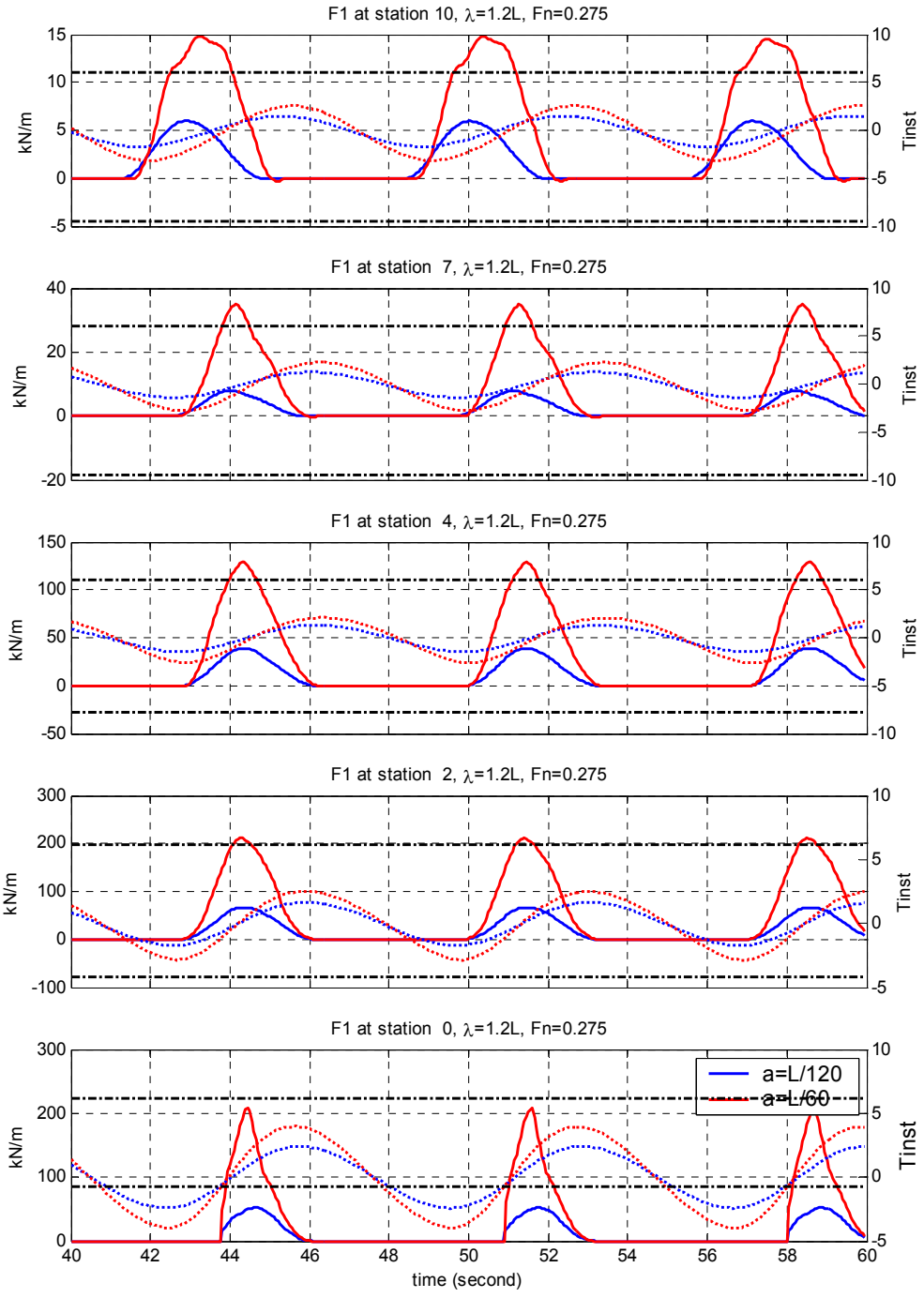

Figure 4.10 Flare slamming force (F_1), λ/L=1.2, Fn=0.275 (STN 10~0)

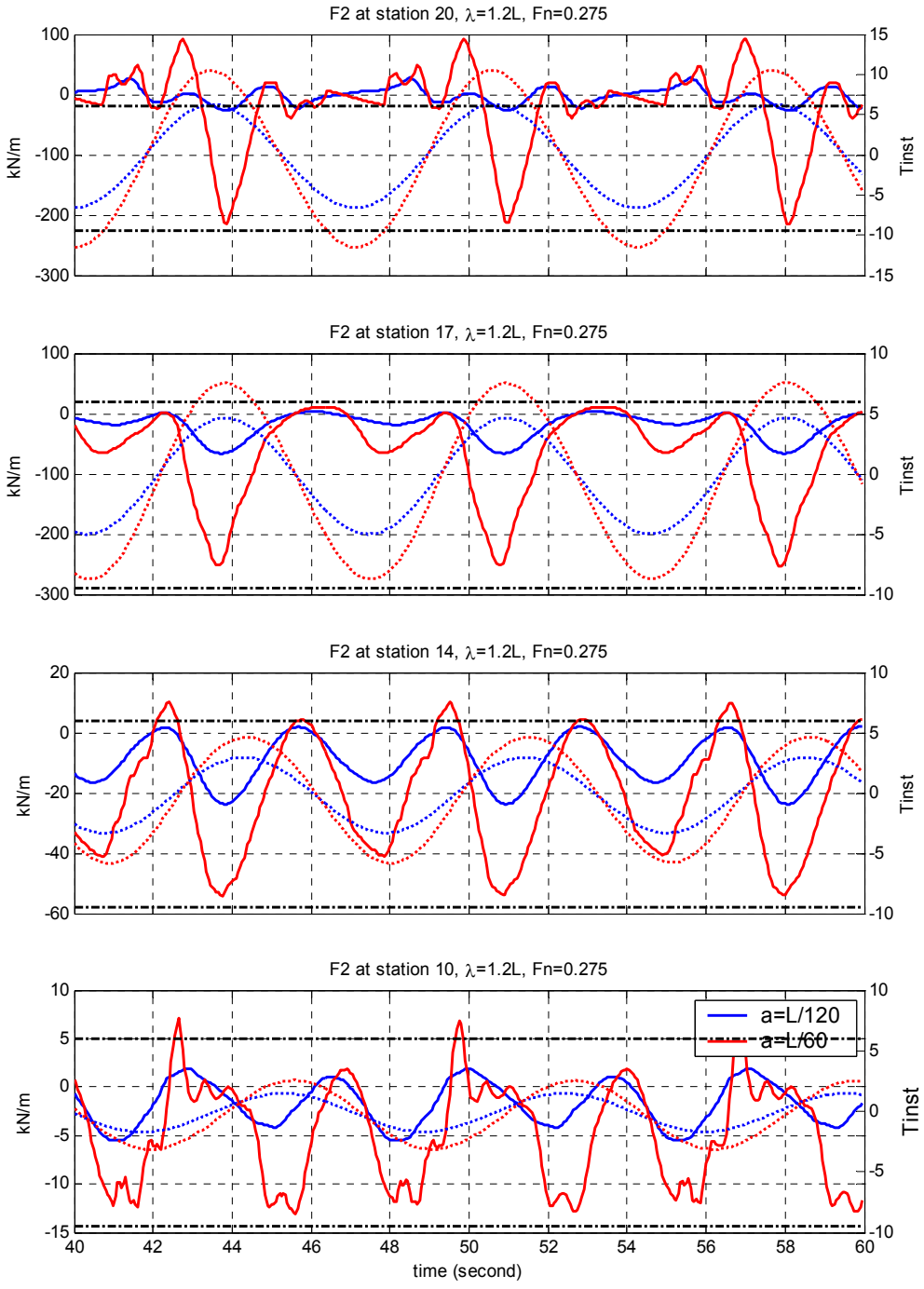

Figure 4.11a Nonlinear modification of added mass force (F_2), λ/L=1.2, Fn=0.275

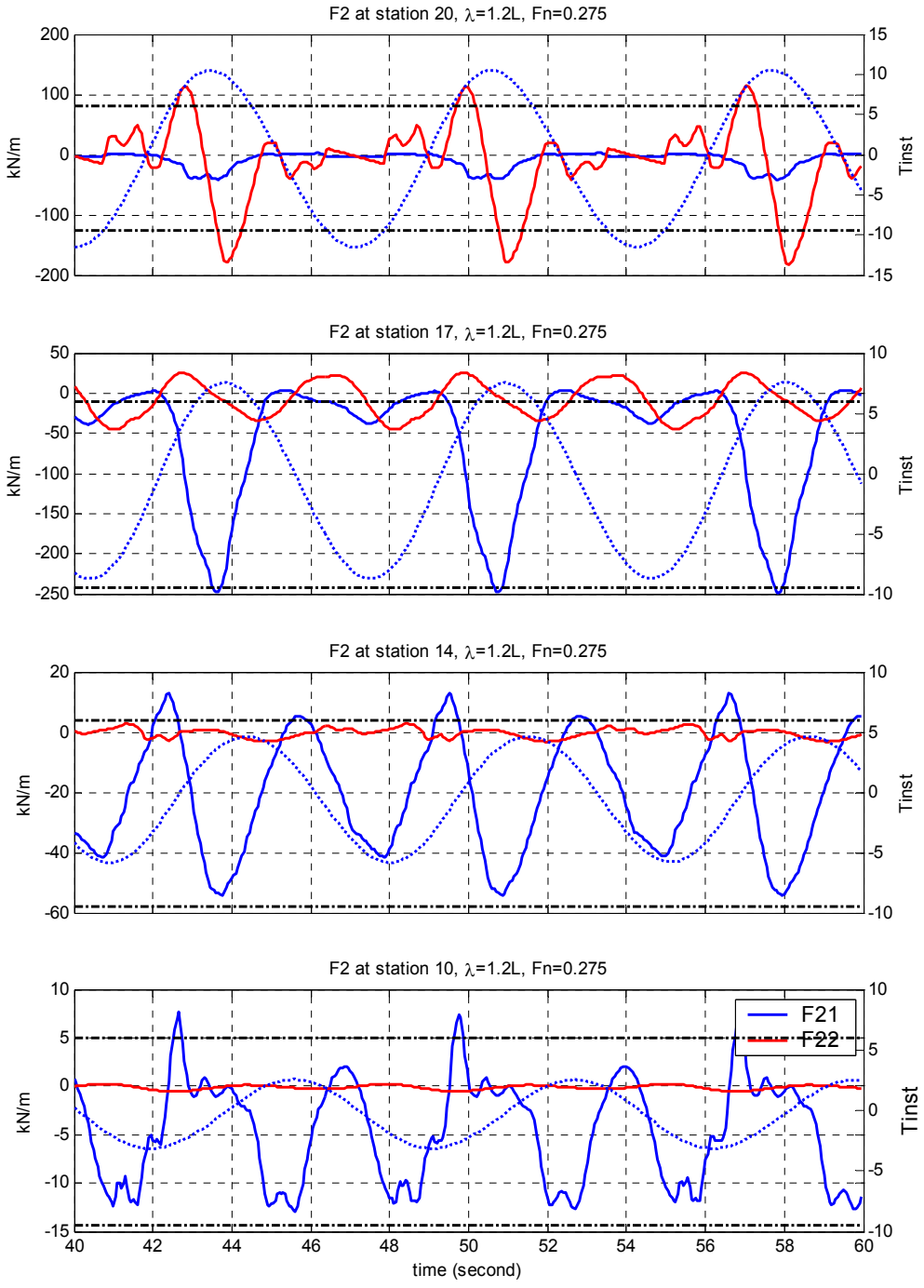

Figure 4.11b Nonlinear modification of added mass force (F_2), λ/L=1.2, Fn=0.275

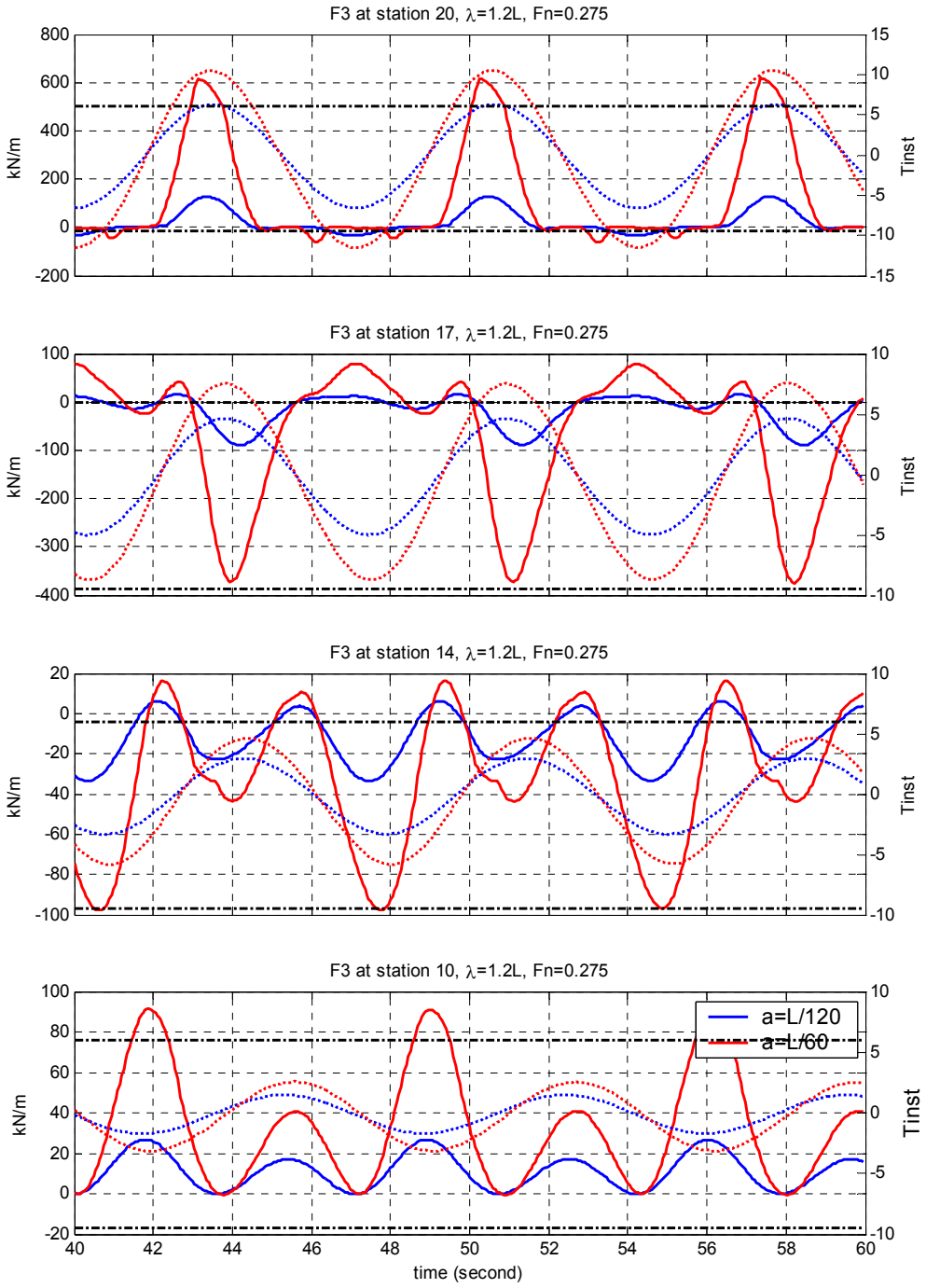

Figure 4.12a Nonlinear modification of fluid damping force (F_3), λ/L=1.2, Fn=0.275

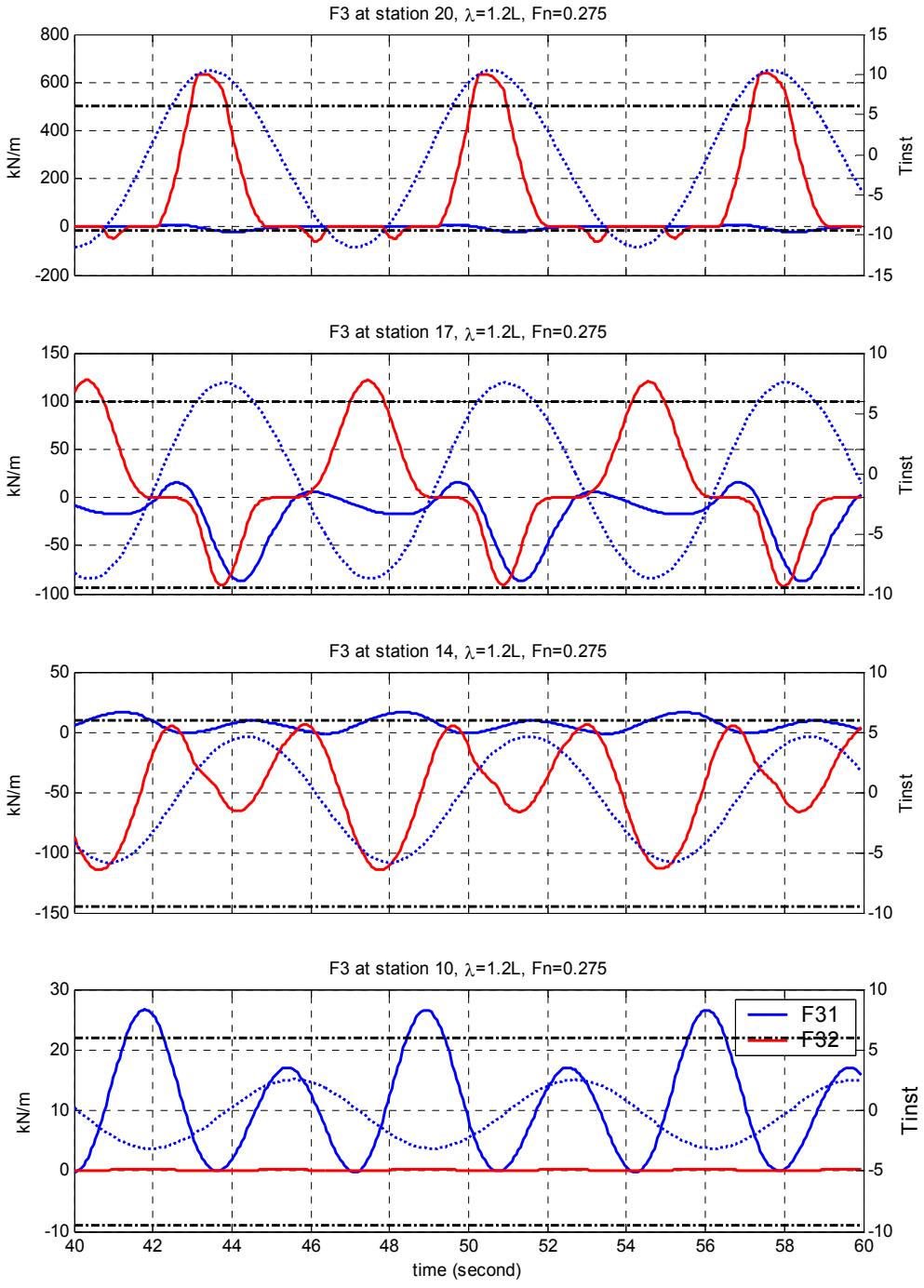

Figure 4.12b Nonlinear modification of fluid damping force (F_3), λ/L=1.2, Fn=0.275

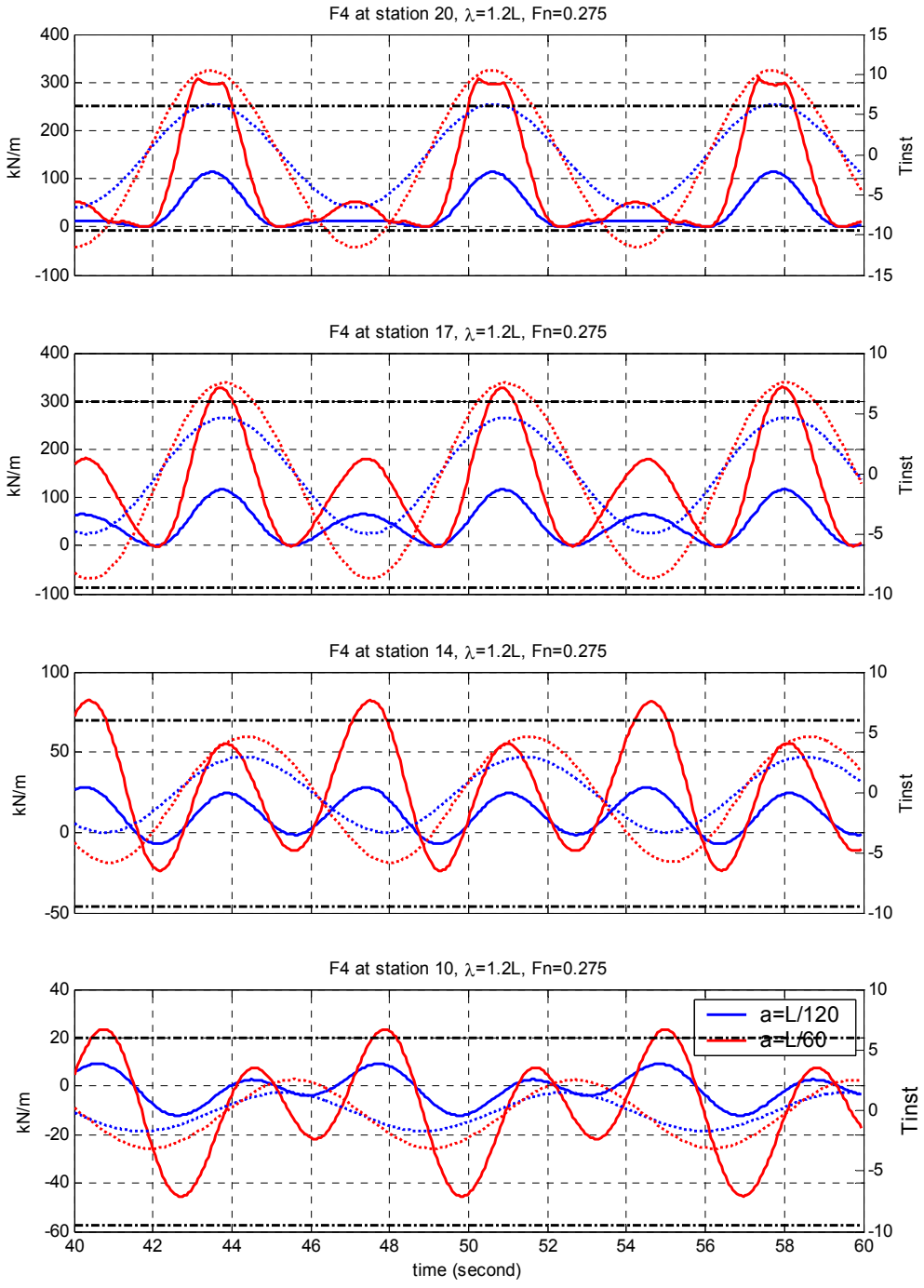

Figure 4.13a Nonlinear Froude-Krylov force and hydrostatic restoring force (F_4), λ/L=1.2, Fn=0.275

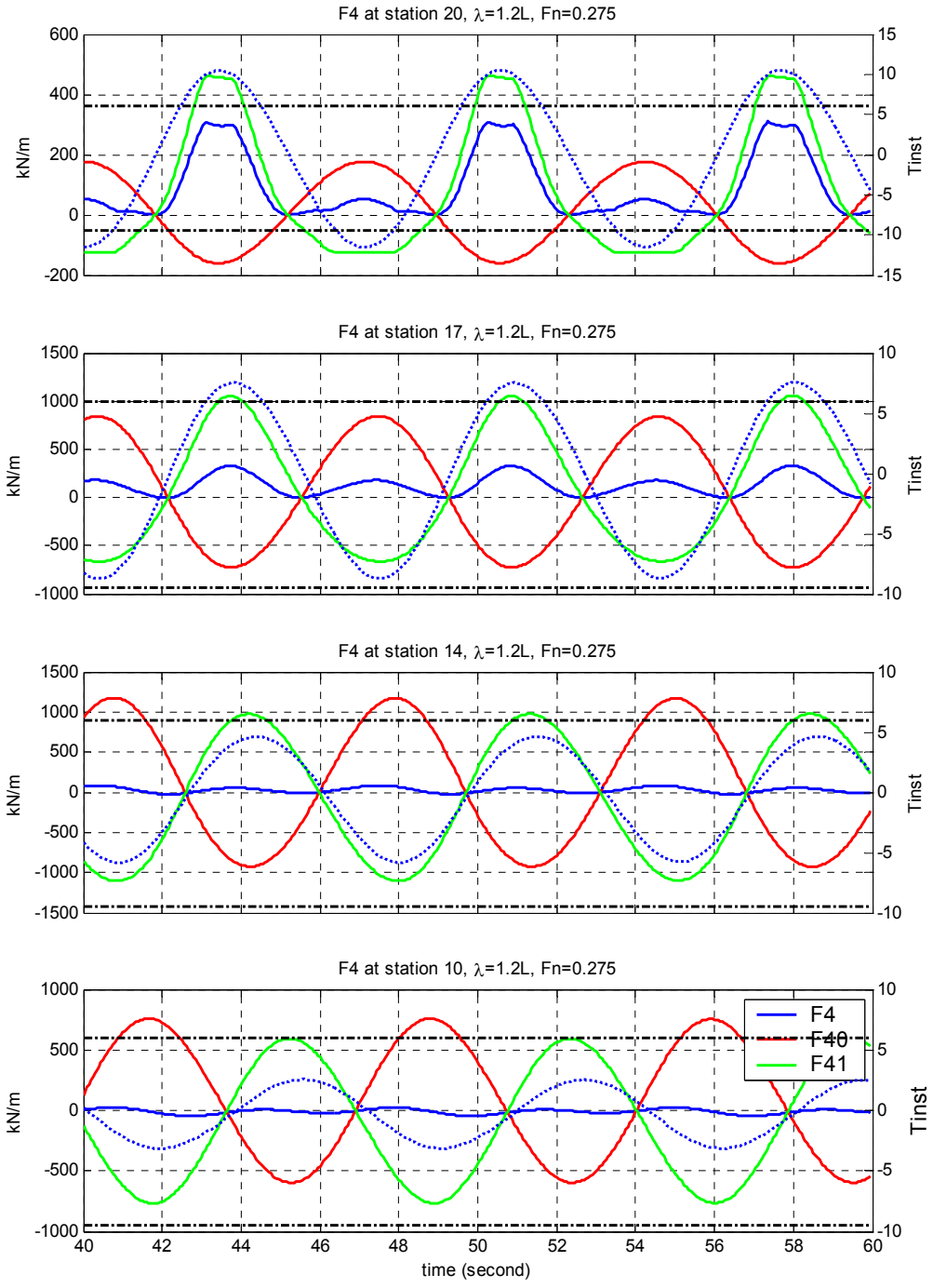

Figure 4.13b Nonlinear Froude-Krylov force and hydrostatic restoring force (F_4), λ/L=1.2, Fn=0.275, a=L/60

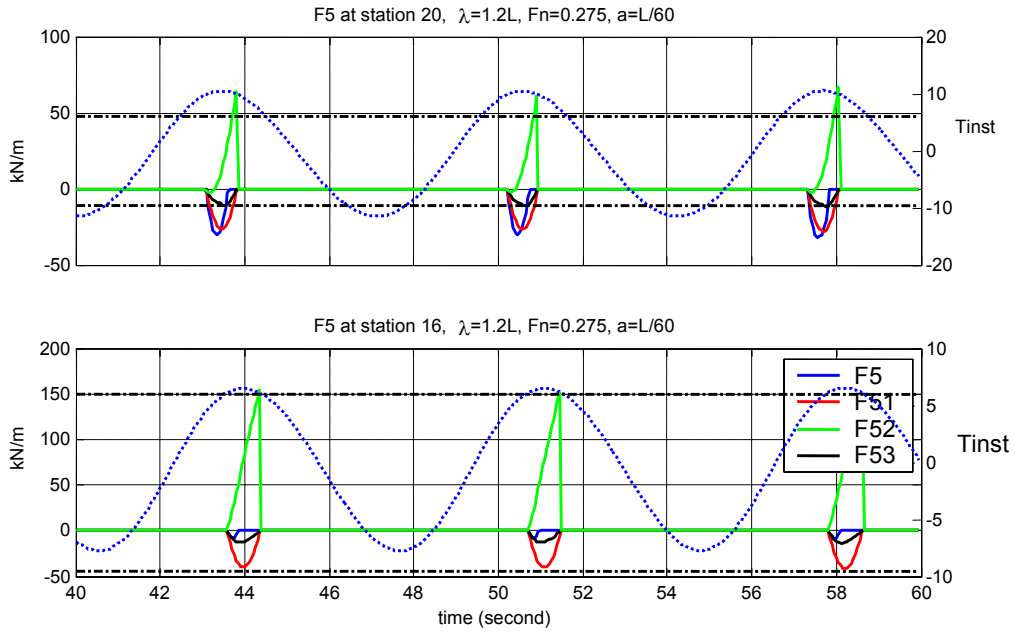

Figure 4.14 Green water force (F_5), λ/L=1.2, a=L/60, Fn=0.275

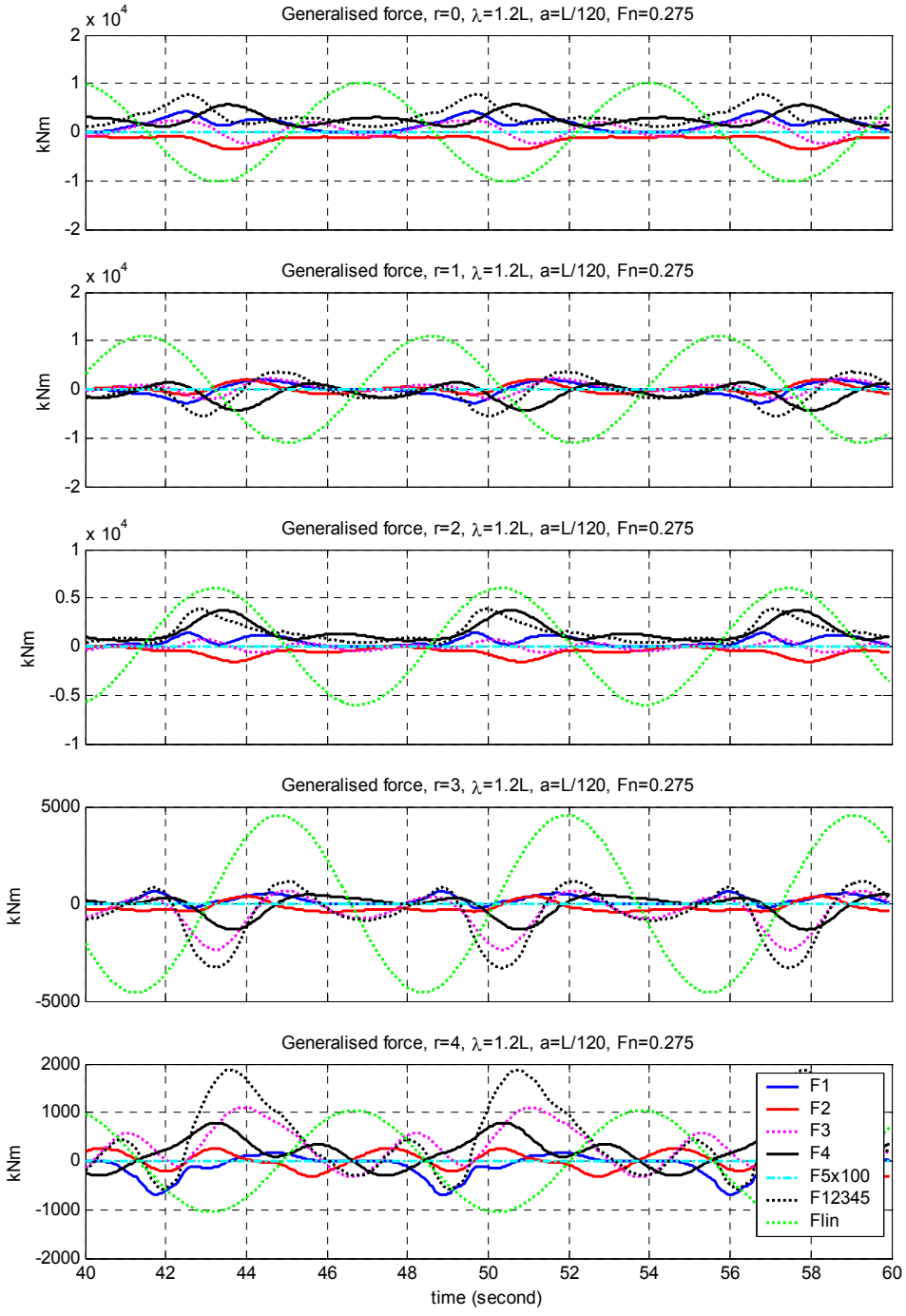

Figure 4.15 Generalised forces (F_1, F_2, F_3, F_4 and F_5), λ/L=1.2, Fn=0.275, a=L/120

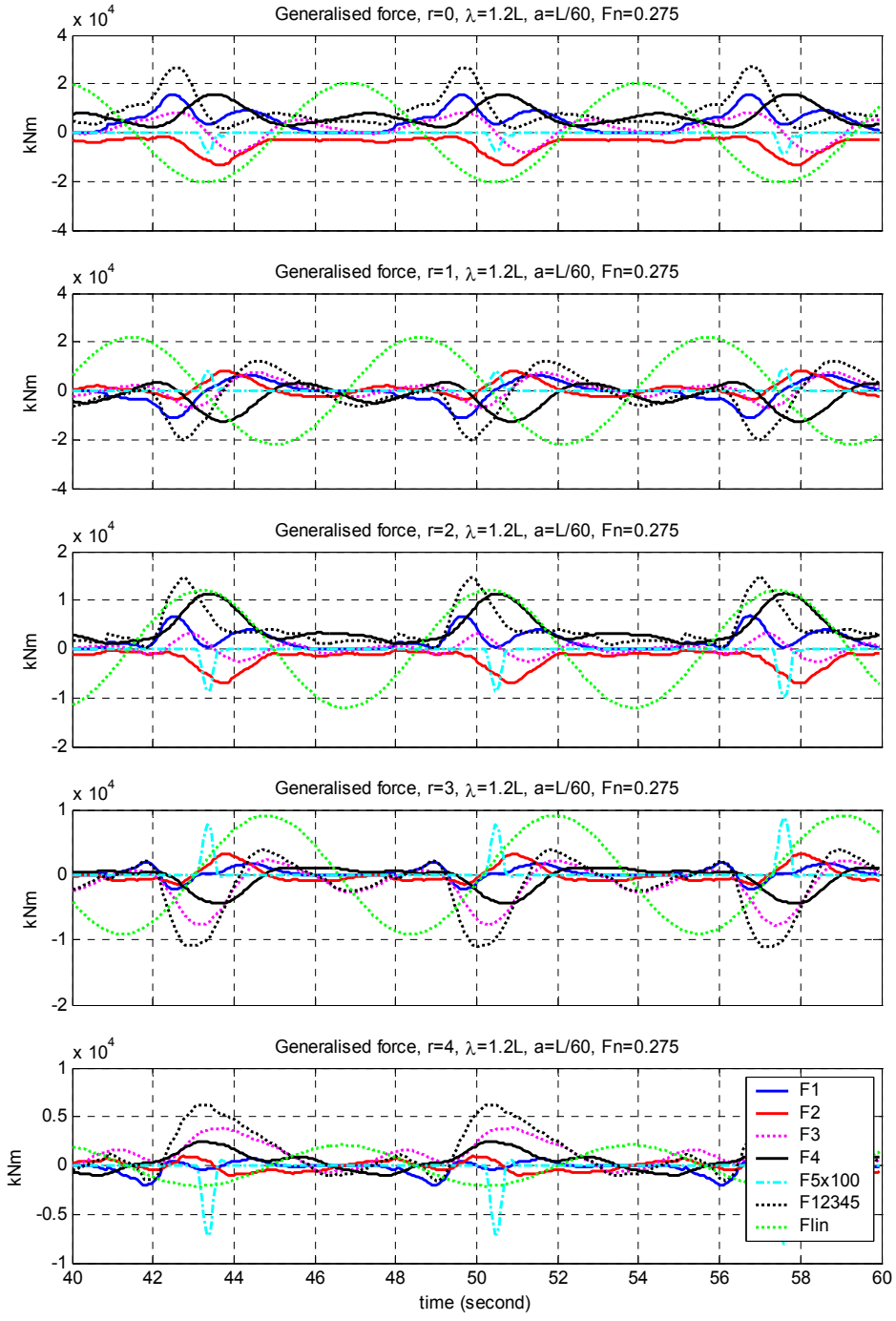

Figure 4.16 Generalised forces (F_1, F_2, F_3, F_4 and F_5), λ/L=1.2, Fn=0.275, a=L/60

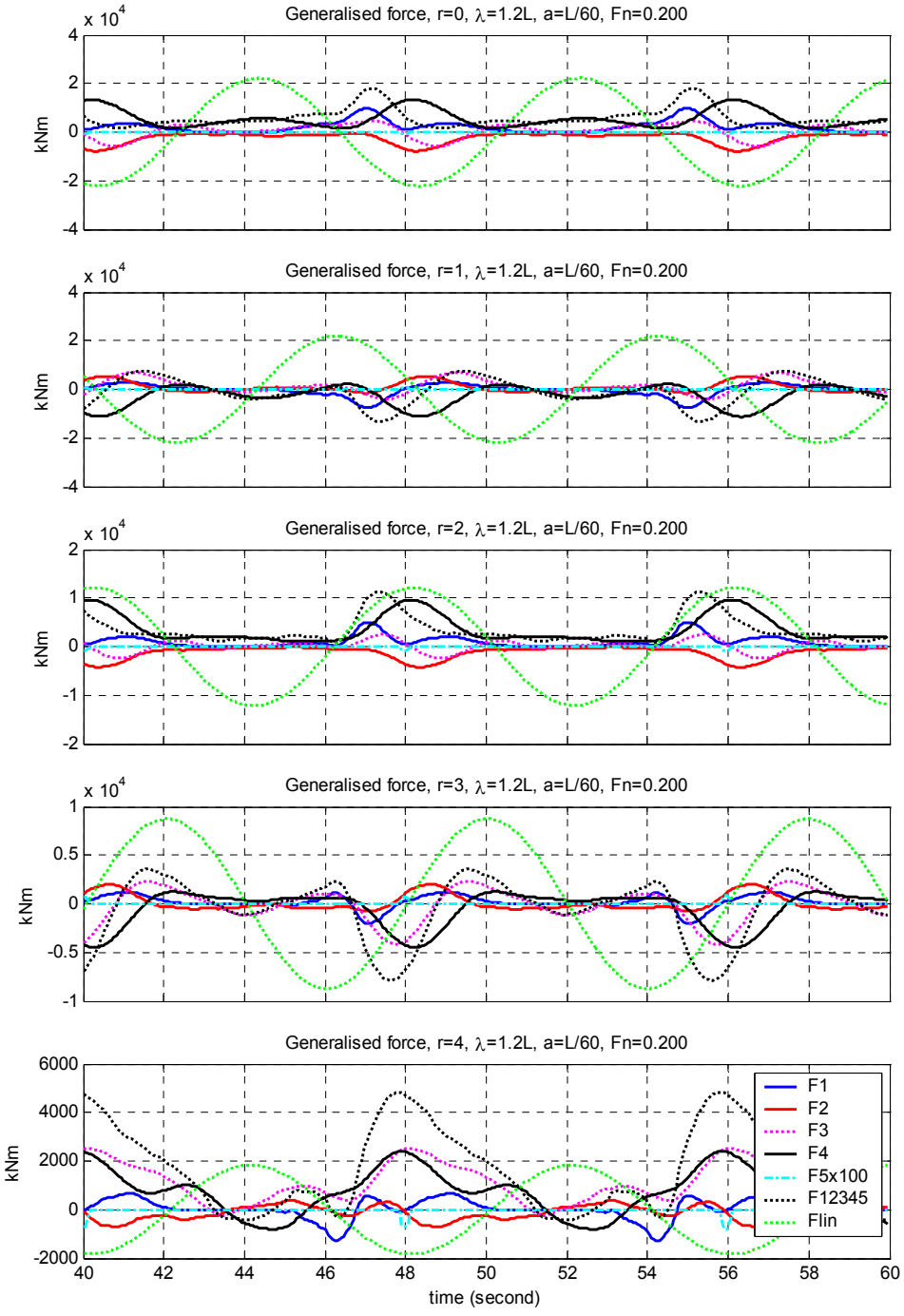

Figure 4.17 Generalised forces (F_1, F_2, F_3, F_4 and F_5), λ/L=1.2, Fn=0.2, a=L/60

4.4 Response to regular waves

4.4.1 Existing experiments

O'Dea et al. (1992) performed an experimental study, with a model of the S175, with the objective of identifying nonlinear effects on vertical motion. The experimental results cover two speeds of advance, corresponding to Fn=0.2 and 0.275 for the vertical motion and acceleration and Fn=0.25 for the vertical bending moment. The wavelengths used were 1.0L, 1.2L and 1.4L, while the wave amplitude was in the range of L/240 to L/40. To investigate the nonlinearity of the motion responses, Fourier analyses were applied to heave, pitch and bow acceleration measurements in regular waves.

To obtain information on wave loads and vertical wave bending moments, a flexural model was used. Watanabe (1989) measured heave, pitch and vertical wave bending moments for the S175 container ship in regular head waves with $\lambda/L=1.2$, $a=L/60$, Fn=0.25. A video camera was equipped on the deck of the model to observe deck wetness. Chen et al. (1999) carried out model tests in CSSRC focusing on the nonlinearity of wave-induced loads. More information is provided on these two experimental set-ups in section 4.4.3, when comparing predicted and measured wave loads.

The calculated results at Fn=0.2, 0.25 and 0.275 using the present method are compared with the existing experimental data.

4.4.2 Ship motions

Calculations were performed for the heave and pitch motions, and the vertical acceleration on the bow at a point located at 0.15 L from F.P. The amplitudes of the first harmonics of heave, pitch and vertical acceleration will be compared with the experimental results. Heave and pitch transfer functions are shown in Figure 4.18 and 4.19 as a function of non-dimensional wave frequency, $\omega_e\sqrt{L/g}$, when the ship advances with Froude number 0.25. These were calculated using F_1, F_2, F_3, F_4 and F_5. The amplitudes are non-dimensionalized by the wave amplitude for heave and by the wave slope for pitch. The estimated wave amplitude was selected varied between L/480 and L/34 and the linear transfer function is also plotted together as reference. The selected wave amplitudes are a/L=1/480, 1/200, 1/120, 1/80, 1/60, 1/50, 1/40, 1/34. The response amplitudes are defined as the first harmonics of a Fourier series of the time history of the response.

Figure 4.18 shows that the linear effect is small below non-dimensional wave frequency 1.9 and above 2.7. Nonlinearity increases around the resonance peak at $\omega_e\sqrt{L/g}$ =2.24. When wave amplitude is L/480 (small amplitude of wave), the heave transfer function is close to a linear solution, so that the asymptotic condition is satisfied. As wave amplitude increases, the heave transfer function reduces. The figure shows that heave responses do not reduce further above a=L/50, because the buoyancy force and hydrodynamic force do not increase anymore when deck wetness occurs. Figure 4.19 shows the nonlinear effect on pitch motions is small above non-dimensional wave frequency 2.75. In the range of 1.6 to 2.5 of $\omega_e\sqrt{L/g}$, nonlinearity increases as the wave amplitude becomes larger. Pitch motion shows a

different aspect to heave, in that when deck wetness occurs pitch motion is still reduced, as wave amplitude increases.

Figures 4.20 and 4.21 show the heave and pitch transfer functions at Fn=0.275 as a function of non-dimensional wave frequency. These figures show similar trends to those at Fn=0.25. The nonlinearities appear to be a little more pronounced. Figures 4.22 and 4.23 present the second harmonics of the heave and pitch motions, as a function of non-dimensional wave frequency and for several wave amplitudes at Fn=0.25. These higher order effects are small for vertical motions. For heave, the second harmonics are in most cases less than 2% of the first harmonics (compared with Figure 4.18). The second harmonics of pitch motions are slightly larger, but less than 6% of the first harmonics. The second harmonics of heave motion show the magnification of amplitude around the resonance frequency. The largest magnitudes of the second harmonics occur for waves with high slope.

4.4.2.1 Combination of nonlinear force components

Three nonlinear force schemes are presented: one (COMP 1) includes only flare slamming (F_1) and hydrostatic restoring and the Froude-Krylov force (F_4); another (COMP 2) adds the modification of hydrodynamic force (F_2, F_3) and the third (COMP 3) adds green water load (F_5). The transfer functions of heave, pitch and bow acceleration (at 0.15L from A.P.) are presented in Figures 4.24 and 4.25, for Fn=0.2 and 0.275, respectively, and three different λ/L values in the ship-wave matching region. The calculations are carried out for different wave steepness ratio ka. Heave amplitudes are non-dimensionalized by the wave amplitude, pitch amplitudes by the wave slope and the vertical acceleration at the bow amplitudes by ga/L. In Figure 4.24, at Fn=0.2, COMP 2 (F_1+F_2+F_3+F_4) and COMP 3 (F_1+F_2+F_3+F_4+F_5) show better agreement to experiments (O'Dea et al. 1992) than COMP 1 (F_1+F_4) for pitch

and bow acceleration, which show more nonlinearity. For heave motions, COMP 1 is in better agreement to measurements in general. This figure also shows that F_5 force occurs when wave steepness is larger than 1.0, where its influence can be seen. F_5 has a relatively large influence on heave and pitch motion at λ/L=1.2 and F_5 has little influence at λ/L=1.0 and 1.4. When the ship advances at Fn=0.275 (Figure 4.25), COMP 2 and COMP 3 present better agreement to measurements and exhibit more effects of nonlinearity. The responses of heave, pitch and acceleration, in general, are close to measurements in general. The calculated heave motion at λ/L=1.4 and 1.2 is slightly larger than the experiments; however the trend against wave steepness is close to experiments. For higher wave steepness values (ka>1.0), nonlinearity does not increase for the heave motion at λ/L=1.4 in the case of COMP 2. With reference to F_5, for either Froude number, it is difficult to judge whether its inclusion results in better agreement with the measurements, as these are scarce when green water occurs.

4.4.2.2 Parameter study of hydrodynamic force modification (F_2, F_3)

Nonlinear modification of the hydrodynamic force of added mass (F_2) and fluid damping (F_3) is presented in Equations 2.48 and 2.49, respectively. Because the magnitude of the damping coefficient in the low frequency range is not small and is comparable to the added mass, as shown in Figures 4.1 and 4.2, the effect of the nonlinear forces F_2 and F_3 were checked in three different ways. The first (Type 1) is all the hydrodynamic force modifications at incident wave encounter frequency; this is what has been used so far in all the result shown. The second (Type 2) is all the hydrodynamic force modifications at infinite frequency where the damping coefficient is negligible. The third (Type 3) is that the nonlinear modification of the radiation force is calculated for the infinite frequency and the modification of the diffraction force is estimated for the incident wave encounter frequency. The heave,

pitch and acceleration responses are presented in Figures 4.26 and 4.27, according to three types of hydrodynamic force modification for the S175 travelling at Fn=0.2 and Fn=0.275, respectively. F_1, F_2, F_3 and F_4 forces are included in the calculation. These figures show that Type 1 shows better agreement with experiments for all responses. Type 2 and Type 3 are not much different from each other; this means that the modification of the diffraction force does not have much influence. In Type 2, the hydrodynamic force is estimated at infinite frequency, so that the damping force is negligible. Comparing Type 1 with Types 2 and 3, one may conclude that the modification of damping force F_3 has a large influence on the responses.

4.4.2.3 Total derivatives of relative displacement z_{rel} and the influence of hull flexibility on estimating nonlinear force

The nonlinear forces in Equations 2.47 to 2.50 are expressed as a function of the relative displacement and its total derivatives. This relative displacement and total derivatives were expressed in Equation 2.55 to 2.59. The modal summation was carried out up to the third distortion mode (i.e. N=4). The effect of higher modes, i.e hull flexibility, for nonlinear force is shown in Figure 4.28. The displacement total derivatives in Equations 2.56 to 2.57 were calculated by mode summation up to N=2 and N=4 using Type 1 concept for F_2 and F_3. A practical approach in nonlinear time domain simulation is to estimate the nonlinear fluid loading for rigid body motion (N=1) only (e.g. Romos et al. 2000). On the other hand, Wu and Hermundstad (2002) and Domnisoru and Domnisoru (1997) include all flexible modes in estimating the nonlinear forces. The figure shows that the two graphs for N=2 and N=4 are very close to each other for all motions and vertical acceleration. It is concluded that hull flexibility of higher modes has only a small influence on the nonlinear motion response. It is noted that this mode summation is applied only in calculating the nonlinear force, while all the resultant linear and nonlinear responses

of motions (i.e. relative motion and derivatives) and wave loads were calculated by mode summation with N=4.

Responses for displacement, velocity and acceleration are obtained by convolution integral between the nonlinear forces and the impulse response functions of h(t), $h_v(t)$ and $h_a(t)$, respectively, in the Equations 4.2 to 4.4 . The convolution integral is rather time intensive, so another proposal is that velocity and acceleration may be calculated by time derivatives of displacement and velocity. That is:

$$\dot{p}(t) = \frac{p(t) - p(t - \Delta t)}{dt}, \tag{4.5}$$

$$\ddot{p}(t) = \frac{\dot{p}(t) - \dot{p}(t - \Delta t)}{dt}. \tag{4.6}$$

Two calculated results are shown in Figure 4.29, using Type 1 method for F_2 and F_3. One is for velocity and acceleration estimated by convolution integral and the other is when they were estimated by numerical differentiation. The figure shows for both cases heave and pitch responses are very close and accelerations are slightly different.

4.4.3 Wave loads

The vertical bending moment calculated at amidships is shown in Figures 4.30 and 4.31 for Fn=0.25 and a range of wave amplitude $L/480 \le a \le L/34$. F_1, F_2, F_3, F_4 and F_5 were used, with F_2, F_3 following Type 1 method. The first and second harmonics of bending moment are non-dimensionalized by $\rho g a B L^2$ where a is wave amplitude and B is ship beam. Figure 4.30 shows the transfer function of bending moment at midship for several wave amplitudes. The amplitudes are amplified around the resonance of the motions (around non-dimensional wave

encounter frequency of 2.5). The second harmonic of amidships bending moment shown in Figure 4.31, also has peak at $\omega_e\sqrt{L/g}\approx 2.5$.

The first harmonics of bending moment transfer function depend slightly on wave amplitudes and show small differences to linear values. It is interesting to note that application of the nonlinear method produces values higher than the linear except for $a \geq L/40$. The second harmonics of bending moment depend strongly on wave amplitudes (Figure 4.31). The vertical bending moment contains strong high-order effects. The second harmonics of the bending moment at amidships can be as high as 45% of the first harmonics at the largest wave amplitude of a/L=34 and 29% at a/L=60.

Figures 4.32 and 4.33 show the transfer functions of the vertical shear force at station 15 for several wave amplitudes corresponding to same operational parameters and calculation method as for the bending moment. The first and second harmonics of bending moment are non-dimensionalized by $\rho gaBL$. The variations with wave encounter frequency are very similar to the bending moment at amidships, as shown in Figures 4.30 and 4.31. The first harmonics of shear force transfer function are amplified in the range of 2 to 3 of non-dimensional wave encounter frequency. The magnitudes of the first harmonics of shear force are larger than these linear predictions for all wave amplitudes used, and they are amplified most at $\omega_e\sqrt{L/g}\approx 2.5$, which is higher than the resonance in heave and pitch motion. This tendency was also observed in the vertical bending moments. The second harmonics in Figure 4.33 can be significant and they strongly depend on wave amplitude. The maximum magnitude of the second harmonics is about 50% of the first harmonics at wave amplitude a/L=1/34 and about 30% at a/L=1/60.

Figure 4.34 shows the first and second harmonics of vertical bending moment, together with comparisons with experimental values, at three stations (5, 10 and 15). The calculations were performed for the S175 travelling at a speed of Fn=0.25 in a regular wave with wave amplitude a/L=1/60. In the figure, the first harmonic is non-dimensionalized by $M/\left(\rho gaBL^2\right)$, and the second harmonic by $M/\left(\rho ga^2BL^2/T\right)$, where T is mean draught as per the experiments. The circle marks and plus marks are the results measured by Watanabe et al (1989) and in CSSRC by Chen et al. (1999), respectively. The first harmonics of bending moment show good agreement with experiments at station 5 and 10. At station 15, the calculated results are rather smaller, around λ/L=1.2, compared to those by both Watanabe and Chen et al, even for the Type 1 method. For the measured results of the second harmonics of bending moment, Watanabe's results are in general larger than these by Chen et al. In Figure 4.34, the calculated magnitudes of the second harmonics are, in general, larger than the measurements by Watanabe et al. (1989) at stations 5 and 10, while the calculated results are close to the experimental measurement at station 15 (See Type 1).

Another important aspect of wave loads is asymmetry of peaks. Figure 4.35 presents the positive peaks (sagging) and negative peaks (hogging) of bending moment at stations 5, 8, 10 , 12 and 15 for the ship travelling at Fn=0.25 in regular waves of λ/L=1.2 and a/L=1/60. The figure shows the strong asymmetry of the positive and negative peaks, the sagging peaks being much larger than the hogging peaks. The maximum ratio between sagging and hogging peaks occurs at station 15, reaching about 5. It is a results of the nonlinearities due to the flared section in the fore part of the ship. The calculated results in Figure 4.35 are in good agreement for the hogging condition and slightly larger in the sagging condition, except the foremost station (station 15) measurements were taken by Watanabe et al. (1989). Once again the

differences between the measurements by Watanabe et al. (1989) and Chen et al. (1999) can be seen.

Investigations along the same lines using different methods for evaluating F_2 and F_3 (namely Types 1, 2 and 3) as in Section 4.4.1 were carried out for the vertical bending moment, and the results are shown in Figures 4.34 to 4.35. Figure 4.34 shows that Type 1 (the modification of hydrodynamic force at incident wave encounter frequency) gives the best fit to experiments for the first harmonics of amidships bending moment. It can also seen that the differences between predictions using Type 1 and Type 2 and 3 only begin to emerge forward of amidships also confirmed in Figure 4.35. For 2^{nd} harmonics, results predicted with Type 1 method are larger than those with Type 2 or 3 in stations 5 and 15.

Watanabe et al. (1989) used a 4.5m long flexible S175 model made of synthetic resin and foam urethane to simulate the bending rigidity of the a real ship. Chen at al. (1999, 2001) used the plastic material (ABS702 material) satisfying the geometrical similarity of the hull form, hydrodynamic similarity, together with the structural similarity for the global vertical bending and shearing. The principal particulars of both models are shown in Table 4.1, with those for the real ship. Comparing the two models, the bending rigidities at midship (EI) are different from each other and the 2-node natural frequency in the 'dry' mode also shows a difference. However, it is hard to say whether this causes the differences in second harmonics of midship bending moment seen in Figure 4.34. More verification for the model tests may be needed.

Table 4.1 Principal particulars of S175 and its model

Items	Real ship	Watanabe (1989)	Chen (2001)
Lbp	175.0	4.5	3.6
Beam, m	25.4	0.653	0.523
Depth, m	15.4	0.596	0.317
Draught, m	9.5	0.244	0.195

Displacement, tonnes	24742	0.412	0.21525
GM, m	1.0	0.0227	0.021
EI, midship, kg mm^2	2.28×10^{18}	3.61×10^{18}	10.66×10^{9}
Dry 2-node frequency	1.60	10.0	12.57
Structural damping		0.051	

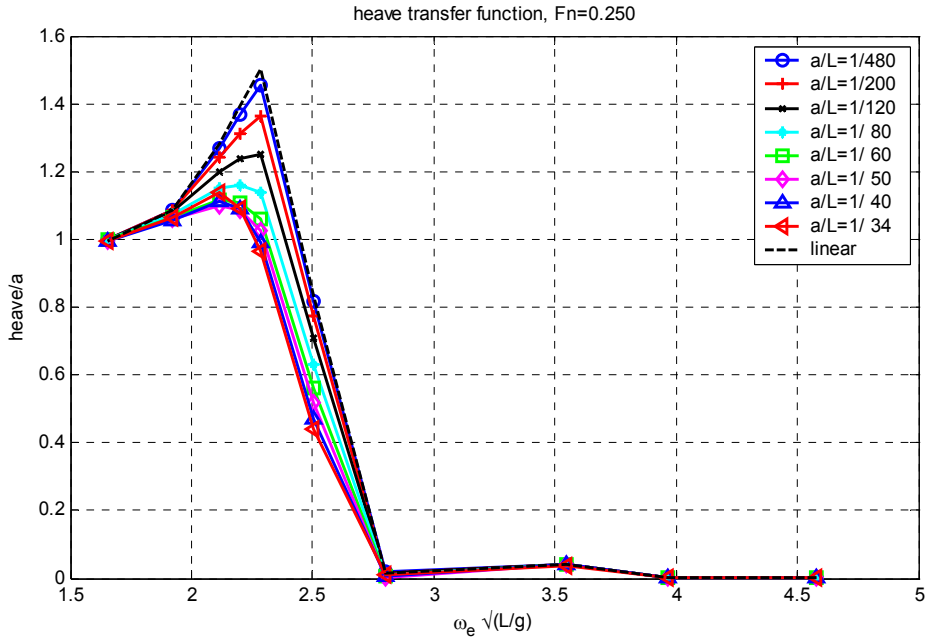

Figure 4.18 Heave transfer function, Fn=0.25

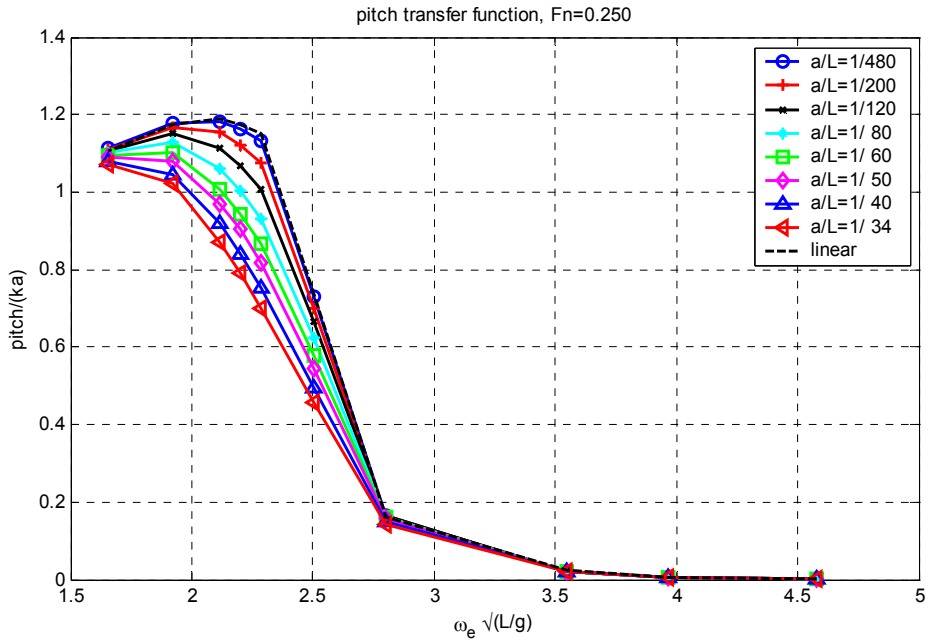

Figure 4.19 Pitch transfer function, Fn=0.25

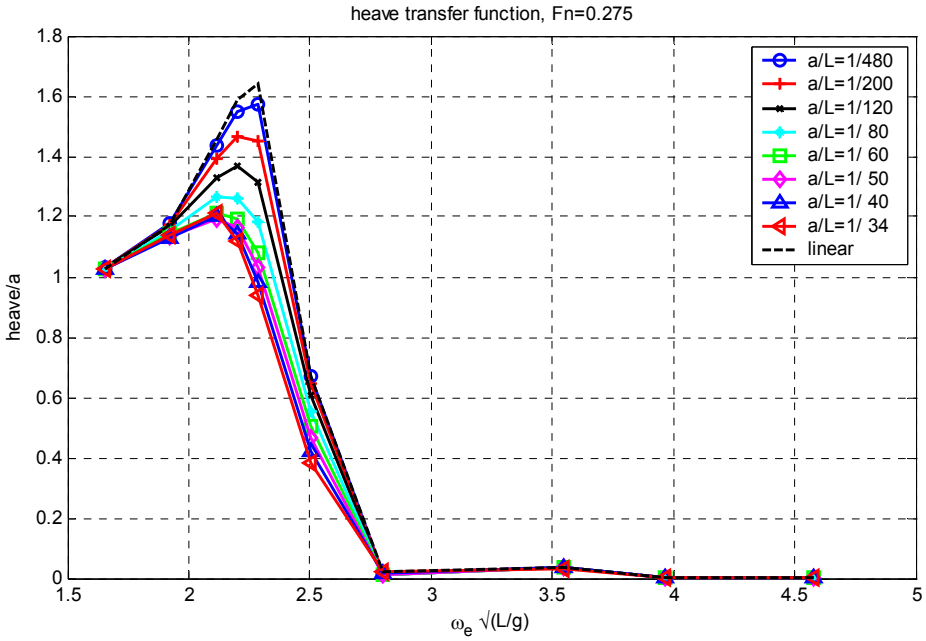

Figure 4.20 Heave transfer function, Fn=0.275

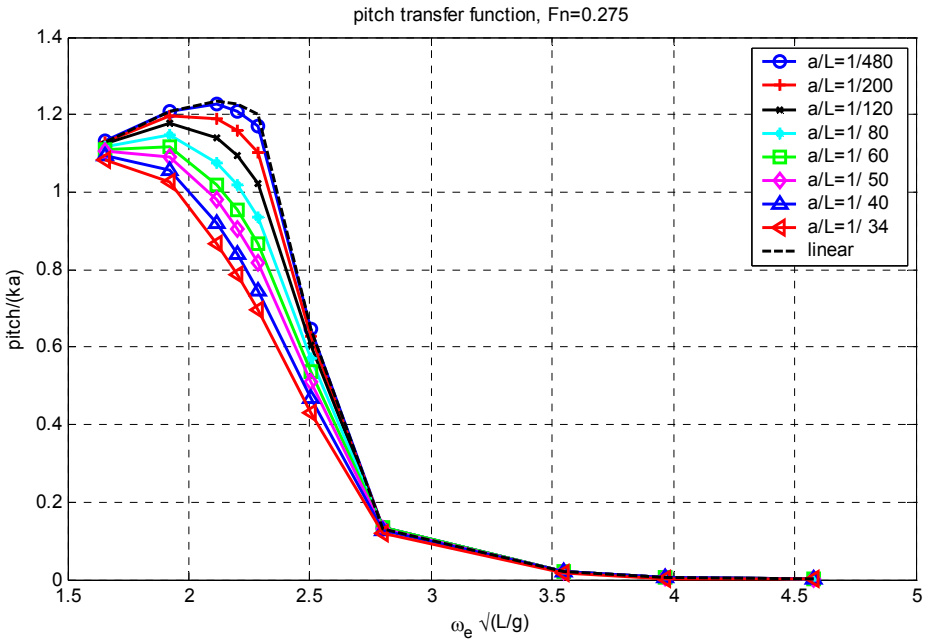

Figure 4.21 Pitch transfer function, Fn=0.275

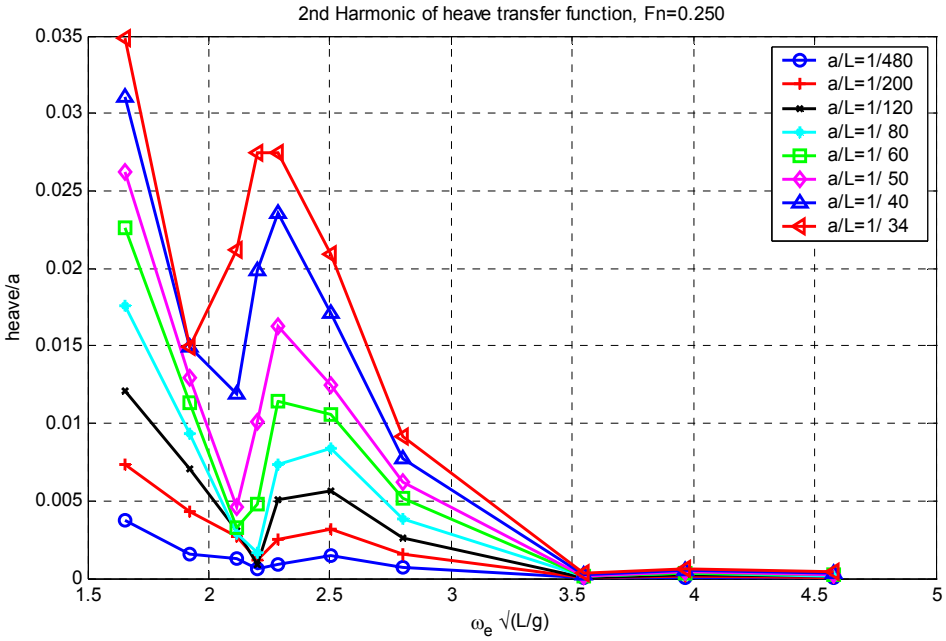

Figure 4.22 Second harmonic of heave transfer function, Fn=0.25

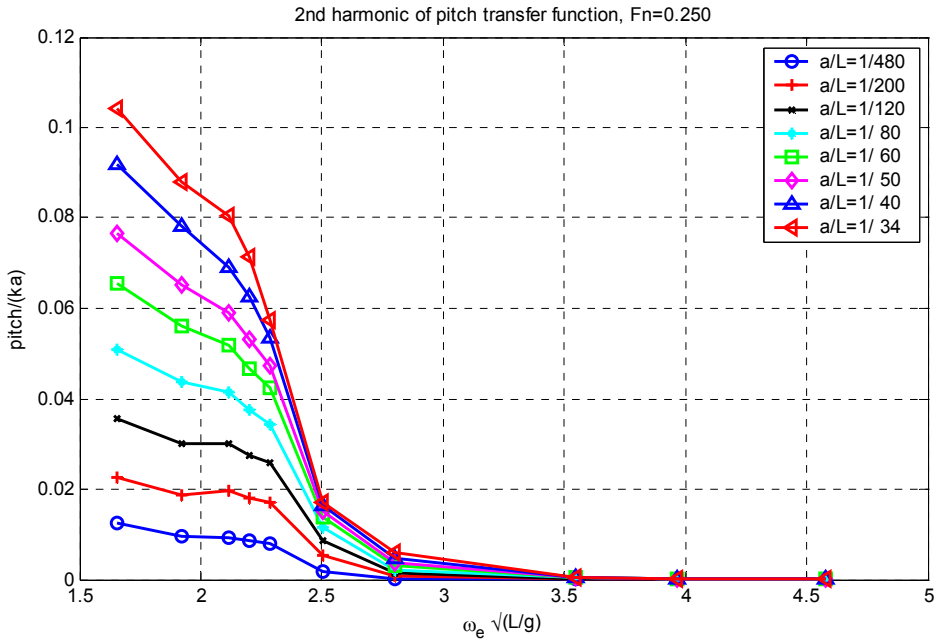

Figure 4.23 Second harmonic of pitch transfer function, Fn=0.25

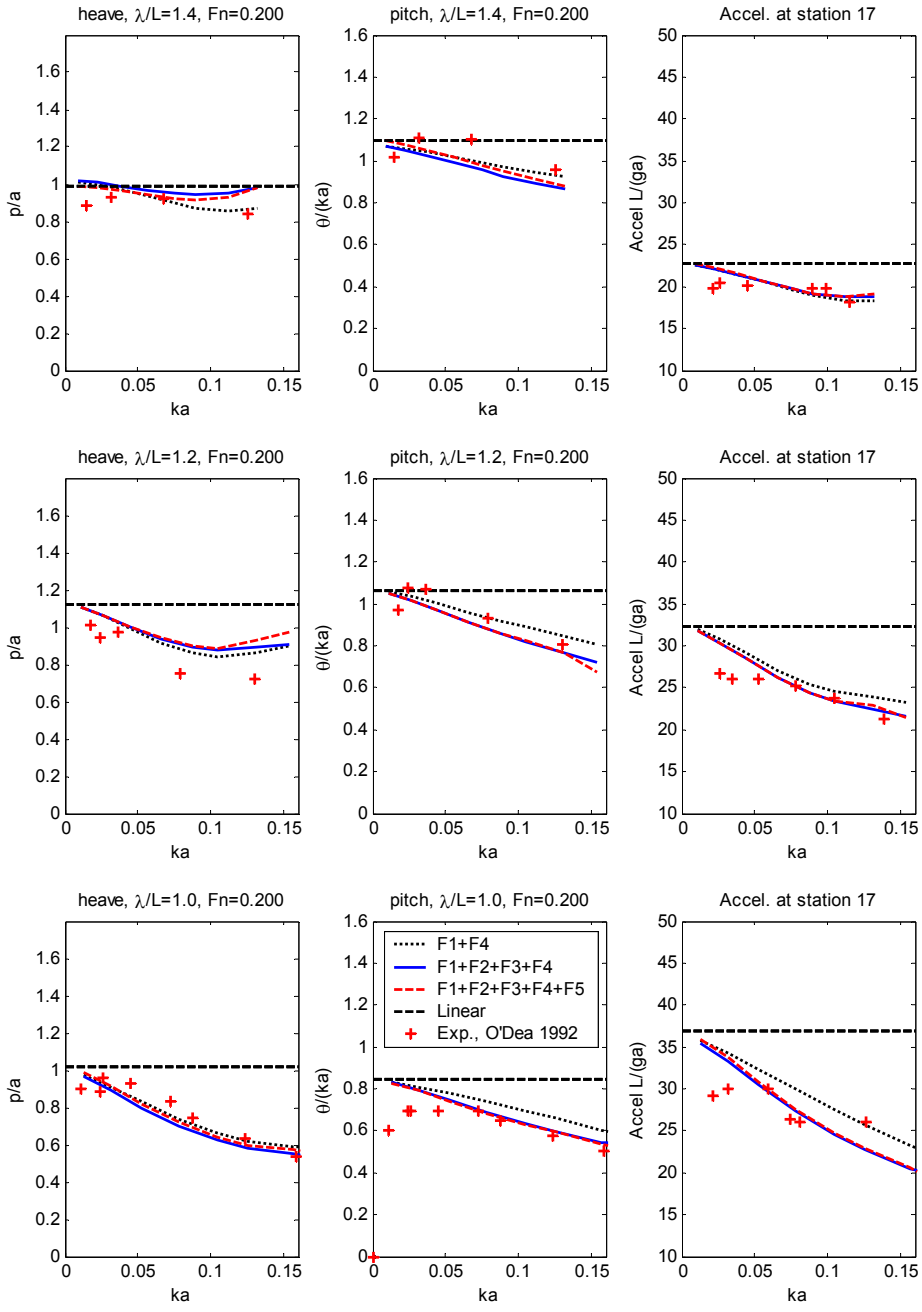

Figure 4.24 Heave, pitch and bow acceleration at station 17 with respect to wave steepness in comparison with experiment data, Fn=0.2

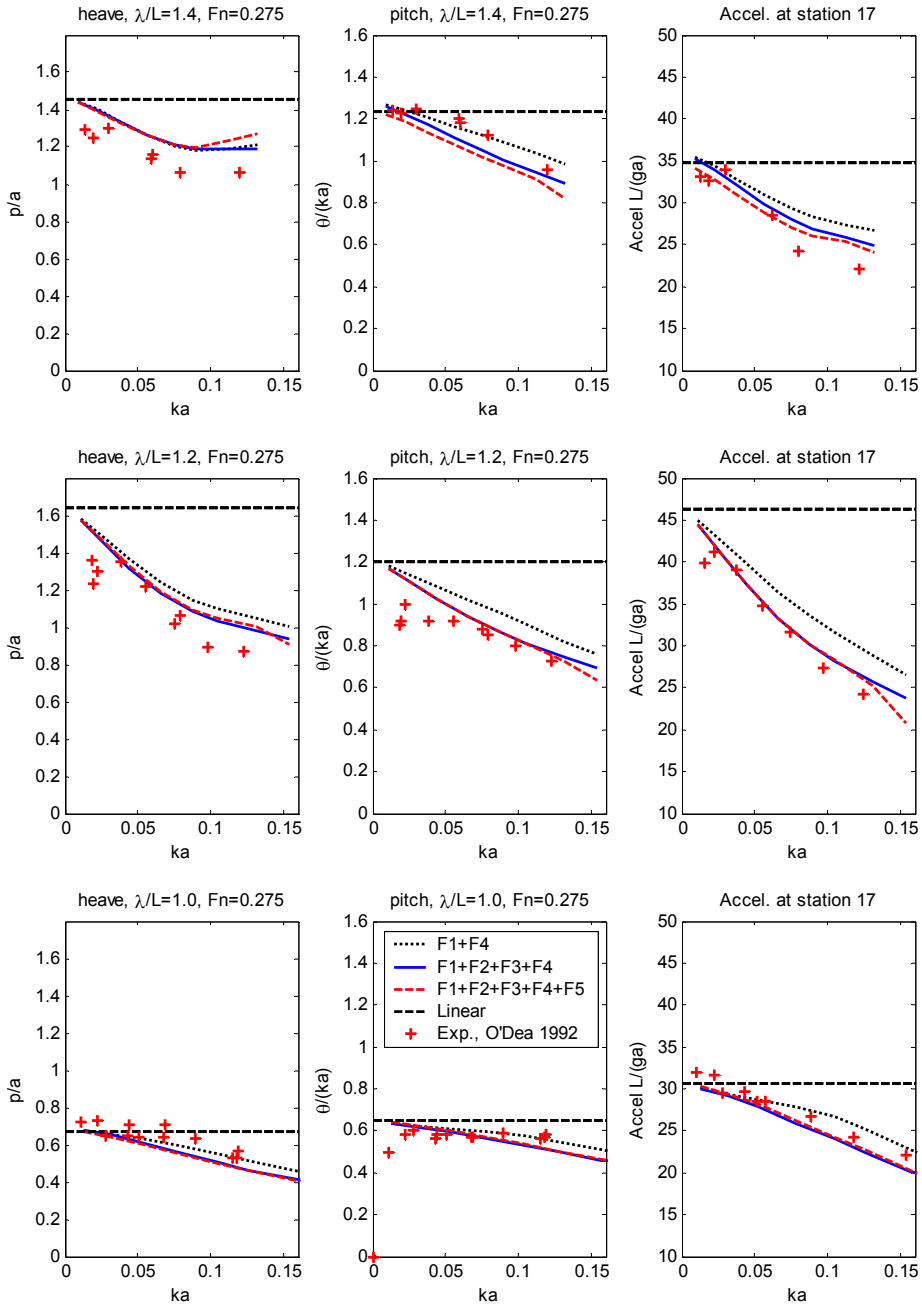

Figure 4.25 Heave, pitch and bow acceleration at station 17 with respect to wave steepness in comparison with experiment data, Fn=0.275

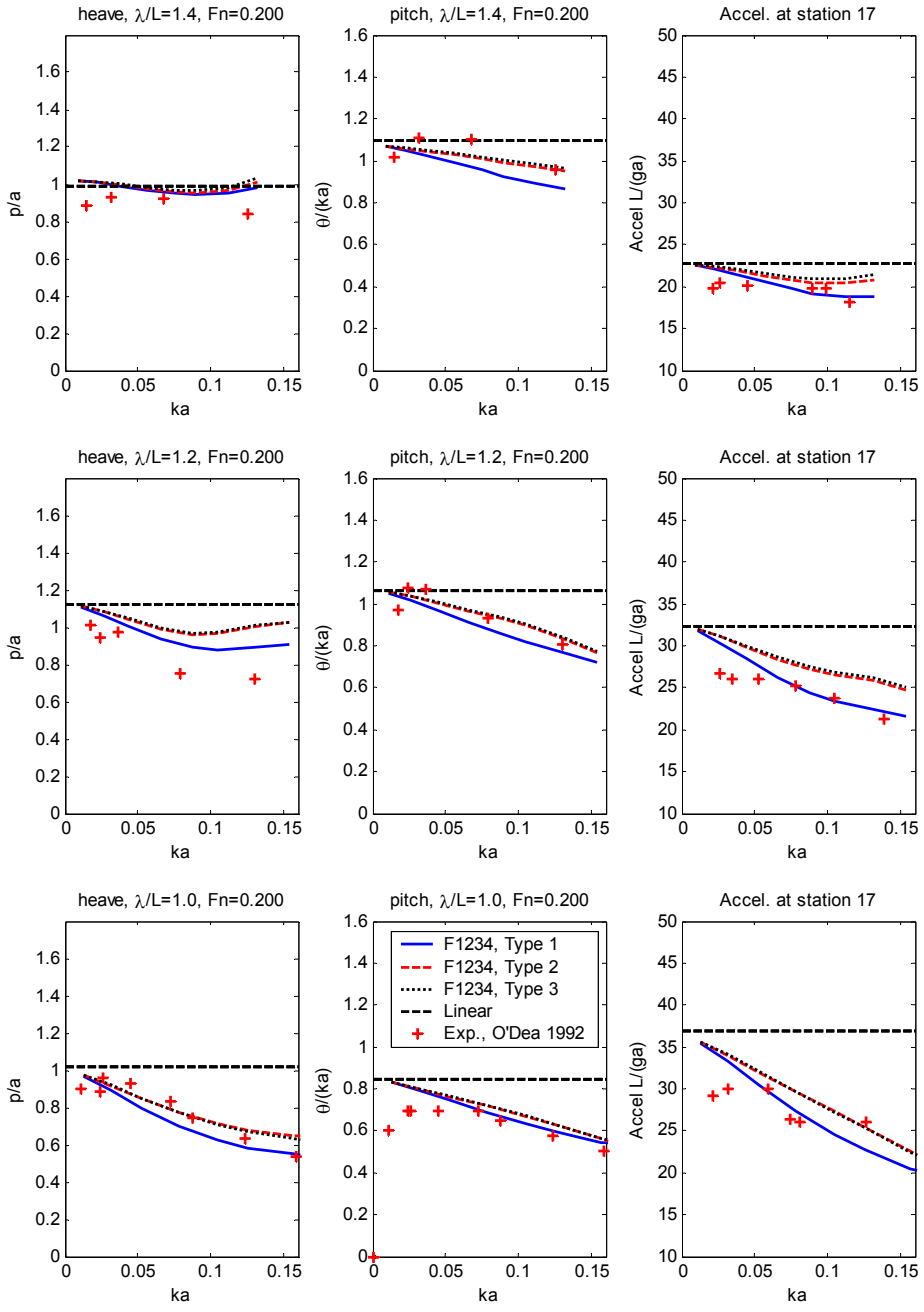

Figure 4.26 Parameter study of damping coefficients on heave, pitch and bow acceleration (at station 17) with respect to wave steepness, Fn=0.2

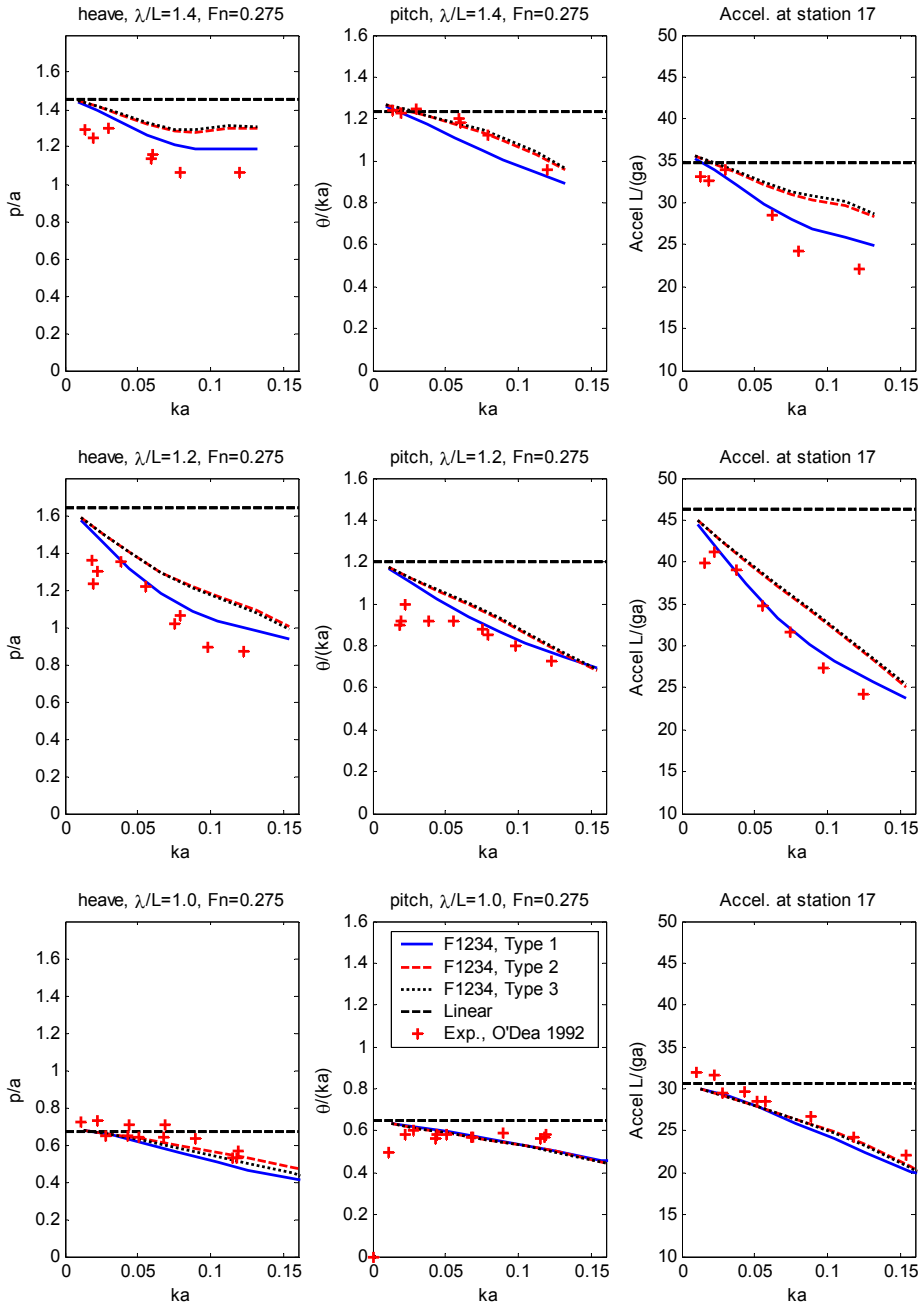

Figure 4.27 Parameter study of damping coefficients on heave, pitch and bow acceleration (at station 17) with respect to wave steepness, Fn=0.275

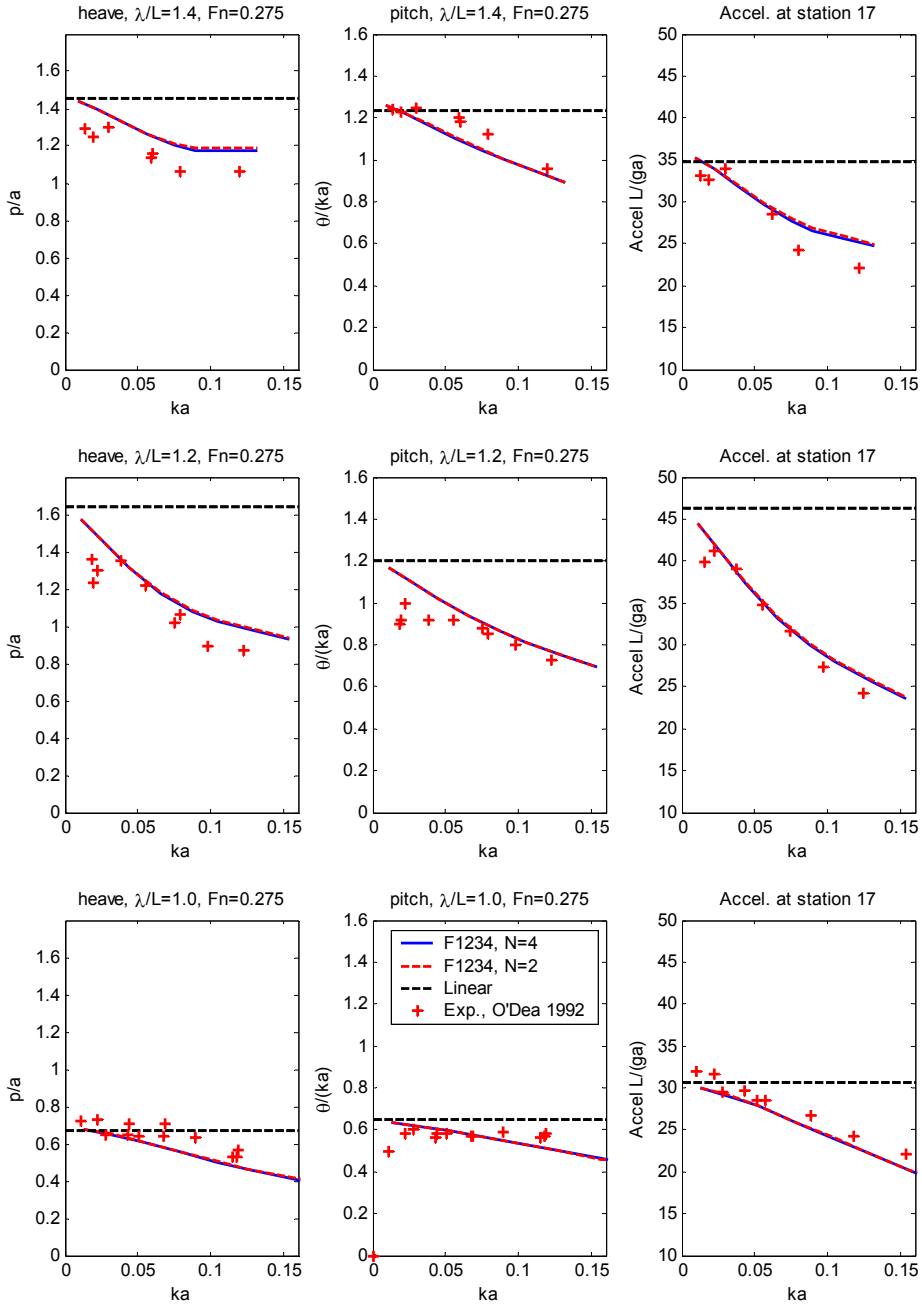

Figure 4.28 Sensitivity to hull flexibility effect estimating fluid forces on ship motion with respect to wave steepness, Fn=0.275

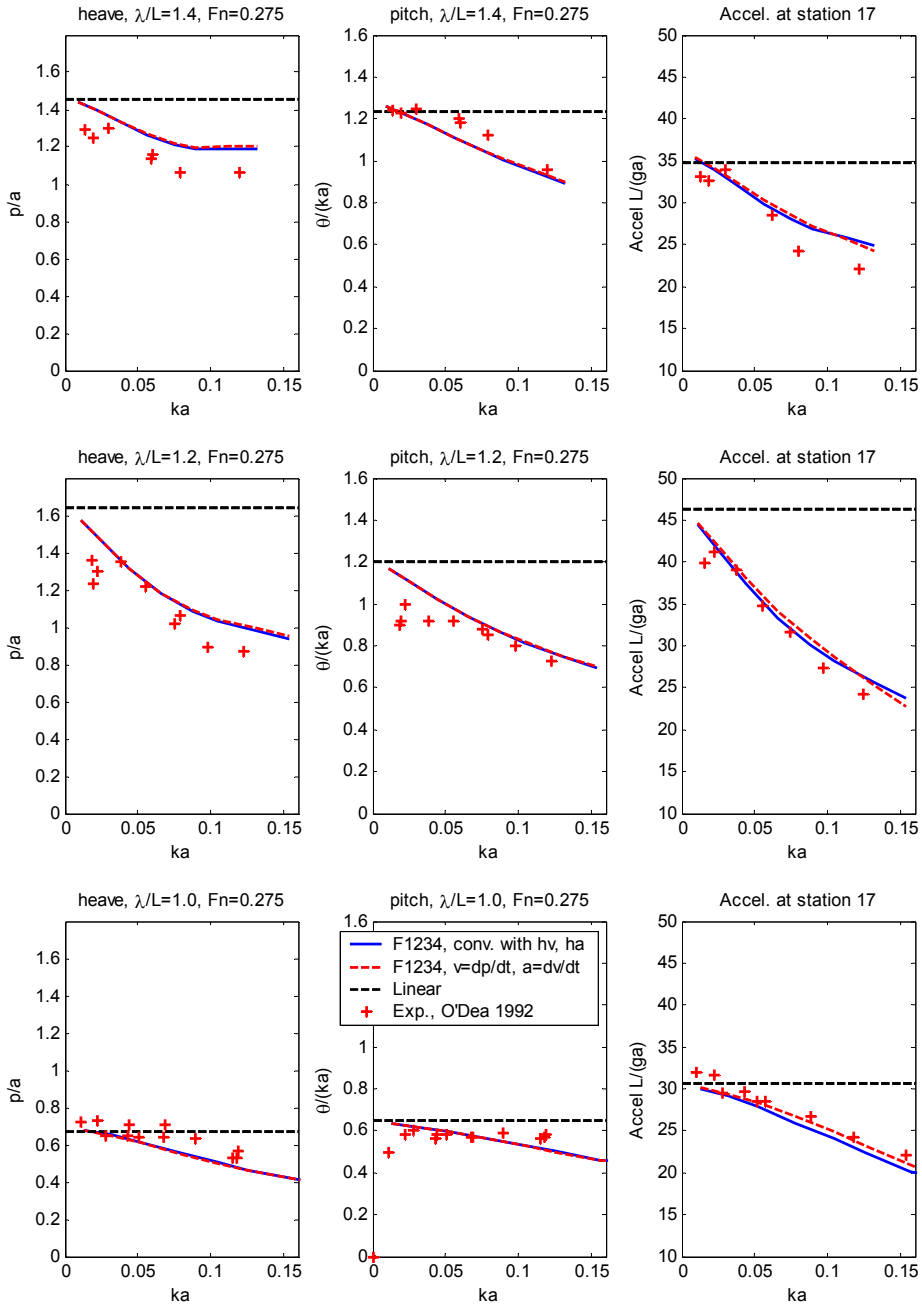

Figure 4.29 Heave, pitch and bow acceleration at station 17 with respect to wave steepness by two differentiating methods, Fn=0.275

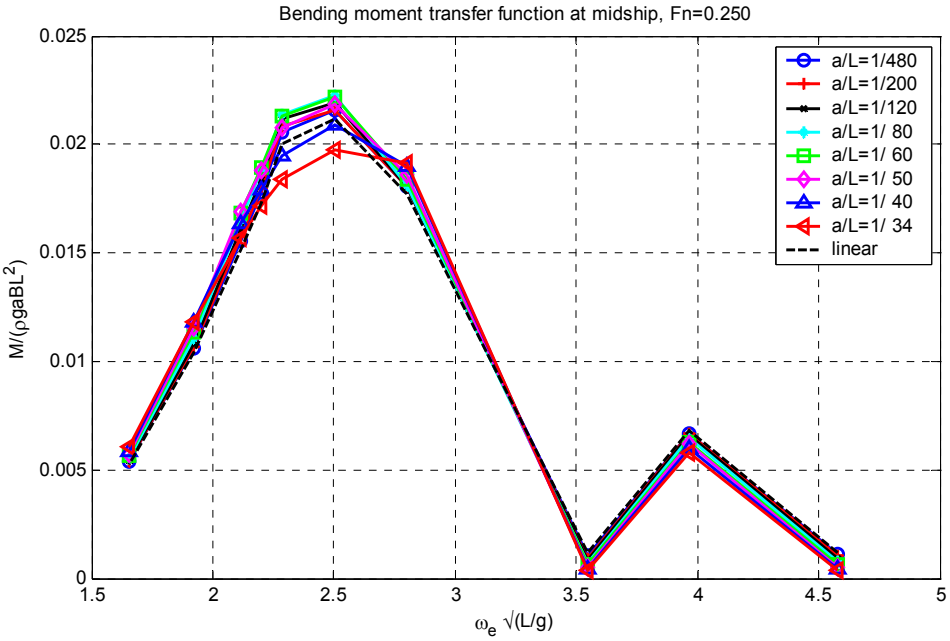

Figure 4.30 First harmonic of midship bending moment, Fn=0.25

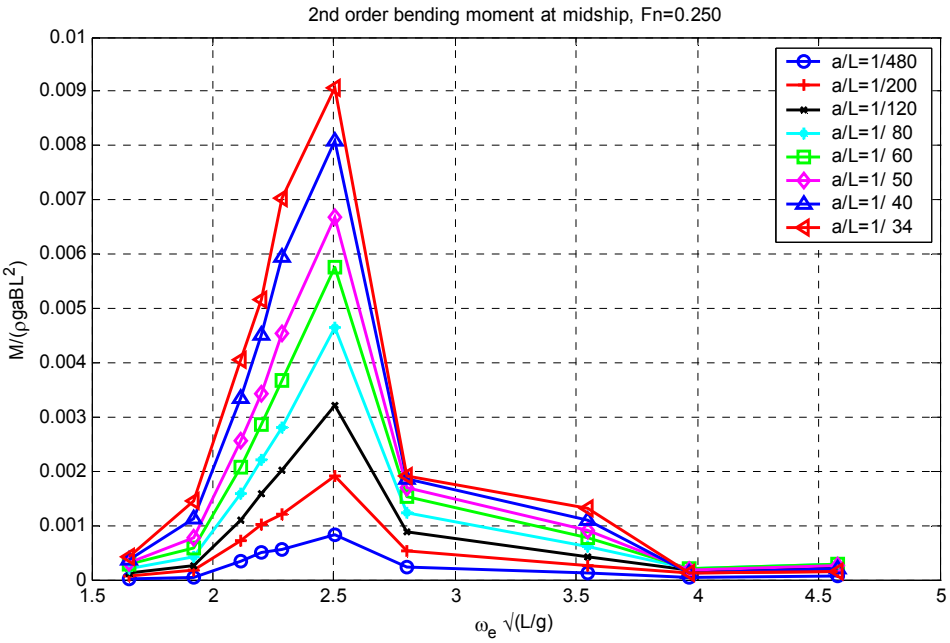

Figure 4.31 Second harmonic of midship bending moment, Fn=0.25

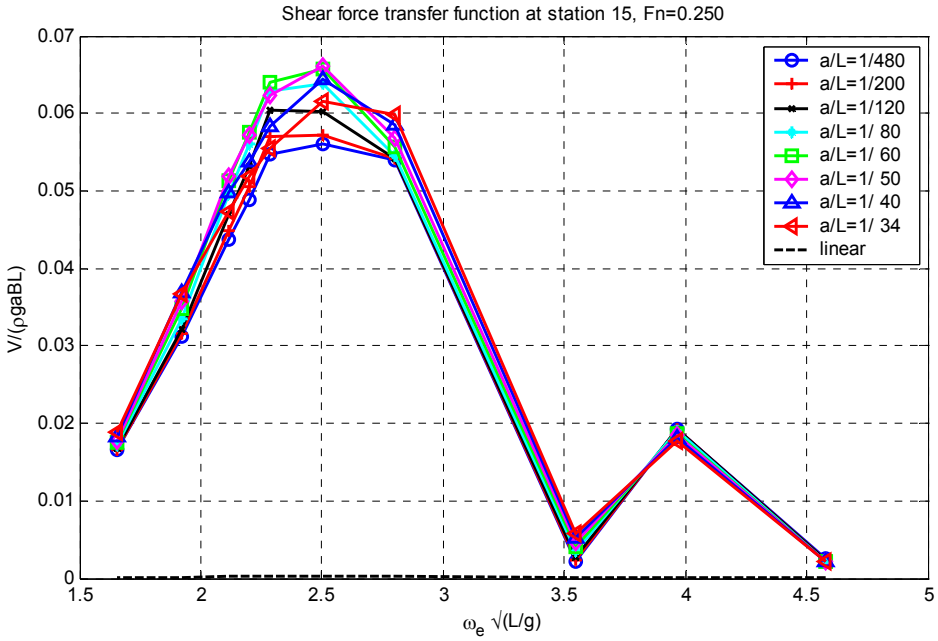

Figure 4.32 1st harmonic of shear force at 0.75 L, Fn=0.25

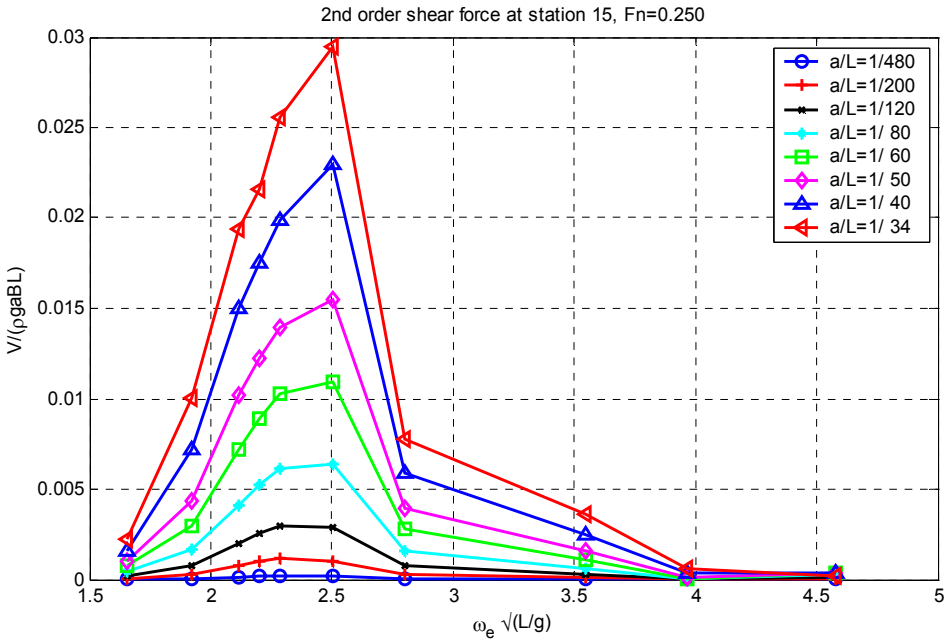

Figure 4.33 2nd harmonic of shear force at 0.75 L, Fn=0.25

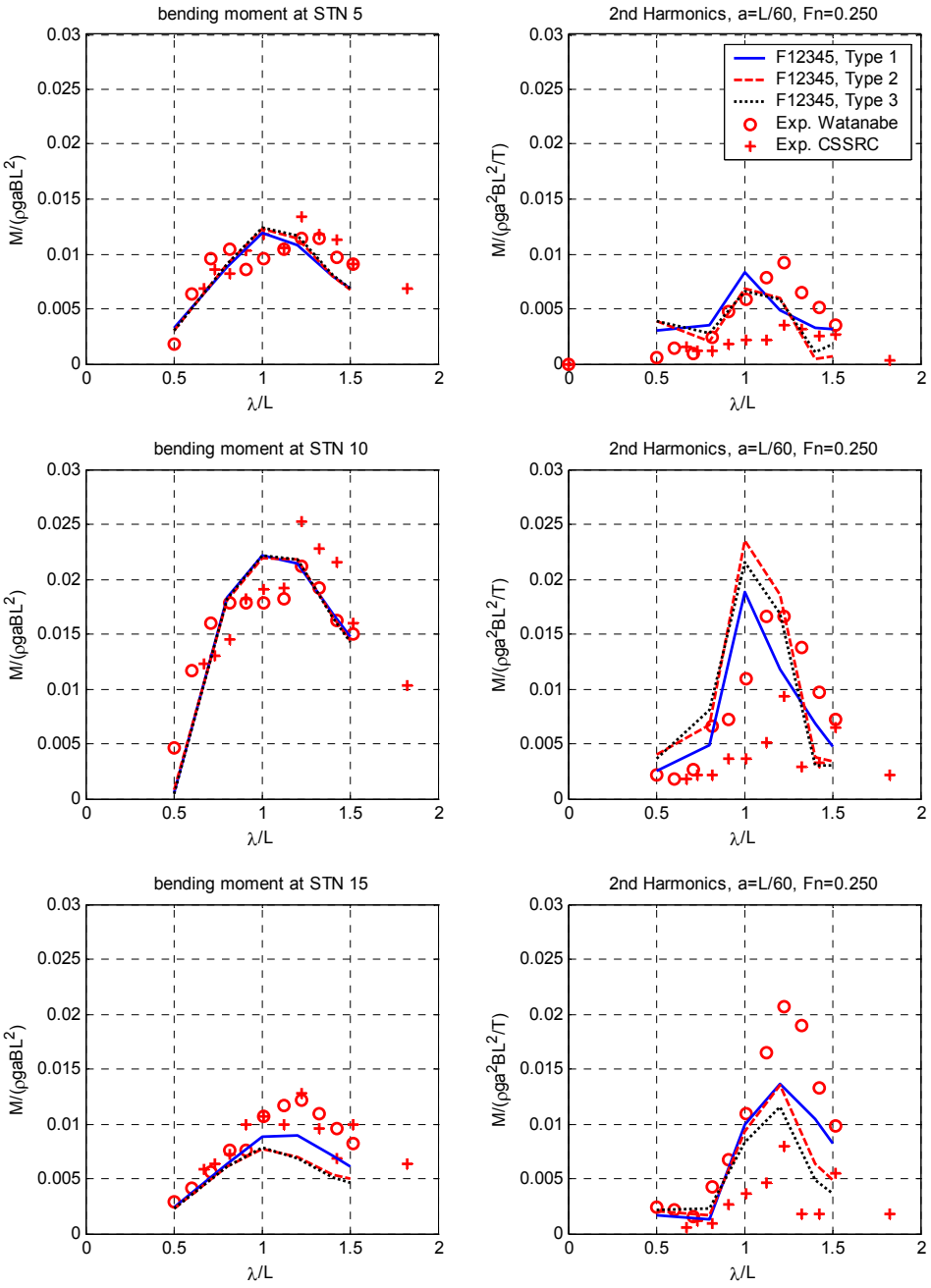

Figure 4.34 First and second harmonics of bending moment compared with experiments, a=L/60, Fn=0.25, non-dimensionalized with

$M/(\rho gBL^2a)$ for 1st and $M/(\rho gBL^2a^2/T)$ for 2nd

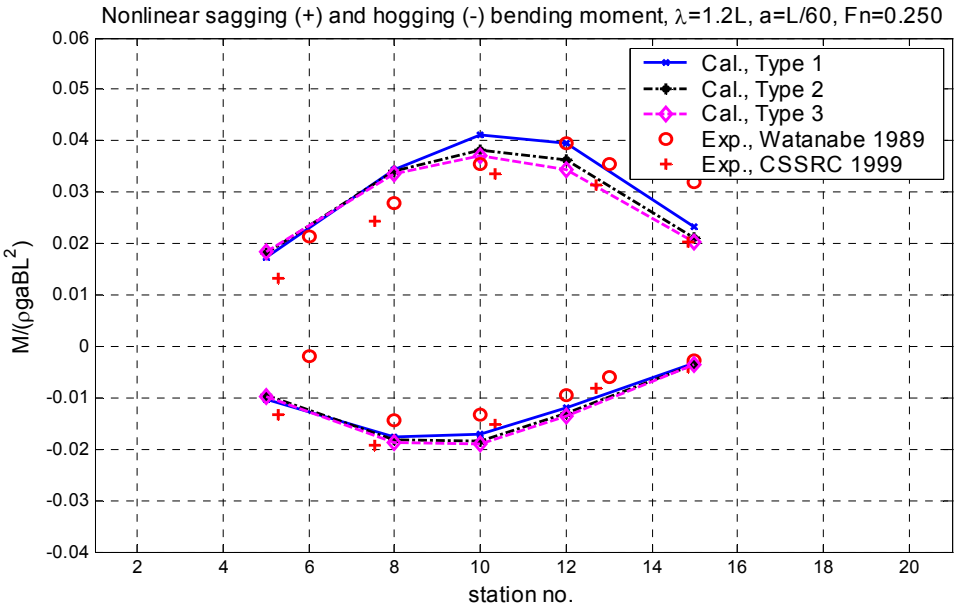

Figure 4.35 Nonlinear sagging and hogging moment according to modifications of hydrodynamic force, F12345, λ/L=1.2, a=L/60, Fn=0.25

4.5 Response to bottom impact load

Figure 4.36 shows the sectional bottom slamming force (F_6), at four sections at the fore part and one at the stern of the ship with time steps of 0.01 seconds. The impact time variation was calculated according to the Kawakami's (1977) assumption (i.e. Equation 2.67) and the maximum pressure according to Stavovy and Chuang (1976) (i.e. Equation 2.64). The figure shows that a time interval of 0.01 second reflects time variation of the impact force well. The bottom slamming force occurs when the hull bottom re-enters the wave, as observed in this figure. The stern slamming is also observed as shown in the fourth graph in Figure 4.36. The green dashed line shows the instantaneous draught at each section. The ship is travelling in regular head waves, $\lambda/L=1.2$, $a=L/60$ and $Fn=0.275$. The instantaneous draught was determined using linear and nonlinear motions, the latter with F_1, F_2 and F_3 (Type 1), F_4 and F_5. F_6 force is combined with the other nonlinear force components at each time step, and the responses are calculated by convolution integral, as per Equation 4.2. The corresponding motions and wave loads of the ship are presented in Figure 4.37. The blue solid line indicates the response for the linear case, the black line indicates the nonlinear response, including F_6, and the red line indicates the response excluding F_6, i.e. $F_1+F_2+F_3+F_4+F_5$. The figure shows that heave and pitch motions are little affected by the bottom slamming force, while bow acceleration, bending moment and shear force are amplified by the slamming force. Compared between the black and red lines in Figure 4.9, it can be seen that bottom impact has greater influence than flare slamming on bow acceleration, bending moment and shear force. When hull bottom impacts water surface, severe high-frequency vibration responses are observed in the time history of bending moment and shear force. In order to evaluate the high frequency responses, Fourier transform is applied to the time history of the bending moment. In Figure 4.38 and 4.39, the solid blue line denotes the response due to F_1, F_2, F_3, F_4 and F_5 nonlinear forces, while the solid red line presents

responses including the bottom slamming force (F_6). The figure shows that the high frequency bending moments are much affected by the impact loads. Around 8.4 rad/s, which is the resonance frequency of 2-node hull girder vibration, the whipping peak occurs.

The transfer function of heave, pitch and bow acceleration (at 0.85 L) are presented in Figures 4.40 and 4.41, for Fn=0.2 and 0.275, respectively, and three different λ/L values of 1.0, 1.2 and 1.4, as shown in Figures 4.24 and 4.25. These figures show that the responses, including the bottom slamming force (F_6) (the solid blue line) are slightly smaller than the responses due to Fi, i=1,…,5 (the dashed red line). The first harmonics of bending moment due to nonlinear forces including F_6 are very close to those without F_6 and the second harmonics of bending moment show a small difference between them at stations 5, 10 and 15, as shown in Figure 4.42. It may be noted that heave, pitch and bow acceleration (i.e. the first harmonics of motion), and the first and second harmonics of bending moment are little affected by the impact loads.

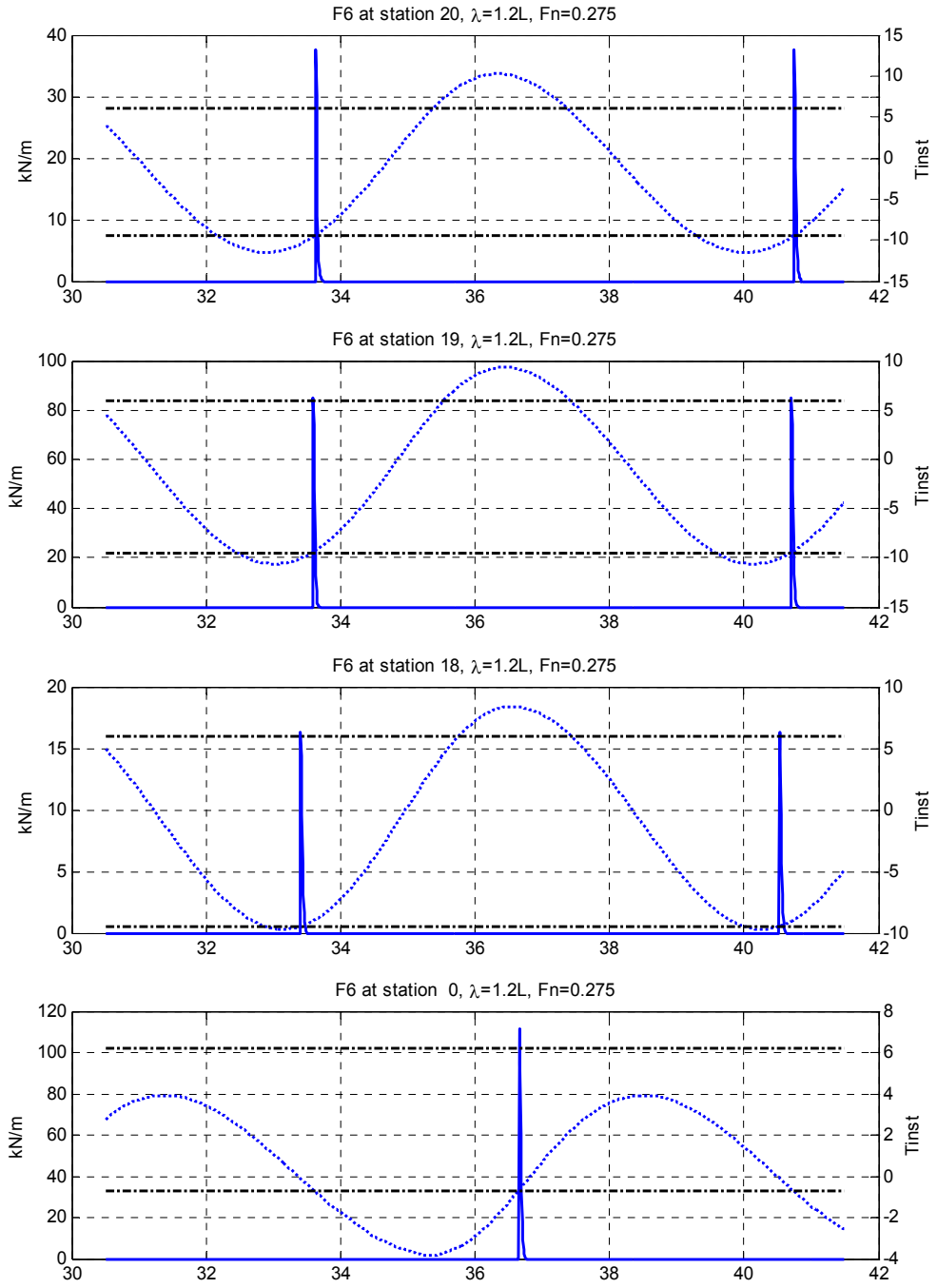

Figure 4.36 Time history of bottom slamming force (F_6) , λ/L=1.2, a=L/60, Fn=0.275

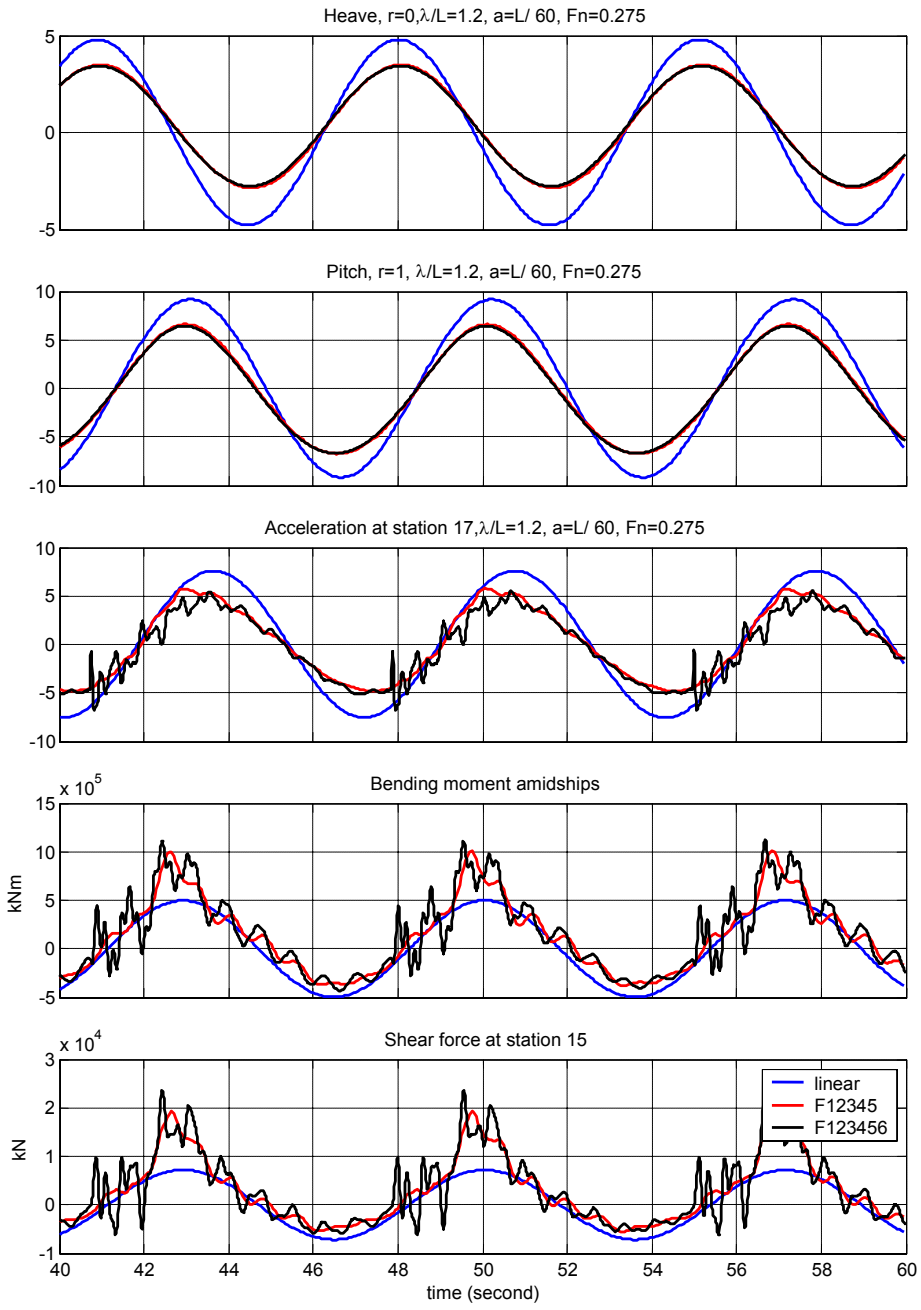

Figure 4.37 Time simulation of heave and pitch motions, bow acceleration, bending moment and shear force, λ/L=1.2, a=L/60, Fn=0.275

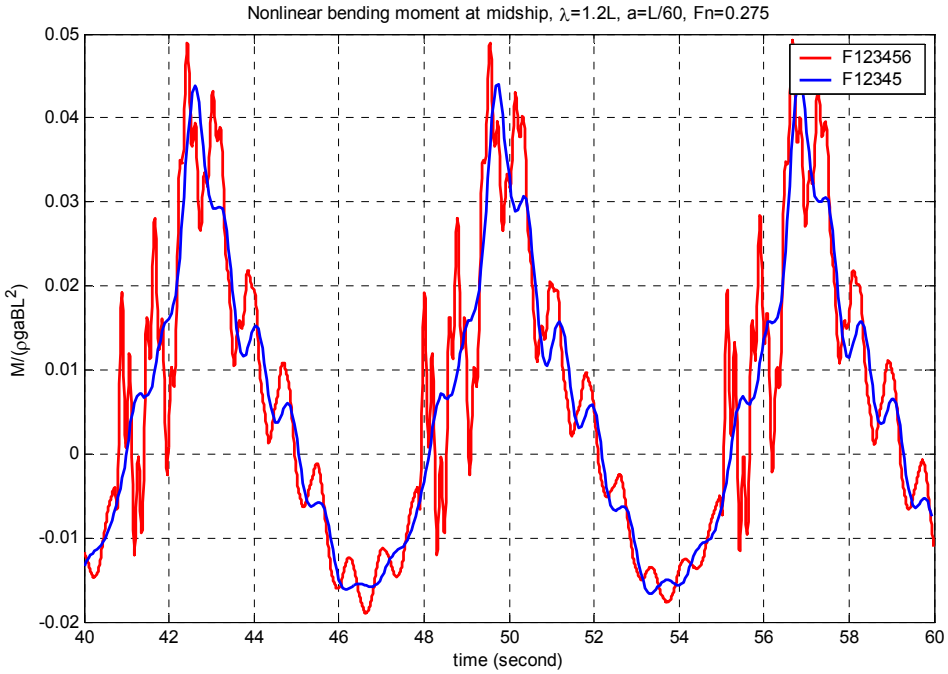

Figure 4.38 Time history of bending moment amidships, F12345 vs. F123456, λ/L=1.2, a=L/60, Fn=0.275

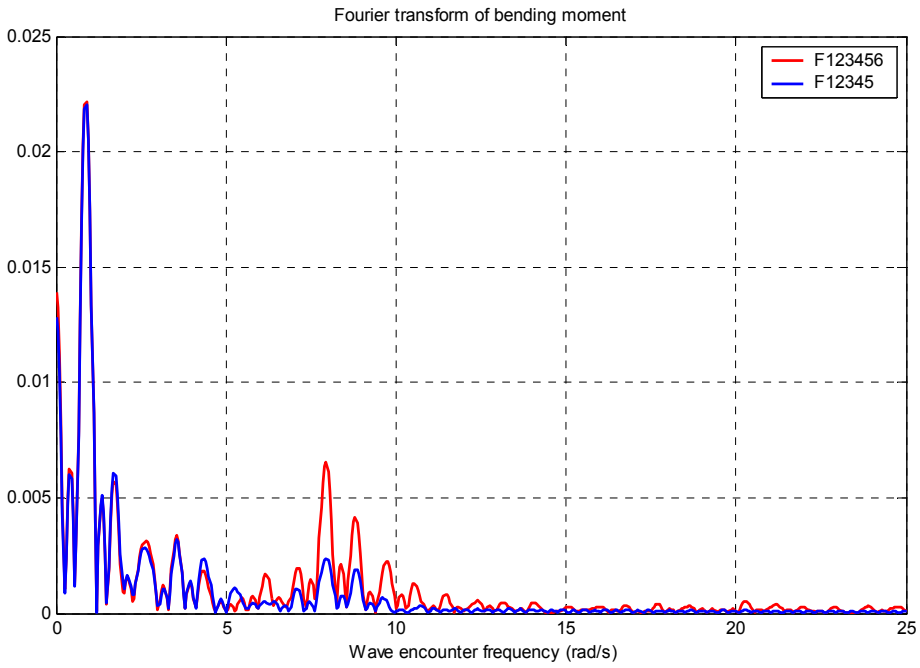

Figure 4.39 Fourier transfer of bending moment with/without bottom slamming force, F12345 vs. F123456, λ/L=1.2, a=L/60, Fn=0.275

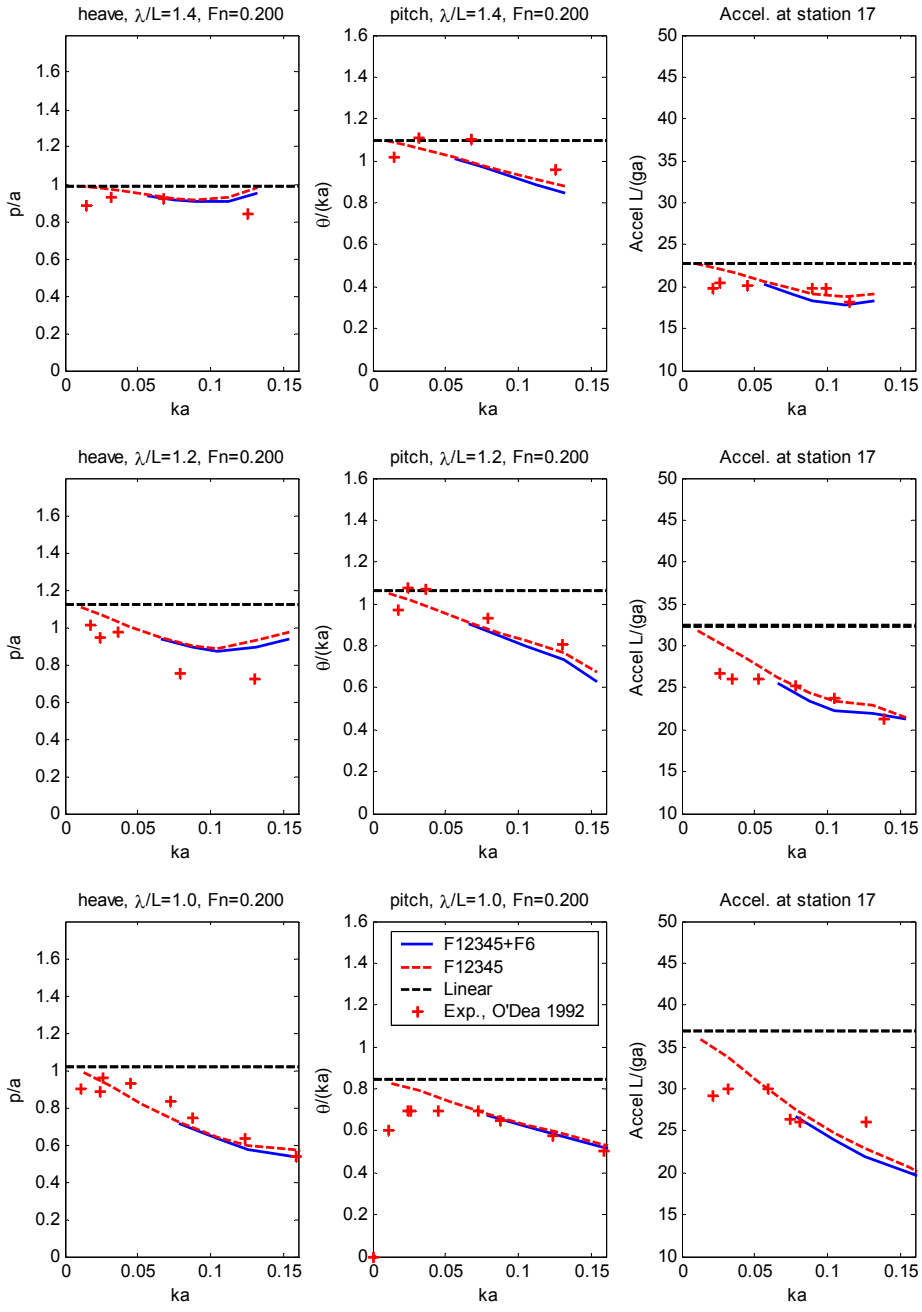

Figure 4.40 Heave, pitch and bow acceleration (at station 17) including bottom slamming force, Fn=0.2

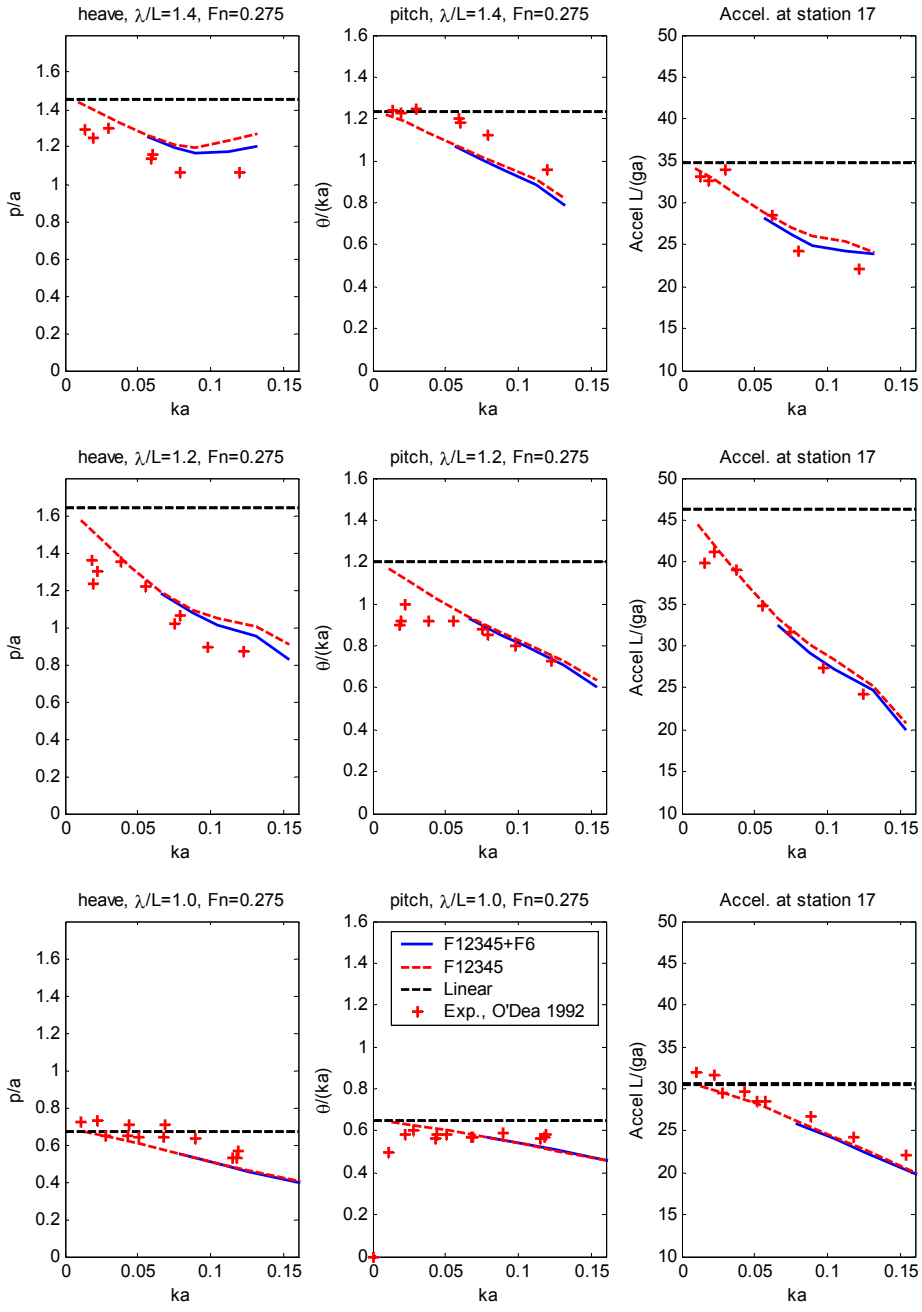

Figure 4.41 Heave, pitch and bow acceleration (at station 17) including bottom slamming force, Fn=0.275

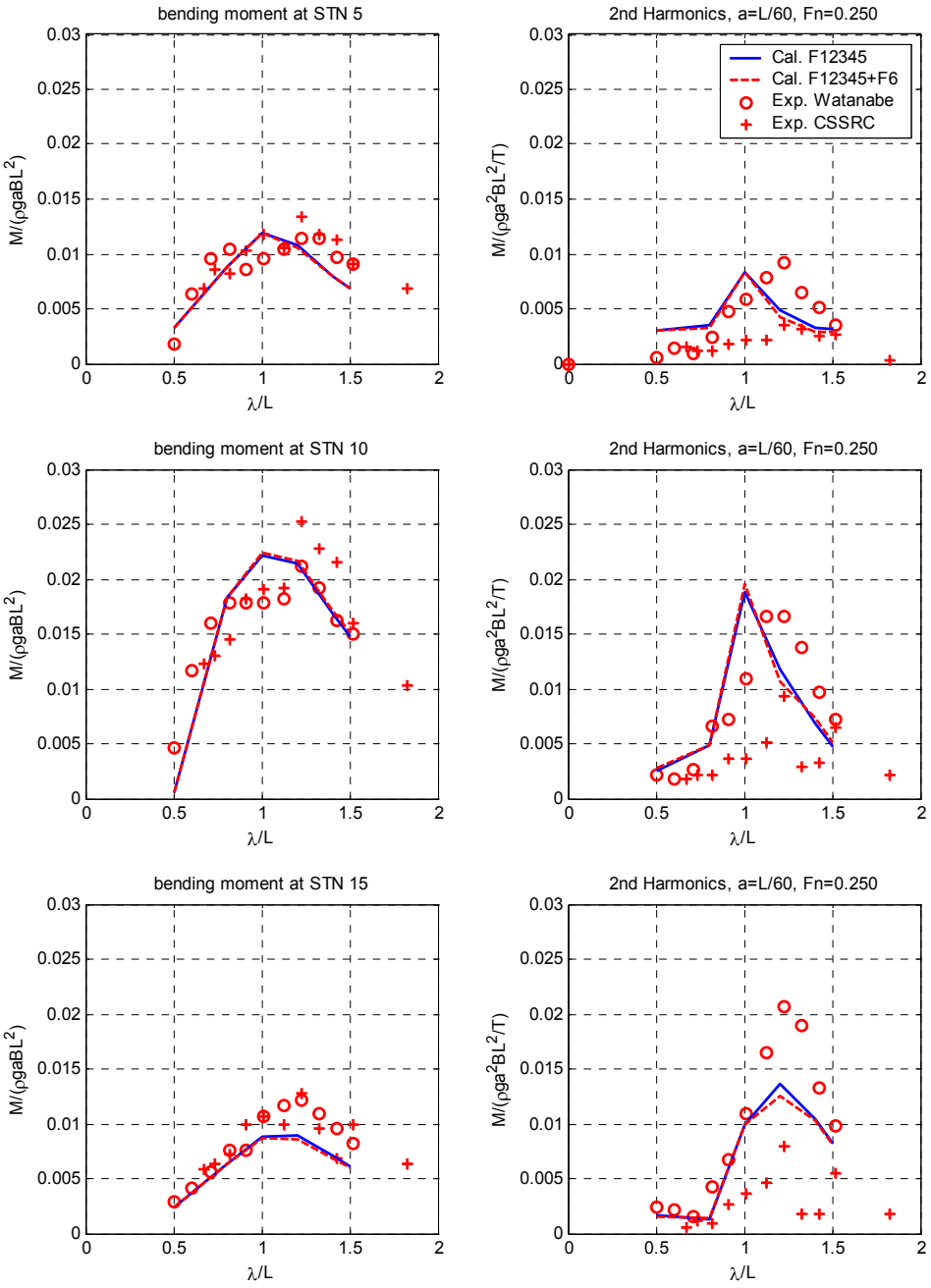

Figure 4.42 First and second harmonics of bending moment with/without bottom slamming force (F_6), a=L/60, Fn=0.25,

4.6 Conclusive remarks

1. The influence of each nonlinear force component (F_i, i=1,…,6) according to the variation of instantaneous draught is verified in the time domain simulation. Bow emergence/deck immersion conditions and the large variation of hydrodynamic force at bow flared sections are well reflected in estimating the nonlinear forces.

2. In general, the amplitude of the nonlinear wave excitation force F_1, F_2, F_3 and F_4 is not so different as to indicate a dominant force among them. F_5 (Green water) does not occur for a regular wave when the wave amplitude is below L/60 (a<L/60) and is small when it occurs.

3. COMP 2 (including F_1, F_2, F_3 and F_4) and COMP 3 (including F_1, F_2, F_3, F_4 and F_5) for pitch and bow acceleration show, in general, better agreement to experiments and exhibit more effects of nonlinearities than COMP 1 (including F_1 and F_4). It means that the modification of hydrodynamic forces (F_2 and F_3) is important as well as the flare slamming force (F_1) and the hydrostatic Froude-Krylov force (F_4).

4. The responses of motions and wave loads of Type 1 (the modification of hydrodynamic force at incident wave encounter frequency) show better agreement with experiments than those of Type 2 (the modification of hydrodynamic force at infinite frequency) and Type 3 (radiation force at infinite frequency and diffraction force at incident wave encounter frequency).

Comparing Types 1, 2 and 3, it may be concluded that the modification of damping force F_3 has a large influence on responses.

5. The motion responses calculated by mode summation with N=2 and N=4 are very close to each other, so it is concluded that hull flexibility with higher distortion modes has only a small influence on the nonlinear motion responses.

6. The calculated results of the first harmonics of bending moment are in good agreement with experiments at stations 5 and 10, while at station 15 the calculated results are rather smaller. The second harmonics of bending moment, in general, are larger than the measurements at stations 5 and 10, while the calculated results are close to the experimental measurements at station 15. The calculated results are in good agreement with experiments for the hogging condition and slightly larger in the sagging condition.

7. The calculated high frequency bending moment is much affected by the impact loads (F_6) and the whipping peaks are apparently observed around the resonance frequency of 2-node hull girder vibration. Heave, pitch, bow acceleration and the first and second harmonics of bending moment are little affected by the impact loads.

Chapter 5

Alternative Method for Prediction of Nonlinear Ship Motions and Wave Loads

5.1 Introduction

In Chapter 2, a method for the prediction of the hydroelastic responses of ships in large amplitude motions was presented, based on the convolution integral method, whereby the nonlinear effects were applied as modifications and the linear and nonlinear responses combined (see Equation 2.44 and 2.45). In Chapter 3, the convolution integral method is compared to the direct integral method for linear responses in the time domain. Based on the excellent agreement observed, it was concluded that the responses estimated in the two methods are close to each other for a specific wave frequency in linear analysis. In Chapter 4, the influence of the nonlinear force components on ship motions and wave loads was evaluated, based on Equation 2.44 and 2.45. this method will hence forward will be referred to as Method 1.

In this chapter an alternative method (Method 2) is introduced for the nonlinear problem for ships in large amplitude of motions and wave loads. In this method, all hydrodynamic coefficients are varied with the instantaneous draught of each hull section. The bottom impact (F_6) and green water (F_5) are estimated in the same manner as in Chapter 2 and included among the total hydrodynamic forces. The flexible modes of the ship hull girder, represented by Timoshenko beam theory, are included as before, N=4.

The calculations were performed for the S175 container ship and the predicted results are compared with those estimated by Method 1 and experiments, described in Chapter 4.

5.2 Theoretical background for alternative method

According to STF linear strip theory (Salvesen et al. 1970), when a ship oscillates in a regular wave, the vertical force on the ship hull can be expressed as, combining Equations 2.21 and 2.29

$$F(x,\omega_e) = -\frac{D}{Dt}\left[\left\{m(x,\omega_e) + \frac{i}{\omega_e}N(x,\omega_e)\right\}\frac{Dz_{rel}(x,t)}{Dt}\right] - \rho g B(x) z_{rel}(x,t) \quad (5.1)$$

Theoretically, this expression is suitable for response predictions of wall sided sections heaving in small amplitude incident waves.

For a slender ship advancing in large-amplitude incident regular waves, this equation can be generalised by setting B(x), $m(x,\omega_e)$, $N(x,\omega_e)$ to vary with time t, i.e. instantaneous draughts of the hull. The vertical relative displacement of each section to wave elevation at an instant is

$$z_{rel}(x,t) = w(x,t) - \bar{\zeta}(x,t). \quad (5.2)$$

As per linear theory the fluid force of Equation 5.1 can be split into radiation, hydrostatic restoring force and diffraction force but with time (or instantaneous draught) dependent values. Then the hydroelastic equation of motion can be expressed as follows:

$$\left[a + A(\omega_e,t)\right]\ddot{p}(t) + \left[b + B(\omega_e,t)\right]\dot{p}(t) + \left[c + C(t)\right]p(t) = F(t) \quad (5.3)$$

where the matrices [a], [b], and [c] are the generalised structural mass, damping and stiffness respectively, and $[A(\omega_e,t)]$, $[B(\omega_e,t)]$ and $[C(t)]$ are the added mass, fluid damping and hydrostatic restoring force estimated at instantaneous draught, respectively. F(t) is the incident wave excitation force, consisting of the diffraction force and the Froude-Krylov force. $[A(\omega_e,t)]$, $[B(\omega_e,t)]$, $[C(t)]$ and F(t) are obtained by following the formulation in the linear method (see Appendix 2). However, B(x), $m(x,\omega_e)$, $N(x,\omega_e)$ and their derivatives are estimated at instantaneous draught.

The product of a time rate of change of added mass (fluid damping is dismissed by assumption in Section 2.3) and the square of the section's vertical relative velocity is defined as F_1 force (i.e. flare slamming) in Equation 2.54 (Gu et al. 2003). In this method (Method 2), Equation 5.3 does not contain F_1, so that F_1 force is treated separately and added. The bottom slamming force (F_6, in Equation 2.66) and green water force (F_5 in Equation 2.61) are also considered when these forces vary according to the instantaneous draught.

In consequence, the hydroelastic equations of motion for ships in large amplitude waves is expressed as: (Gu et al. 2003)

$$[a + A(\omega_e,t)]\ddot{p}(t) + [b + B(\omega_e,t)]\dot{p}(t) + [c + C(t)]p(t) = F(t) + F_1(t) + F_5(t) + F_6(t) \quad (5.4)$$

.

Equation 5.4 was numerically solved in the time domain step by step using the Newmark-beta direct integration method, as introduced in Chapter 3.4.2.2.

5.3 Results and comparisons

Figure 5.1 shows heave and pitch motions, bow acceleration at 0.85L, midship bending moment and shear force at 0.75L for a regular wave amplitude a=L/60 with Fn=0.275 and λ/L=1.2. Compared with the results predicted by Method 1 in Figure 4.9, the nonlinear responses by Method 2 in Figure 5.1 are close to those by Method 1. The fluctuations of bending moment by Method 2 decrease, comparing Figure 4.9

.

Excluding the flare slamming force (F_1), green water force (F_5) and bottom impact slamming force (F_6) from Method 2 and using Method 1 with F_2, F_3 (Type 1) and F_4, then both methods are directly comparable. The heave, pitch and bow acceleration (station 17) transfer functions calculated by the alternative method (Method 2) are presented in Figures 5.2 and 5.3 in comparison with those by the convolution integral method (Method 1) for Fn=0.2 and 0.275. Figure 5.2 shows that heave, pitch and bow acceleration transfer functions estimated by Method 2, are close to those by Method 1, in the case of low amplitude waves (below ka=0.05). Above that range, the heave responses of Method 2 are smaller than Method 1. Pitch and bow acceleration responses are close to each other. This trend is also seen in Figure 5.3, for Fn=0.275.

Figures 5.4 and 5.5 show the heave, pitch and bow acceleration, including F_1 and F_5 forces, comparing Method 1 and Method 2 as well as experimental results. In this figure, Method 2 denotes the solution with F(t) only (see Equation 5.4). One can also see the influence of subsequently adding F_1 and F_5 to the prediction by Method 2. The largest influence, as expected, is due to Force F_1. The influence of green water (F_5) is only seen at high values of ka. Predictions by Method 1 and 2, with equivalent

nonlinear influences, are very close to each other. This confirms the validity of both methods and numerical procedures used.

The vertical bending moment is shown in Figure 5.6, comparing predictions by Method 1 and 2, with and without bottom slamming, and experimental results for a regular wave of amplitude a=L/60 at Fn=0.275. The figure shows that the first harmonics of the amidships bending moments estimated by Method 2 are close to those by Method 1 and agree well with experiments. Bending moments predicted by Method 2 at the quarter length points are a little closer to the experimental values. The second harmonics of bending moment by Method 2 are a little smaller than those of Method 1 for a short wave ($\lambda/L<1.0$) and larger above $\lambda/L>1.0$. In the later region predicted bending moments (2^{nd} harmonics) by Method 2 are closer to the experimental measurements than Method 1. The bottom slamming force (F_6) has only a small effect on the first and second harmonics of bending moments, as seen in Figure 5.6.

From Figures 5.1 to 5.6, it may be concluded that the nonlinear hydroelastic response of ship motion and wave loads calculated by both Method 1 and Method 2 compared reasonably well to experimental measurements.

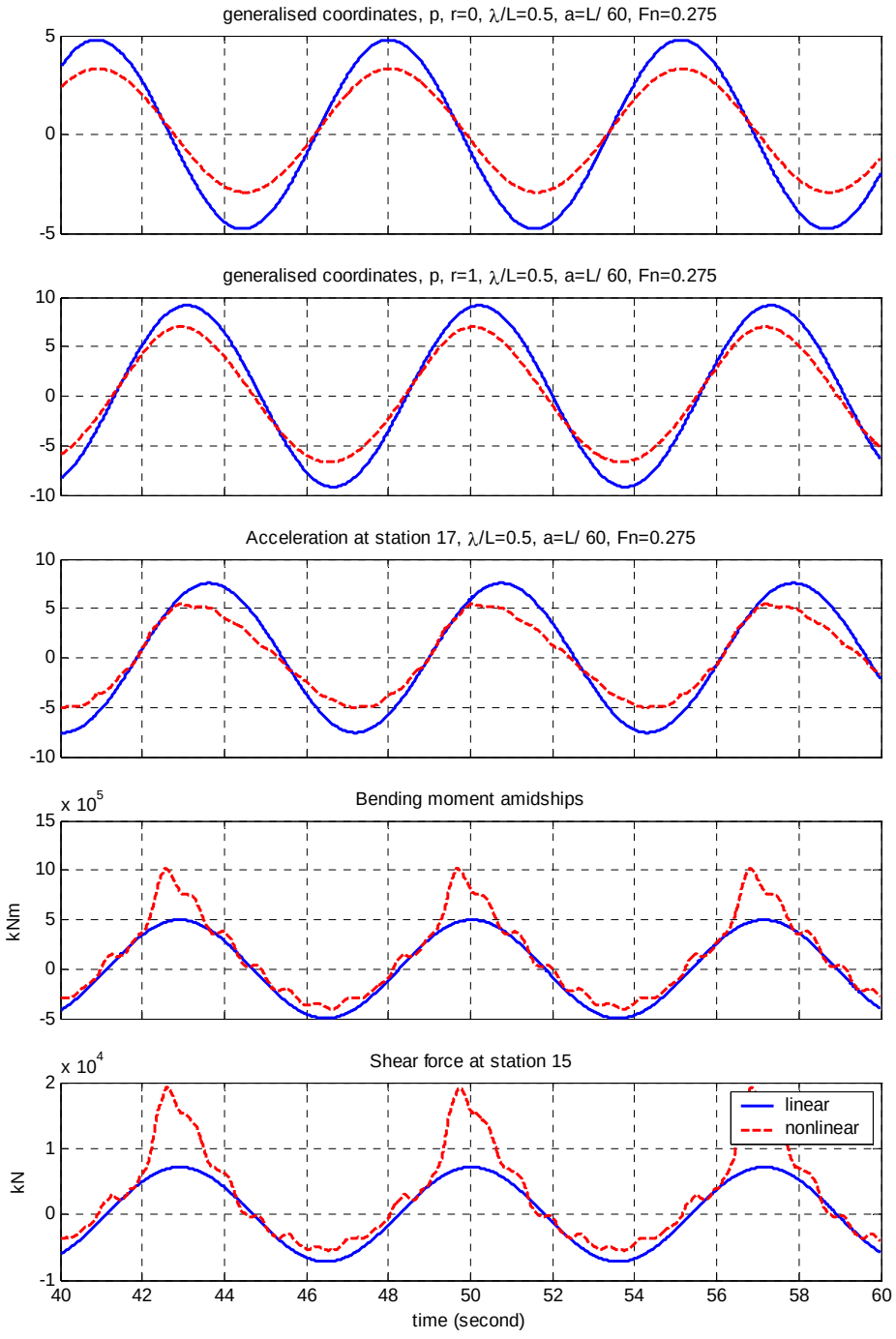

Figure 5.1 Time simulation of heave and pitch motions, bow acceleration at 0.85L, bending moment and shear force at 0.75L by Method 2, λ/L=1.2, a=L/60, Fn=0.275

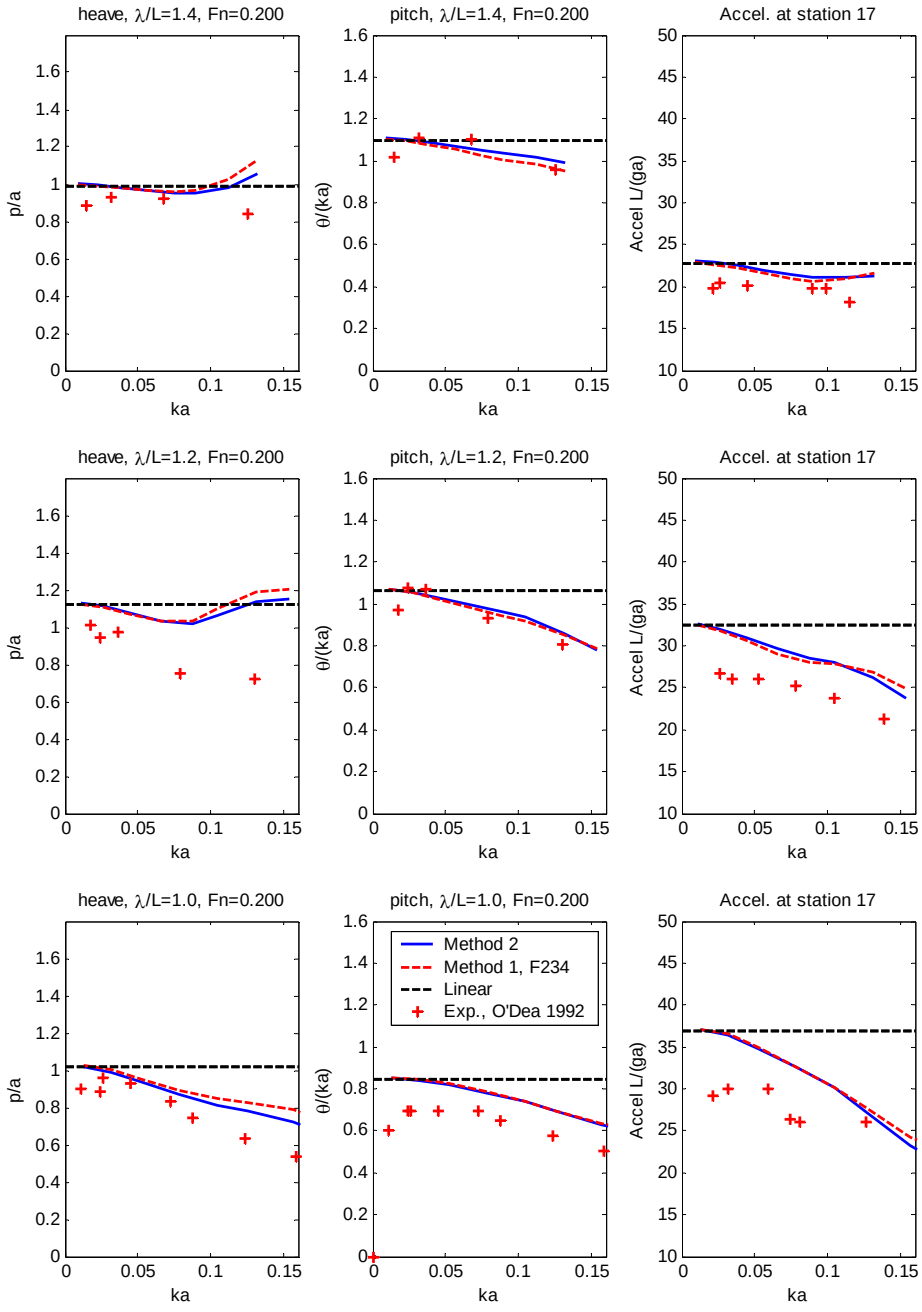

Figure 5.2 Ship motions and bow acceleration at station 17 with respect to wave steepness; comparison between Method 1 and Method 2, Fn=0.2

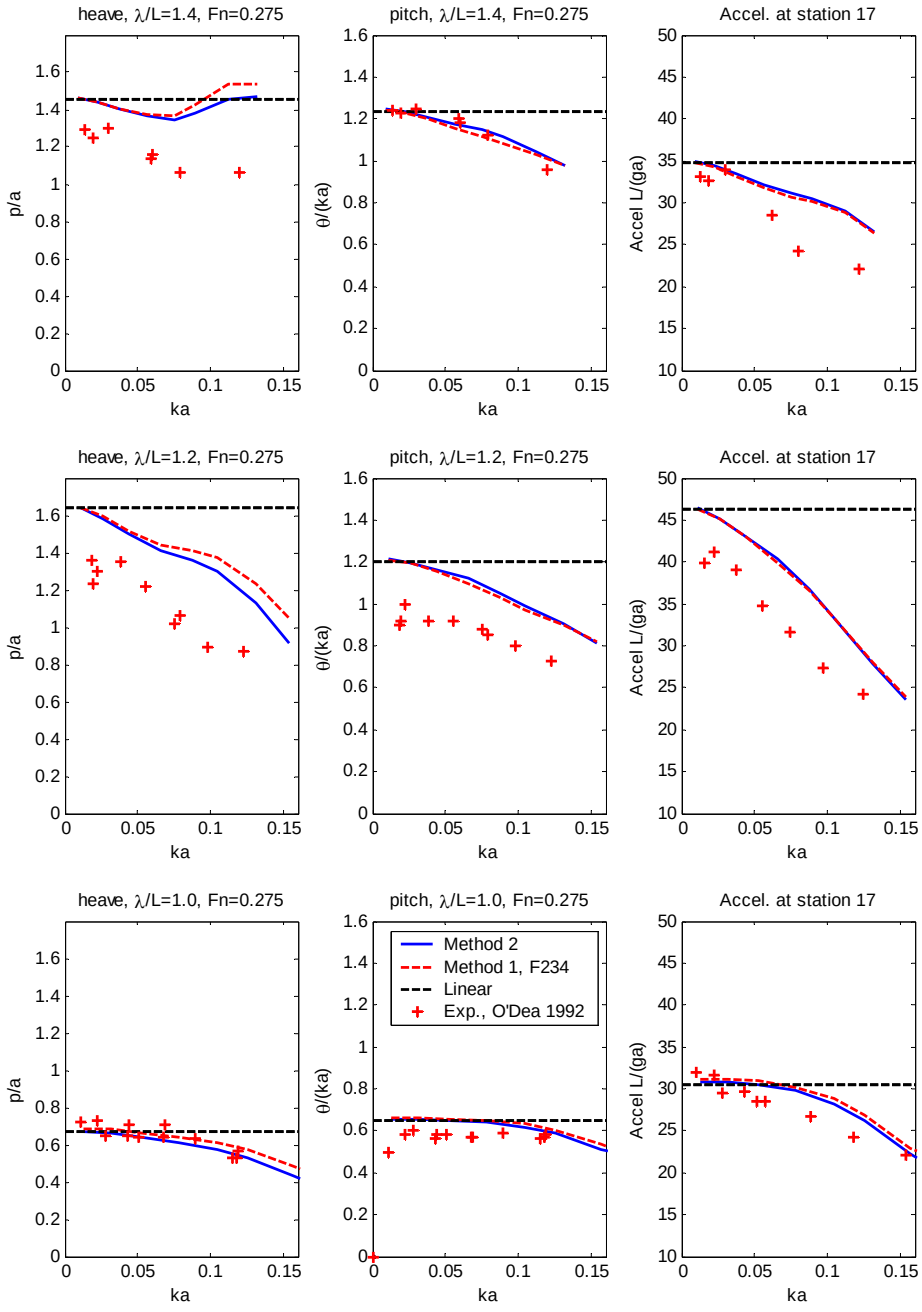

Figure 5.3 Heave, pitch and bow acceleration at station 17 with respect to wave steepness; comparison between Method 1 and Method 2, Fn=0.275

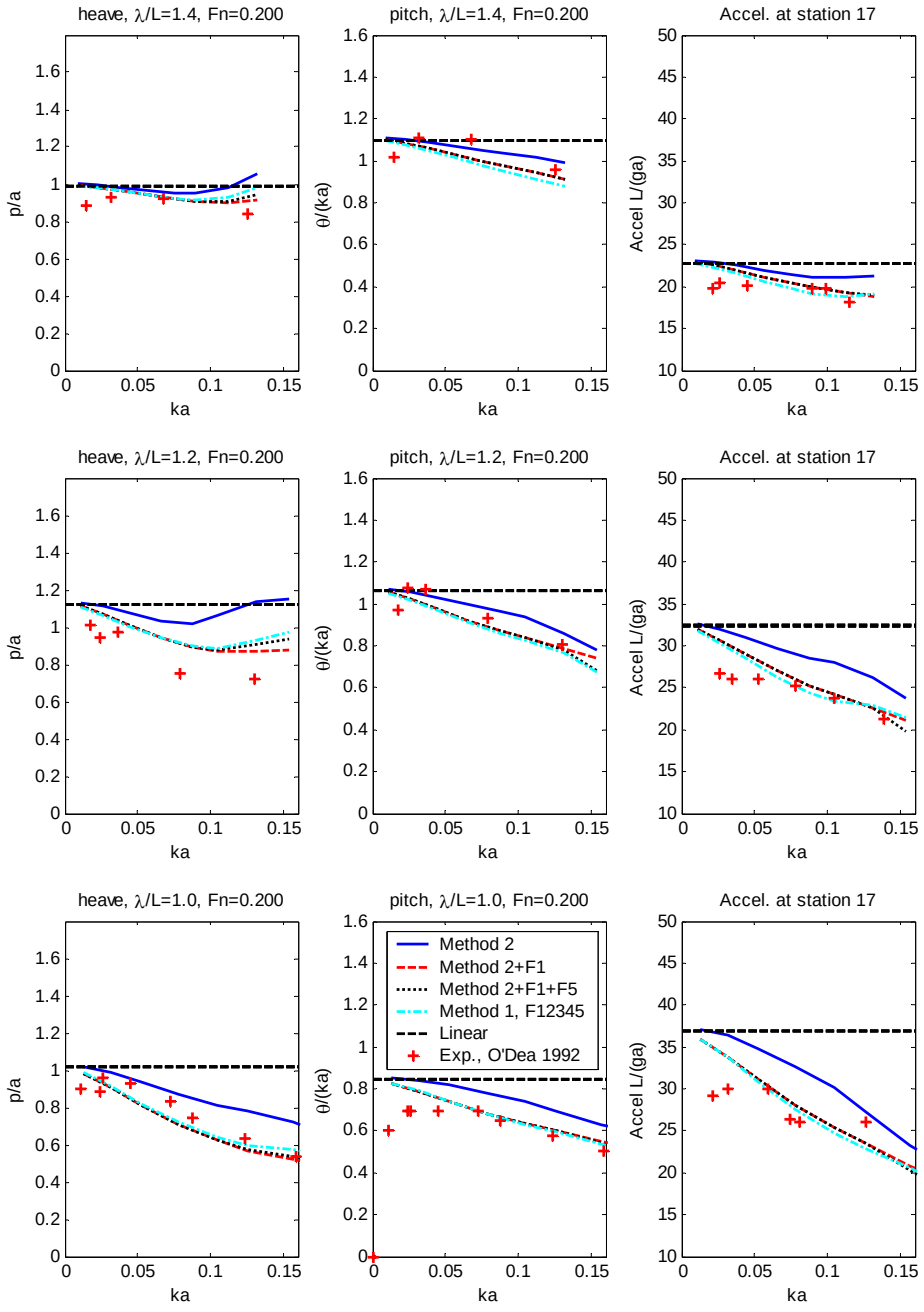

Figure 5.4 Heave, pitch and bow acceleration at station 17 as a function of wave steepness using Method 1 and 2, Fn=0.2

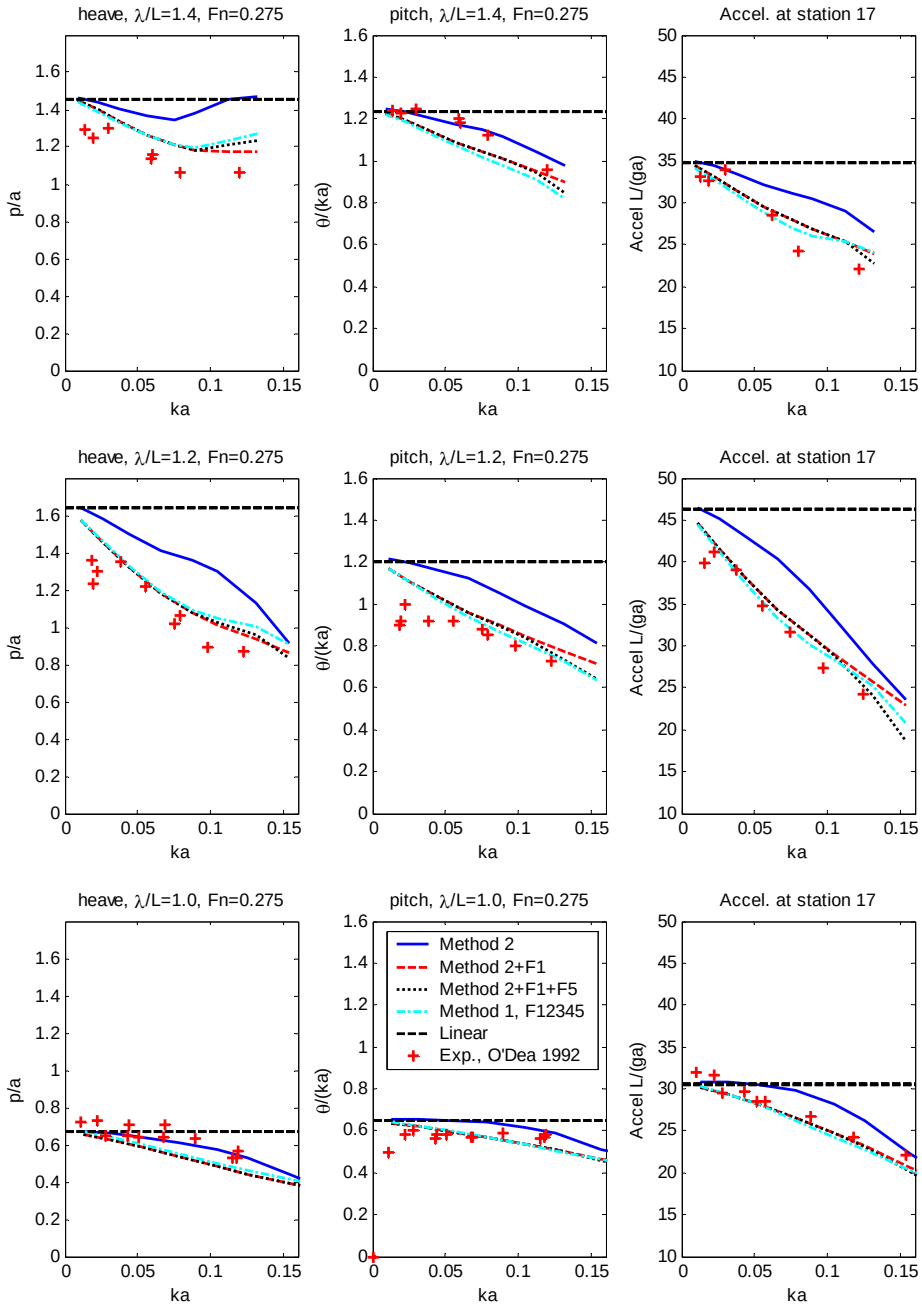

Figure 5.5 Heave, pitch and bow acceleration at station 17 as a function of wave steepness using Method 1 and 2, Fn=0.275

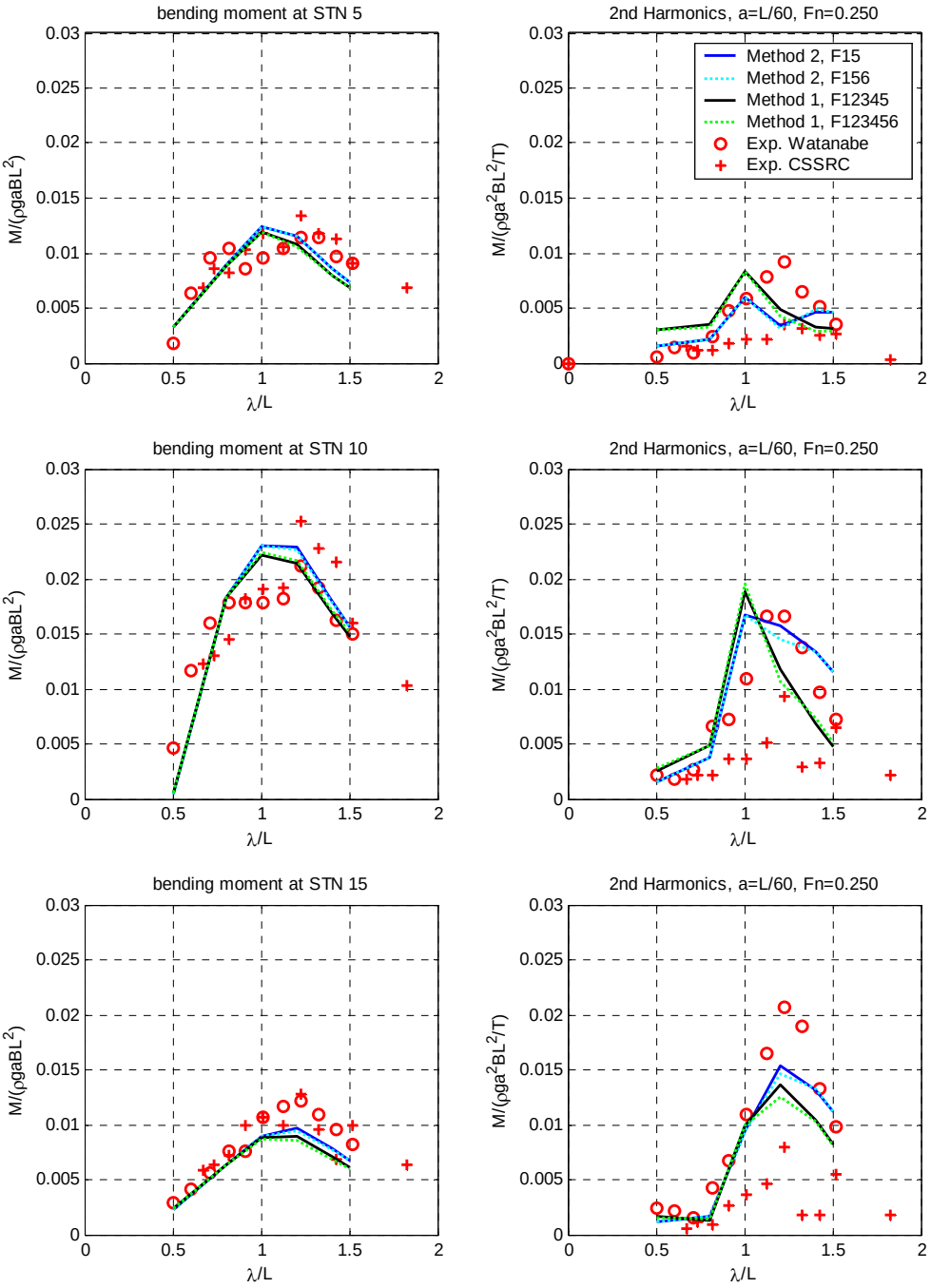

Figure 5.6 First and second harmonics of bending moment with/without bottom slamming force (F_6); comparison between Methods 1 and 2, a=L/60, Fn=0.25

Chapter 6

Conclusions

6.1 Conclusion

1. The linear response in regular waves is obtained both in frequency and time domain, the latter using convolution and direct integration methods, in order to ascertain the most suitable method for the nonlinear analysis. An investigation is carried out for the nonlinear solution, in order to understand the importance of the various force components and their numerical issues. The nonlinear solutions (both methods 1 and 2) developed in this study provide consistent and acceptable results over a range of speeds and wave steepness for rigid body motions, bow acceleration and sagging/hogging bending moments. This is based on comparison with extensive experimental measurements for the S175 container ship.

From the linear time domain analysis

2. The rigid body motion is little affected by the number of mode summations, while the vertical bending moments vary up and down according to the number of mode summations. The first five modes are adequate to ensure convergence.

3. The convolution integral method using the impulse response function estimated by the inverse Fourier transformation may give correct results for the whole frequency range of excitation while the system matrix for the Hamiltonian method and the Newmark method need to be modified in order to calculate transient response.

From the nonlinear time domain analysis

4. The nonlinear modifications of radiation and diffraction force (F_2 and F_3) are important as well as flare slamming force (F_1) and nonlinear hydrostatic Froude-Krylov force (F_4). Furthermore, it is observed, from the parametric study, that the modification of damping force has a large influence on the responses.

5. The whipping peaks on the bending moment due to the impact loads (F_6) are apparently observed around the resonance frequency of 2-node hull girder vibration, which contributes larger peak values in hogging and sagging responses. Heave, pitch and bow acceleration (i.e. the first harmonics of motions), and the first and second harmonics of bending moment are little affected by the impact loads.

From the alternative method

6. Predictions by Method 1 (the convolution integral method) and Method 2 (the alternative method based on the direct numerical integration method), with equivalent nonlinear influences, are very close each other. This confirms the validity of both methods and numerical procedures used. The nonlinear hydroelastic response of ship motion and wave loads calculated by Method 1 and 2 compared reasonably well to experimental measurements.

6.2 Recommendations for further work

1. Through the present research work, the hydroelasticity analysis for symmetric dynamic behaviour of ships in waves was carried out in regular waves. The method can extend to estimate the vertical responses to irregular waves. In

the linear analysis, the irregular seaway is expressed as the superposition of the regular waves. However the nonlinear responses may not be estimated the sum of responses corresponding to regular waves because the nonlinear fluid forces vary with current draught as well as frequency. One of the suggestion method for estimating the responses in irregular waves based on the present method (i.e. convolution integral method), is that the linear responses are calculated by the sum of responses to regular waves and the nonlinear forces estimated at instantaneous draught are calculated for a certain wave frequency (e.g. the heave/pitch resonance frequency) (Gu et al. 2003). The total responses are obtained by sum of linear and nonlinear responses.

2. For the short-term and long-term predictions, it is important to investigate the motions and loads in all directional waves. The container ship may suffer the highest stresses in oblique waves. In order to predict hydroelastic responses of the horizontal and torsions modes based on the present method using strip theory, a thin-walled beam model is applicable (Bishop and Price 1979). Estimating the two-dimensional hydrodynamic coefficient, the multi-parameter conformal mapping technique is utilised for asymmetric sections below water line (Westlake et al. 2000).

References

1 Adegeest, L.J.M, Braathen, A.and Loseth, R.M, 'Use of non-linear sea-loads simulation in design of ships', Proc. of Practical Design of Ships and Mobile Units, pp.53-58, 1998.

2 Aertssen, G. and Sluys, M.F., ‘Service performance and seakeeping trials on a large containership’, Trans. RlNA., Vol.114, 1972.

3 Aksu, S., Price, W.G and Temarel, P., 'Steady state and transient responses of bulk carriers and tankers in random seas', Trans. Royal Institute of Naval Architects, pp.72-95, 1995.

4 Aksu, S., Price, W.G., Suhrbier, K.R. and Temarel, P., 'Comparison study of the dynamic behaviour of a fast patrol boat travelling in rough seas', Marine Structures, Vol.6, pp.421-441, 1993.

5 Baarholm, G.S. and Jensen, J.J, 'Influence of whipping on long-term vertical bending moment', Journal of Ship Research, Vol.48, No.4, pp.261-272, 2004.

6 Ballard, E.J., Hudson, D.A, Price, W.G and Temarel, P., 'Time domain simulation of symmetric ship motions in waves', International Journal of Maritime Engineering, pp.89-108, 2003.

7 Beck, R.F, Cao, Y., Scorpio, S. and Schultz, W., "Nonlinear ship motion computations using the desingularized method', Proc. Of 20th symposium on Naval Hydrodynamics, p227-246, 1994.

8 Belik, Ö., Bishop, R.E.D. and Price, W.G., 'On the slamming response of ships to regular head waves', Trans. of RINA, Vol.121, pp.325-337, 1980.

9 Belik, Ö., Bishop, R.E.D. and Price, W.G., 'Influence of bottom and flare slamming on structural reponses', Trans. RINA, Vol.129, pp.261-275, 1987.

10 Bishop, R.E.D, Clarke, J.D. and Price, W.G., 'Comparison of full scale and predicted responses of two frigates in severe weather trial', Trans. RINA, Vol.126, pp.123-66, 1984.

11 Bishop, R.E.D, Price, W.G. and Tam, P.K.Y., 'A unified dynamic analysis of ship response to waves', Trans. RINA, Vol.119,pp.363-390, 1977.

12 Bishop, R.E.D, Price, W.G. and Tam, P.K.Y., 'A unified dynamic analysis of antisymmetric ship response to waves', Trans. RINA, Vol.120, 1978a.

13 Bishop, R.E.D., Price, W.G. and Tam., P.K.Y., 'On the dynamics of slamming', Trans. RINA, Vol.120, 259-280, 1978b.

14 Bishop, R.E.D., Price, W.G. and Tam., P.K.Y., 'Hydrodynamic coefficients of some heaving cylinders of arbitrary shape', International Journal of Numerical methods in Engineering', Vol.13, pp.17-33, 1978c.

15 Bishop, R.E.D and Price, W.G., 'Hydroelasticity of ships', Cambridge University Press, 1979.

16 Bishop, R.E.D, Price, W.G. and Wu, Y., 'A general linear hydroelasticity theory of floating structures moving in a seaway', Philosophy Trans. of Royal Society of London, A316,pp.375~426, 1986.

17 Buchner, B. 'On the impact of green water loading on ship and offshore unit design', 6th International Symposium on Pratical Design of Ships and Mobile Units, PRADS'95, pp.1.430-1.443, 1995.

18 Chan, H.S, Altar, M. and Incecik, A., 'Global wave loads on intact and damaged Ro-Ro ships in regular oblique waves', Marine Structures, Vol. 16, pp.323-344, 2003.

19 Chen, R.Z, Du, S.X., Wu, Y.S., Lin, J.R. Hu, J.J. and Yue, Y.L, "The experiment on extreme wave loads on a flexible model of the S175 container ship', China ship scientific research center report, 1999

20 Chen, R.S., Du, S.X., Wu, Y.S., Lin, J.R. Hu, J.J. and Yue, Y.L., 'Experiment on extreme wave loads of a flexible ship model', PRADS' 2001, September Shanhai, China, pp.871-878, 2001.

21 Chui, F. and Fujino, M., 'Nonlinear prediction of vertical motions of a fishing vessel in head sea', Journal of Ship Research, 35, 1, pp.32-39, 1991.

22 Cummins, W.E, 'The impulse response function of ship motions', Schiffstechnik, 7, pp.101-109, 1962.

23 de Jong, B., 'Computation of the hydrodynamic coefficients of oscillating cynlinders, Neth. Res. Centre TNO Report, 145a, 1955.

24 Dobrovol'skaya, Z.N., 'On some problems of similarity flow of fluid with a free surface', Journal of Fluid Mechanics, 36, pp.805-829, 1969.

25 Domnisoru, L. and Domnisoru, D, 'The unfied anslysis of springing and whipping phenomena', Trans. RINA, pp.19-36, 1997.

26 Du, S., Hudson, D.A, Price, W.G and Temarel, P., 'Comparison of numerical evaluation techniques for the hydrodynamic analysis of a ship travelling in waves', Trans. RINA, pp.236-258, 1999.

27 Faltinsen, O.M., 'A study of the two dimensional added mass and damping coefficients by the Frank's close fit method', Det Norske Veritas report 69-10-S, 1969.

28 Faltinsen, O. and Zhao, R., 'Numerical predictions of ship motions at high forward speed', Phil. Trans. of Royal Society of London, Vol.334, pp.241-252, 1991.

29 Faltinsen, O.M., 'Sea loads on ships and offshore structures', Cambridge: Cambridge University Press, p.297, 1990.

30 Flokstra, C., 'Comparison of ship motion theroies with experiments for a container ship', International Shipbuilding Progress, Vol.21,pp.168-189, 1974.

31 Fonseca, N. and Guedes Soares, C., 'Time-domain analysis of large-amplitude vertical ship motions and wave loads', Journal of Ship Research, Vol.42,

pp.139-153, 1998.

32 Gerritsma, J and Beukelman, W., 'Analysis of the modified strip theory for the calculation of ship motions and wave bending moments', International Shipbuilding Progress, Vol.14, 1967.

33 Gu, M., Wu, Y. and Xia, J., 'Time domain analysis of non-linear hydroelastic response of ships', Proc. of 4th International Symposium on Practical Design of Ships and Mobile Units, 4, pp.145, 1989.

34 Gu, X.K., Shen, J.W. and Moan, T., 'Efficient and simplified time domain simulation of nonlinear responses of ships in waves', Journal of ship Research, Vol.47, pp.262-273, 2003.

35 Guedes Soares, C, 'Transient response of ship hulls to wave impact', International Shipbuiding Progress, Vol.36, pp.137-156, 1989.

36 Hermundstad, O.A, Aarsnes, J.V. and Moan, T., 'Linear hydroelastic analysis of high-speed catamarans and monohulls', Journal of Ship Research, Vol.43-1, pp.48-63, 1999.

37 Hirdaris, S.E, Price, W.G and Temarel, P., 'Two- and three-dimensional hydroelastic modelling of a bulker in regular waves', Marine Structures 16, pp.627-658, 2003.

38 Hooft, J.P., 'Advanced dynamics of marine structures', John Wiley and sons, 1982.

39 Huang, Y. and Sclavounos, P., 'Nonlinear ship motions', Journal of Ship Research, Vol.42, pp.120-130, 1998.

40 Hughes. O.F, 'Ship structural design', John Willey & Sons, 1983.

41 Inglis, R.B and Price, W.G, ‘Calculation of the velocity potential of a translating, pulsating source’, Trans. RINA, Vol.123, pp.163-175, 1981.

42 Inglis, R.B and Price, W.G, ‘Motions of ships in shallow water’, Trans. RINA, 121, pp.269-282, 1980.

43 Inglis, R.B. and Price, W.G, ‘A three-dimensional ship motion theory: Calculation of wave loading and responses with forward speed”, Trans. RINA, Vol.123, pp183-192, 1982.

44 Inglish, R.B. and Price, W.G., 'A three dimensional ship motion theory – comparison between theoretical predictions and experimental data of the hydrodynamic coefficients with forward speed’, Trans. RINA, pp.141-157, 1981.

45 International Ship and offshore Structures Congress, 13th, Committee I.2, Loads, Trondheim, Norway, 1997.

46 ISSC, 14th, Special task committee VI.1, Extreme hull girder loading, Nagasaki, Japan., 2000.

47 Janardhanan K. and Price, W.G., 'Generalised fluid impulse functions for oscillating marine structures', Journal of Fluids and Structures, Vol.6, pp.207-

222, 1992.

48 Jensen, J.J, and Dogliani, M., 'Wave-induced ship hull vibrations in stochastic seaways', Marine Structures, 9, pp.353-387, 1995.

49 Jensen, J.J, 'Load and global response of ships', Elsevier, 2001.

50 Jensen, J.J. and Mansour, A.E., ‘Estimation of the effect of green water and bow flare slamming on the wave-induced vertical bending moment using closed-form expressions’, Hydroelasticity in Marine Technology, Oxford, UK, pp.155-161, 2003.

51 Jensen, J.J. and Pedersen, P.T., 'Wave-induced bending moments in ships - a quadratic theory', Trans. RINA, pp.151-161, 1979.

52 Kaplan, P., “Analysis and prediction of flat bottom slamming impact of advanced marine vehicles in waves,” International Shipbuild. Progress, 34, pp.44-53, 1987.

53 Kawakami, M., Michimoto, J. and Kobayashi, K., ‘Prediction of long term whipping vibration stress due to slamming of large full ships in rough seas,’ International Shipbuilding Progress, 24, 83-110, 1977.

54 Korvin-Kroukovsky, B.V and Jacobs, W.R, 'Pitching and heaving motions of a ship in regular waves', Trans. SNAME, Vol.65, 1957.

55 Kumai, T., 'Damping factors in the higher modes of ship vibration of Lewis’ section cylinder with finite length', Trans. West JSNA, 50, 173-80, 1958.

56 Kvålsvold, J. and Faltinsen, O.M., 'Hydroelastic modelling of wet deck slamming on multihull vessels', Journal of Ship Research, 39, 3, pp.225-239, 1995.

57 Leibowitz, R.C., 'A method for predicting slamming forces and responses of a ship hull', DTMB Report No.1961, 1963.

58 Lin, W.M and Yue, D.K.P., 'Numerical solutions for large amplitude ship motions in the time domain', Proc. 18th symposium on Naval Hydrodynamics, Ann Arbor, pp.41-66, 1990

59 Lin, W.M. and Yue, D.K.P., 'Time-domain analysis for floating bodies in mild-slope waves of large amplitude', Proc. 8th International Workshop on Water Waves and Floating Bodies, St. Johns, Newfoundland, Canada, 1993

60 Lin, W.M, Meinhold, M.J, Salvensen, N. and Yue, D.K.P, ‘Large-amplitude motions and wave loads for ship design’, Proc. 20th symposium on naval hydrodynamics’, Santa Barbara, pp.205-226, 1994.

61 Lundgen, J., Price, W.G. and Wu, Y., 'A hydroelastic investigation into the behaviour of a floating dry dock in waves', Trans. RINA, Vol.131, pp.213-231, 1989

62 Meek, M., Adams, R. and Chapman, J.C. , ‘The structural design of the O.C.L. container ships', Trans. RINA, Vol.114, pp.241-292, 1972.

63 Miao, S.H, Temarel, P. and Hampshire, J.K., 'Dynamic loads on a trimaran travelling in irregular seaways including slamming', Hydroelasticity in Marine Technology, 2003.

64 Nakos, D.E. and Sclavounos, P.D., ‘Ship motions by a three-dimensional Rankine panel method’, 18th Symposium on naval hydrodynamics, Ann Arbor, Michgan, pp.21-39, 1990.

65 Nakos, D.E., Kring, D.C and and Sclavounos, P.D., ‘Rankine panel methods for time-domain free surface flows', 6th International conference on Numerical Ship Hydrodynamics, 1993.

66 Ochi, M.K. and Motter, L.E., 'A method to estimate the slamming characteristics for ship design', Mar. Tech., 8, pp.219-32, 1971.

67 O'dea, J., Powers, E. and Zselecsky, J., 'Experimental determination of non-linearities in vertical plane ship motions', Proc. of 19th Symposium on Naval Hydrodynamics, 1992.

68 Ogilivie, T.F and Tuck, E.O, 'A rational strip theory of ship motions: Part I', Department of Naval Architecture, The University of Michgan, Rep. No. 013, 1969.

69 Price, W.G. and Bishop, R.E.D, 'Probabilistic theory of ship dynamcis', Chapman and Hall, London, 1974

70 Price, W.G, Temarel, P. and Keane, A.J, 'Hydroelastic analysis of a SWATH in waves', Proceedings of the First International Conference on Hydroelastic in Marine Technology, Norway, pp.231-243, 1994.

71 R.W. Clough and J. Penzien, “Dynamics of structures,” McGraw-Hill, Inc., 1975.

72 Ramos, J., Incecik, A. and Guedes Soares, C., 'Experimental study of slam-induced stresses in a containership', Marine Structures, 13, pp.25-51, 2000.

73 Salvesen, N, Tuck, E.O. and Faltinsen, O., 'Ship motions and sea loads', Trans. SNAME, Vol.78, pp.250-287, 1970.

74 Sclavounos, P.D., Kring, D.C, Huang, Y., Mantzaris, D.A., Kim, S, Kim, Y., 'A computational methods as an advanced tool of ship hydrodynamic design', Trans. SNAME, 105, pp.375-397, 1997

75 Schmitke, R.T., 'Ship sway, roll and yaw motions in oblique seas', Trans. SNAME, 1986.

76 Shin, Y.S., Chung, J.S, Lin, W.M, Zhang, S. and Engle, A., 'Dynmaic loadings for structural analysis of fine form container ship based on a non-linear large amplitude motions and loads methed', Trans. SNAME, Vol.105, pp.127-154, 1997.

77 St. Denis, M. and Pierson, W.J, 'On the motions of ships in confused seas', Trans. SNAME, Vol.61, pp.280-354, 1953.

78 Stavovy, A.B and Chuang, S.L, 'Analytical determination of slamming

pressures for high-speed vehicles in waves', Journal of Ship Research, Vol. 20, pp.190-198, 1976.

79 Stiansen, S.G, Mansour, A. and Chen., Y.N., 'Dynamic response of large great lakes bulk carriers to wave-excited loads', Trans. SNAME, Vol.85, pp.174-208, 1978.

80 Storhaug, G., Vidic-Perunovic, J., Rüdinger, F., Holtsmark, G., Helmers, J.B. and Gu, X., 'Springing/whipping response of a large ocean going vessel – A comparison between numerical simulations and full-scale measurements', Hydroelasticity in Marine Technology, pp.117-129, 2003.

81 Tasai, F., 'Formula for calculating hydrodynamic force of a cylinder heaving on a free surface (N-parameter family)', Res. Inst. Appl. Mech. Kyushu Univ. report 31, pp.71-74, 1960.

82 Tasai, F. and Takaki, M., 'Theroy and calculation of ship responses in regular waves', Symposium on Seaworthiness of Ships, Japan Society of Naval Architects, 1969.

83 Ursell, F., 'On the heaving motion of a circular cylinder in the surface of a fluid', Quart. J. Mech. Appl. Maths, 2, pp.218-131, 1949.

84 Vidic-Perunovic, J. and Jensen J.J., 'Springing response due to directional wave field excitation', 9th Symposium on Practice Design of Ships and Other Floating Structures', pp.869-875, 2004.

85 Wang, Z., Jensen, J.J. and Xia, J., 'On the effect of green water on deck on the wave bending moment', Proc. 7th Int. Symposium on Pratical Design of Ships and Mobile Units, PRADS'98, the Hague, 1998.

86 Watanabe, I. , Ueno, M. and Swada, H., 'Effects of bow flare shape to wave impact pressure', Journal of the Society of Naval Architects of Japan, 166, pp.259-266, 1989.

87 Watanabe, I. and Guedes Soares, C., 'Comparative study on the time-domain analysis of non-linear ship motions and loads', Marine Structures, 12, pp.153-170, 1999.

88 Weaver, W. and Johnson, P.R., 'Structural dynamics by finite elements', 1987

89 Weems, K., Zhang, S., Lin, W.M, Bennett, J. and Shin, Y.S., 'Structural dynamic loadings due to impact and whipping', Proc. Practical Design of Ships and Mobile Units, pp.79-85, 1998.

90 Wu, M.K. and Moan, T., 'Linear and nonlinear hydroelastic analysis of high-speed vessels', Journal of Ship Research, Vol.40, 2, pp.149-163, 1996.

91 Wu, M. and Hermundstad, O.A, 'Time-domain simulation of wave-induced non-linear and loads and its applications in ship design', Marine Structures, 15, pp pp.561-597, 2002.

92 Xia, J. and Wang, Z., 'Time-domain hydroelasticity theory of ships responding to waves', Journal of Ship Research, Vol.41, pp.286-300, 1997.

93 Xia, J., Wang, Z. and Jensen J.J., 'Non-linear wave loads and ship responses by a time-domain strip theory', Marine Structures, 11, pp.101-123, 1998.

94 Zhao, R. and Faltinsen, O., “Water entry of two-dimensional bodies”, Journal of Fluid Mechanics, Vol.246, pp.593-612, 1993.

Appendix 1 Derivation of Froude-Krylov force

The vertical sectional force can be obtained form Equation 2.20, using Gauss integral theorem as

$$F_A = -\iint_A \frac{\partial p}{\partial z} dA \tag{A1.1}$$

where the integrals extent over the instantaneous wetted sectional area *A*.

Figure A1 shows a sketch of sections at rest and after vertically moved in waves. Here $\zeta(x,t)$ is wave elevation and w(x,t) is the vertical displacement of the hull. (Jensen 2001)

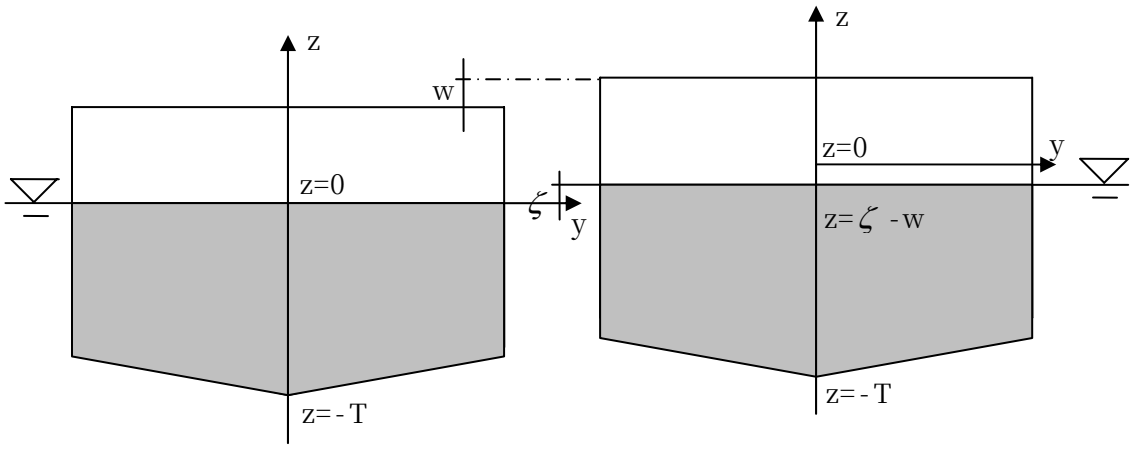

(a) (b)

Figure A1 Sketch of section at different times: (a) section at rest; (b) section after vertical motion in waves

The integral in Equation A1.1 can be written in the equilibrium coordinate system as

$$F_A = -\int_{-T}^{\zeta - w} \frac{\partial p}{\partial z} B(x,z) dz \tag{A1.2}$$

where T is the draught of the section with respect to mean water line and B(x,z) is the ship breadth as function of z.

The derivative in Equation A1.2 can be represented using the global coordinate Z as

$$\frac{\partial p}{\partial z} = \left.\frac{\partial p}{\partial Z}\right|_{Z=z+w} . \tag{A1.3}$$

Then the vertical sectional force of Equation A1.3 becomes

$$F_{FKz}(x;\zeta,w,t) = -\int_{-T}^{\zeta-w} \left.\frac{\partial p}{\partial Z}\right|_{Z=z+w} B(x,z)dz . \tag{A1.4}$$

For the linear wave, the pressure is as shown in Equation 2.18, then

$$\left.\frac{\partial p}{\partial Z}\right|_{Z=z+w} = \left.\frac{\partial(p_a - \rho g z + \rho g e^{kz}\zeta)}{\partial z}\right|_{Z=z+w} = -\rho g + \rho g k \zeta e^{k(z+w)} \tag{A1.5}$$

Finally, Equation A1.5 becomes

$$\begin{aligned} F_{FKz} &= \rho g \int_{-T}^{\zeta-w} B(x,z)dz - \rho g k \zeta \int_{-T}^{\zeta-w} e^{k(z+w)} B(x,z)dz \\ &= \rho g \int_{-T}^{0} B(x,z)dz + \rho g \int_{0}^{\zeta-w} B(x,z)dz - \rho g k \zeta \int_{-T}^{\zeta-w} e^{k(z+w)} B(x,z)dz \end{aligned} \tag{A1.6}$$

The first term in Equation A1.6 is the hydrostatic force in calm water and the remaining terms are the sectional force due to the dynamic pressure in the waves, which is called the Froude-Krylov force.

Appendix 2 Derivation of linear and nonlinear equation of motion

Total vertical fluid force acting on a strip (Equation 2.31) is

$$F(x,t) = -\frac{D}{Dt}\left[\left\{m(x,\omega_e,t) + \frac{i}{\omega_e}N(x,\omega_e,t)\right\}\frac{Dz_r}{Dt}\right] + \rho g\int_0^{\zeta-w} B(x,z)dz \\ -\rho g k\zeta\int_{-T}^{\zeta-w} e^{k(z+w)}B(x,z)dz. \tag{A2.1}$$

The hydrodynamic coefficients are decomposed into linear and nonlinear parts in Equations 2.32 and 2.33 as:

$$m(x,\omega_e,t) = m_o(x,\omega_e) + m_{nl}(x,\omega_e,t) \tag{A2.2}$$

$$N(x,\omega_e,t) = N_o(x,\omega_e) + N_{nl}(x,\omega_e,t) \tag{A2.3}$$

Decomposing the total vertical displacement $w(t)$ also into linear and non-linear parts,

$$w(t) = w_l(t) + w_{nl}(t)\,, \tag{A2.4}$$

then the relative vertical displacement of the ship becomes

$$z_r(x,t) = z_{ro}(x,t) + w_{nl}(x,t)\,,\quad z_{ro}(x,t) = w_l - \overline{\zeta}\,. \tag{A2.5}$$

Substituting Equations A2.2 to A2.3 into Equation A2.1, the vertical fluid force becomes

$$F(x,t) = -\frac{D}{Dt}\left[\left\{\left(m_o(x,\omega_e) + m_{nl}(x,\omega_e,t)\right) + \frac{i}{\omega_e}\left(N_o(x,\omega_e) + N_{nl}(x,\omega_e,t)\right)\right\}\frac{Dz_{rel}}{Dt}\right] \\ +\rho g\int_0^{\zeta-w} B(x,z)dz - \rho g k\zeta\int_{-T}^{\zeta-w} e^{k(z+w)}B(x,z)dz - \rho g B_o(x)z_{ro} + \rho g B_o(x)z_{ro}$$

$$
\begin{aligned}
&= -\frac{D}{Dt}\left[\left\{\left(m_o(x,\omega_e)+m_{nl}(x,\omega_e,t)\right)+\frac{i}{\omega_e}\left(N_o(x,\omega_e)+N_{nl}(x,\omega_e,t)\right)\right\}\frac{Dz_{rel}}{Dt}\right] \\
&+\rho g\int_0^{\zeta-w} B(x,z)dz-\rho gk\zeta\int_{-T}^{\zeta-w} e^{k(z+w)}B(x,z)dz \\
&-\rho gB_o(x)z_o+\rho gB_o(x)(z_r-w_{nl}) \\
&= -\frac{D}{Dt}\left[\left\{m_o(x,\omega_e)+\frac{i}{\omega_e}N_o(x,\omega_e)\right\}\frac{Dz_{ro}}{Dt}\right]-\rho gB_o(x)z_{ro} \\
&-\frac{D}{Dt}\left[\left\{m_o(x,\omega_e)+\frac{i}{\omega_e}N_o(x,\omega_e)\right\}\frac{Dw_{nl}}{Dt}\right]-\rho gB_o(x)w_{nl} \\
&-\frac{D}{Dt}\left[\left\{m_{nl}(x,\omega_e,t)+\frac{i}{\omega_e}N_{nl}(x,\omega_e,t)\right\}\frac{Dz_r}{Dt}\right] \\
&+\rho g\int_0^{\zeta-w} B(x,z)dz-\rho gk\zeta\int_{-T}^{\zeta-w} e^{k(z+w)}B(x,z)dz+\rho gB_o(x)z_r.
\end{aligned}
\tag{A2.6}
$$

Letting the first and second terms of Equation A2.6 as F_l, the third and fourth terms as H_{nl} and the remained terms as F_{nl}, Equation A2.1 can be written as (see Equations 2.36 to 2.39)

$$F(x,t)=F_l(x,t)+H_{nl}(x,t)+F_{nl}(x,t) \tag{A2.7}$$

where

$$F_l(x,t)=-\frac{D}{Dt}\left[\left\{m_o(x,\omega_e)+\frac{i}{\omega_e}N_o(x,\omega_e)\right\}\frac{Dz_{ro}}{Dt}\right]-\rho gB_o(x)z_{ro}, \tag{A2.8}$$

$$H_{nl}(x,t)=-\frac{D}{Dt}\left[\left\{m_o(x,\omega_e)+\frac{i}{\omega_e}N_o(x,\omega_e)\right\}\frac{Dw_{nl}}{Dt}\right]-\rho gB_o(x)w_{nl}, \tag{A2.9}$$

and

$$
\begin{aligned}
F_{nl}(x,t) &= -\frac{D}{Dt}\left[\left\{m_{nl}(x,\omega_e,t)+\frac{i}{\omega_e}N_{nl}(x,\omega_e,t)\right\}\frac{Dz_r}{Dt}\right] \\
&+\rho g\int_0^{\zeta-w} B(x,z)dz-\rho gk\zeta\int_{-T}^{\zeta-w} e^{k(z+w)}B(x,z)dz+\rho gB_o(x)z_r.
\end{aligned}
\tag{A2.10}
$$

The generalised force is obtained by multiplying the mode shapes and integrating

along the ship length. That is to say:

$$F(t) = \int_L w_r(x) F(x,t) dx \,. \tag{A2.11}$$

Substituting Equation A2.7 into Equation 2.5, the hydroelastic equation of motion becomes in a matrix form as

$$[a]\{\ddot{p}\} + [b]\{\dot{p}(t)\} + [c]\{p(t)\} = \{F_l(t)\} + \{H_{nl}(t)\} + \{F_{nl}(t)\} \tag{A2.12}$$

Decomposing the principal coordinates $p(t)$ into linear and non-linear parts

$$\{p(t)\} = \{p_l(t)\} + \{p_{nl}(t)\} \,. \tag{A2.13}$$

The hydroelastic equation motion of Equation A2.13 can be decomposed into linear and nonlinear parts

$$[a]\{\ddot{p}_l\} + [b]\{\dot{p}_l(t)\} + [c]\{p_l(t)\} = \{F_l(t)\} \tag{A2.14}$$

$$[a]\{\ddot{p}_{nl}\} + [b]\{\dot{p}_{nl}(t)\} + [c]\{p_{nl}(t)\} = \{H_{nl}(t)\} + \{F_{nl}(t)\} \,. \tag{A2.15}$$

The linear fluid force $\{F_l\}$ in Equation A2.14 can be decomposed in two parts (Bishop and Price 1979):

$$F_l(t) = -H_l(t) + F_w(t) \tag{A2.16}$$

where $H_l(t)$ is the generalised force due to hull motions (radiation): That is

$$H_l(t) = [A(\omega_e)]\{\ddot{p}_l(t)\} + [B(\omega_e)]\{\dot{p}_l(t)\} + [C]\{p_l(t)\} \tag{A2.17}$$

$$\begin{aligned} A_{rs} = & \int_0^l m_o w_r w_s dx + \frac{U^2}{\omega_e^2} \int m_o w_r' w_s' dx + \frac{U}{\omega_e^2} \int N_o \{w_r' w_s - w_s' w_r\} dx \\ & - \frac{U^2}{\omega_e^2} \left| m_o w_s w_r' \right|_0^l + \frac{U}{\omega_e^2} \left| N_o w_s w_r \right|_0^l , \end{aligned} \tag{A2.18}$$

$$\begin{aligned} B_{rs} = & \int_0^l N_o w_r w_s dx + \frac{U^2}{\omega_e^2} \int N_o w_r' w_s' dx + \frac{U}{\omega_e^2} \int m_o \{w_r' w_s - w_s' w_r\} dx \\ & - \frac{U^2}{\omega_e^2} \left| N_o w_s w_r' \right|_0^l + \frac{U}{\omega_e^2} \left| m_o w_s w_r \right|_0^l \end{aligned} \tag{A2.19}$$

$$C_{rs} = \rho g \int_0^l B_o w_s w_r dx \,. \tag{A2.20}$$

$F_w(t)$ is the generalized linear wave force vector: That is

$$F_w(x,t) = e^{-i\omega_e t} \int_0^l a e^{-k\bar{T}} e^{ikx} \left\{ -\omega^2 \left[m + \frac{UN'}{\omega\omega_e} \right] - i\omega \left[\frac{\omega N}{\omega_e} - Um' \right] + \rho g B \right\} w_s(x) dx \,. \tag{A2.21}$$

The force component $H_{nl}(t)$ in Equation A2.9 is also expressed as

$$H_{nl}(t) = [A(\omega_e)]\{\ddot{p}_{nl}(t)\} + [B(\omega_e)]\{\dot{p}_{nl}(t)\} + [C]\{p_{nl}(t)\}, \tag{A2.22}$$

where $[A(\omega_e)]$, $[B(\omega_e)]$ and $[C]$ are the same in Equation A2.17.

The generalised nonlinear force $F_{nl}(x,t)$ is written as

$$\{F_{nl}(t)\} = \int_L w_r(x) F_{nl}(x,t) dx \,. \tag{A2.23}$$

From Equations A2.17 and A2.21 and Equations A2.22 and A2.23, both linear and nonlinear hydroelastic equation of motion (Equations 2.44 and 2.45) can be written as,

$$[a + A(\omega_e)]\{\ddot{p}_l(t)\} + [b + B(\omega_e)]\{\dot{p}_l(t)\} + [c + C]\{p_l(t)\} = \{F_l(t)\} \tag{A2.24}$$

$$[a + A(\omega_e)]\{\ddot{p}_{nl}(t)\} + [b + B(\omega_e)]\{\dot{p}_{nl}(t)\} + [c + C]\{p_{nl}(t)\} = \{F_{nl}(t)\} \,. \tag{A2.25}$$

Appendix 3 Derivation of nonlinear forces

The sectional nonlinear force in Equation 2.39 is shown as

$$F_{nl}(x,t) = -\frac{D}{Dt}\left[\left\{m_{nl}(x,\omega_e,t) + \frac{i}{\omega_e}N_{nl}(x,\omega_e,t)\right\}\frac{Dz_{rel}}{Dt}\right] + \rho g\int_0^{\zeta-w} B(x,z)dz - \rho gk\zeta\int_{-T}^{\zeta-w} e^{k(z+w)}B(x,z)dz + \rho g B_o z_{rel}\,. \quad \text{(A3.1)}$$

The D/Dt operator is defined as

$$\frac{D}{Dt} = \frac{\partial}{\partial t} - U\frac{d}{dx} \quad \text{(A3.2)}$$

The first term in Equation A3.1 becomes (variable index and function dependence are omitted)

$$\begin{aligned}
&\frac{D}{Dt}\left[\left\{m + \frac{i}{\omega_e}N\right\}\frac{Dz_{rel}}{Dt}\right] = \frac{D}{Dt}\left\{m + \frac{i}{\omega_e}N\right\}\frac{Dz_{rel}}{Dt} + \left\{m + \frac{i}{\omega_e}N\right\}\frac{D^2 z_{rel}}{Dt^2} \\
&= \left(\frac{\partial}{\partial t} - U\frac{\partial}{\partial x}\right)\left[m + \frac{i}{\omega_e}N\right]\frac{Dz_{rel}}{Dt} + \left\{m + \frac{i}{\omega_e}N\right\}\frac{D^2 z_{rel}}{Dt^2} \\
&= \frac{\partial m}{\partial t}\frac{Dz_{rel}}{Dt} + \frac{i}{\omega_e}\frac{\partial N}{\partial t}\frac{Dz_{rel}}{Dt} - U\frac{\partial m}{\partial x}\frac{Dz_{rel}}{Dt} - U\frac{i}{\omega_e}\frac{\partial N}{\partial x}\frac{Dz_{rel}}{Dt} + m\frac{D^2 z_{rel}}{Dt^2} + \frac{i}{\omega_e}N\frac{D^2 z_{rel}}{Dt^2}
\end{aligned} \quad \text{(A3.3)}$$

Substituting Equation A3.3 into A3.1 and arranging according to the time derivatives, added amass and fluid damping terms, the sectional nonlinear force is written as (see Equation 2.46 to 2.50)

$$F_{nl}(x,t) = F_1(x,t) + F_2(x,t) + F_3(x,t) + F_4(x,t) \quad \text{(A3.4)}$$

where

$$F_1(x,t) = -\frac{\partial m_{nl}(z_{rel};x,\omega_e,t)}{\partial t}\frac{Dz_{rel}}{Dt} - \frac{i}{\omega_e}\frac{\partial N_{nl}(z_{rel};x,\omega_e,t)}{\partial t}\frac{Dz_{rel}}{Dt} \quad \text{(A3.5)}$$

$$F_2(x,t) = -m_{nl}(z_{rel};x,\omega_e,t)\frac{D^2 z_{rel}}{Dt^2} + U\frac{\partial m_{nl}(z_{rel};x,\omega_e,t)}{\partial x}\frac{Dz_{rel}}{Dt} \quad \text{(A3.6)}$$

$$F_3(x,t) = -\frac{i}{\omega_e} N_{nl}(z_{rel}; x, \omega_e, t) \frac{D^2 z_{rel}}{Dt^2} + \frac{i}{\omega_e} U \frac{\partial N_{nl}(z_{rel}; x, \omega_e, t)}{\partial x} \frac{Dz_{rel}}{Dt} \qquad \text{(A3.7)}$$

$$F_4(x,t) = \rho g \int_0^{\zeta - w} B(x,z)dz - \rho g k \zeta \int_{-T}^{\zeta - w} e^{k(z+w)} B(x,z)dz + \rho g B_o(x) z_{rel} \qquad \text{(A3.8)}$$

Appendix 4 Definition of impact shape factor G(x)

Assuming the distribution of normal pressure p_n over the bottom one-tenth of the draught at any instant as a linear distribution, the pressure p_n is written as (Bishop and Price 1979)

$$p_n(\alpha) \square\ p_{\max}(y(\alpha)/d) \quad \text{where} \quad d = 0.1T(x) \tag{A4.1}$$

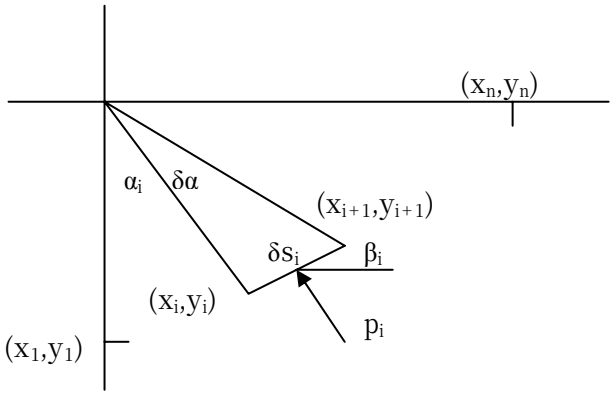

Figure A2 the vertical impact force at the i[th] element of the section

In the figure A2, the vertical force at the i[th] element of the section is given by

$$p_i \cos\alpha_i \delta s_i \tag{A4.2}$$

where

y_1 is d and y_n is 0,

$$p_i = p_{\max}\left(\frac{y_{i+1}+y_i}{2y_1}\right) \quad \text{and} \quad \cos\beta_i = \frac{x_{i+1}-x_i}{\delta s_i}.$$

The total vertical force per unit length on the section is thus

$$F(x) = 2\sum_{i=1}^{n-1} p_i \cos\beta_i \delta s_i = p_{\max}\frac{1}{y_1}\sum_{i=1}^{n}(y_{i+1}+y_i)(x_{i+1}-x_i) \tag{A4.3}$$

From Equation 2.66 without the time variation *f(t)*, the shape factor is denoted as

G(x). Thus by comparing with Equation A4.3,

$$G(x) = \frac{1}{y_1} \sum_{i=1}^{n} (y_{i+1} + y_i)(x_{i+1} - x_i) . \qquad \text{(A4.4)}$$